

國立臺灣大學電機資訊學院電信工程研究所

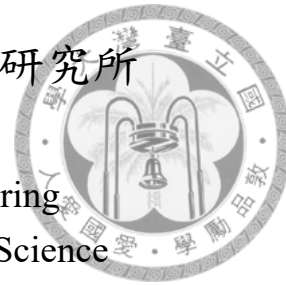
碩士論文

Graduate Institute of Communication Engineering

College of Electrical Engineering and Computer Science

National Taiwan University

Master Thesis



分增益多重接取系統之分析與設計

Analysis and Design of Gain-Division Multiple Access

許永超

Yung-Tsao Hsu

指導教授：林茂昭 博士

Advisor: Mao-Chao Lin, Ph.D.

中華民國 108 年 7 月

July, 2019

國立臺灣大學碩士學位論文
口試委員會審定書
分增益多重接取系統之分析與設計
Analysis and Design of Gain-Division Multiple Access

本論文係許永超君（R06942102）在國立臺灣大學電信工程學研究所完成之碩士學位論文，於民國 108 年 7 月 24 日承下列考試委員審查通過及口試及格，特此證明

口試委員：

林茂仁

(簽名)

王家志

(指導教授)

許永超

蘇賜麟

鄧惟明

系主任、所長

蘇大偉

(簽名)



致謝

感謝指導教授林茂昭老師在研究上提供我許多寶貴的意見並同時給予我充分的發揮空間，不會忘記這兩年來在老師身上所學習到的一點一滴。感謝李世凱教授、李晃昌教授與唐宏驛教授每個假日的指導與交流。感謝陳冠成、李冠廷、林穎塵、謝瑞賢、張倍豪、金揚恩與王會名學長們的提點與經驗分享，也感謝松董、湯神、小劉與智君學姊無私的幫忙。

感謝實驗室可愛的學弟妹們：裕欽、德生、疇尹、薏如和博瀚，祝福各位都能循著自己的規劃成為理想中的自己。感謝同學家俊和亭軒平時的相互鼓勵與支持，在兩年的碩士生活中一同經歷並完成了各式各樣的挑戰，很榮幸能遇見兩位優秀的戰友，也期許我們都能在各自的領域中發光發熱。

能在求學生涯中走到這一步當然也要感謝家人長期以來的無條件支持，也感謝每一個曾經給予我協助與鼓勵的朋友。兩年的時間，時光匆匆卻恍如隔世，回想起來要感謝的人事物實在太多，不如就謝天吧！



中文摘要

多重接取技術為現今通信系統中不可或缺的一部分。在大多數的系統中，能同時進行資料傳輸的使用者數量往往會因為傳輸資源的特性而有所限制。本篇論文介紹了如何使用分增益多重接取技術，在使用者透過不同且獨立的衰弱通道進行資料傳輸的場景中，利用不同的通道係數來區分不同使用者所傳輸的信號。這樣的多重接取技術允許多個使用者共享相同的傳輸資源，使資源的分配可以更有彈性。

這篇論文也針對多重接取的系統架構，基於分群演算法提出了一種通道盲測的技術。所提出的通道估計方法不需要使用額外的引信信號，因此能得到較高的頻譜使用效率。為了要解決在盲測技術中不可避免的相位不定性且同時保有一定的傳輸可靠度，我們在有使用差分編碼的系統中，針對低密度奇偶檢查碼進行最優化，藉此降低差分編碼對於傳輸效能的影響。

關鍵字：多重接取、衰弱通道、通道估計、盲蔽估測、分群演算法、低密度奇偶檢查碼、多邊式低密度奇偶檢查碼、差分編碼、密度演化



Abstract

Multiple access techniques are essential to telecommunication systems nowadays. In this thesis, we investigate a multiple access scheme called gain-division multiple access (GDMA), which allows multiple users to share the same user-specific resource by exploiting distinct channel coefficients when the transmissions are over independent fading channels.

We also propose a blind channel estimation scheme based on the clustering algorithm for GDMA system. The proposed method achieves high spectral efficiency by avoiding the use of pilot signal in channel estimation. To remove the inherent phase ambiguity in estimates derived from blind estimation and also attain an acceptable reliability in transmission, we optimize the outer low-density parity-check (LDPC) codes specifically when an inner differential encoding is cascaded in multi-edge framework and thus relieve the performance degradation introduced by differential encoding.

Key words: Multiple access, fading channel, channel estimation, blind estimation, clustering algorithm, LDPC codes, MET-LDPC codes, differential encoding, density evolution



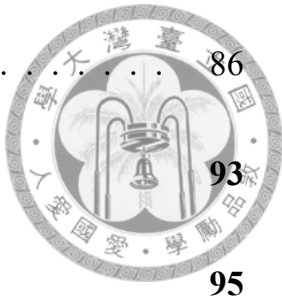
Contents

口試委員會審定書	i
致謝	ii
中文摘要	iii
Abstract	iv
Contents	v
List of Figures	viii
List of Tables	xii
1 Introduction	1
2 Gain-Division Multiple Access	5
2.1 Detection Principle	5
2.2 Bound of Error Rate	11
2.3 Multi-Level Receiver with Error-Correcting Codes	15
2.3.1 Joint Channel Decoding	15
2.3.2 Throughput Performance of Rateless Coding	22
2.4 System Examples	26



2.4.1	Multi-Carrier DS-CDMA	26
2.4.2	Alamouti Space-Time Scheme	30
3	Cluster-Based Channel Estimation	34
3.1	K-Means Algorithm	35
3.1.1	The LBG Algorithm	39
3.1.2	K-Means++ Algorithm	42
3.1.3	Gaussian Mixture Model	44
3.2	Derivation of Channel Coefficients	49
3.3	Resolving Phase Ambiguity	56
3.3.1	Differential Encoding	56
3.3.2	Turbo Principle	59
3.3.3	Joint Decoding	60
3.3.4	Noncoherent Block-Coded Modulation	62
3.4	System Impairments	68
3.4.1	Unknown Timing Drifts	68
3.4.2	Doppler Effect	70
4	Concatenation of LDPC Codes and Differential Encoding in Multi-Edge Framework	72
4.1	Multi-Edge Type LDPC Codes	73
4.2	Ensemble Behavior	77
4.3	Serial Concatenation of LDPC Codes and Differential Encoding .	81
4.3.1	Multi-Edge Representation	82
4.3.2	Decoding Schemes	84
4.3.3	Optimization in Multi-Edge Framework	85

4.3.4	Numerical Results
-------	-------------------	-------



5 Conclusion and Future Works

Bibliography

86

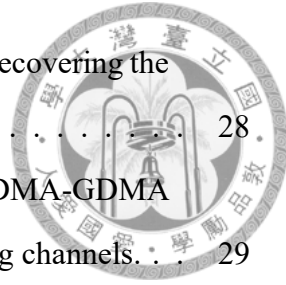
93

95



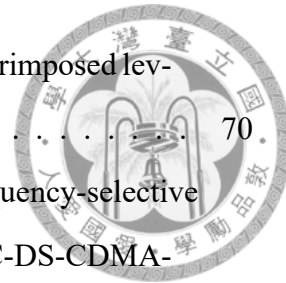
List of Figures

1.1	Schematic diagram for uplink transmission where the number of transmit resources is less than that of users.	2
2.1	Transmitters of P users occupying the same resource.	6
2.2	An example of superimposed levels in the case of $m = 1$ and $P = 2$	7
2.3	Multi-level receiver in GDMA system for recovering the messages of P users.	8
2.4	Separated channel decoding in the case of $m = 1$ and $P = 2$	9
2.5	An example of superimposed levels in the case of $m = 1$ and $P = 3$	10
2.6	Upper bounds and exact BERs for BPSK transmissions.	13
2.7	Upper bounds and exact BERs in the case of $m = 2$	15
2.8	Joint channel decoding in the case of $m = 1$ and $P = 2$	16
2.9	The message passing algorithm along the edges in factor graph.	17
2.10	BLER performances of (256, 128) Polar-coded GDMA-SCD system over quasi-static Rayleigh flat-fading channels.	20
2.11	BLER performances of (1008, 504) LDPC-coded GDMA systems over quasi-static Rayleigh flat-fading channels.	21
2.12	An encoder of a Raptor code.	22
2.13	An example of a Raptor code represented in Tanner graph.	23
2.14	Throughput performances of Raptor-coded GDMA-SCD system over quasi-static Rayleigh flat-fading channels.	25
2.15	Transmitter of user- (k, p) in MC-DS-CDMA-GDMA system.	27



2.16	Multi-level receiver in MC-DS-CDMA-GDMA system for recovering the signals using the k -th spreader.	28
2.17	BLER performances of (1008,504) LDPC-coded MC-DS-CDMA-GDMA system over quasi-static frequency-selective Rayleigh fading channels.	29
2.18	Alamouti space-time transmitter of user- p	30
2.19	Multi-level receiver in STC-GDMA system for recovering the messages of P users.	31
2.20	BER performances of STC-GDMA system over quasi-static Rayleigh flat-fading channels.	33
3.1	Superimposed levels and the corresponding received signals in the case of $m = 1$ and $P = 2$	34
3.2	An example of k-means algorithm and the resultant centroids.	37
3.3	A local minima found by k-means algorithm.	38
3.4	An example of the quantization region designed by the LBG algorithm. .	40
3.5	Splitting from q to get $q + \epsilon$ and $q - \epsilon$ with a perturbation vector ϵ	41
3.6	An example of local minimums found by the LBG algorithm	41
3.7	Grouping result of hard clustering by applying nearest neighbor rule.	44
3.8	An example of EM clustering with GMM.	46
3.9	Derivation of coefficients in the case of $P = 2$ and BPSK transmission. .	49
3.10	Derivation of coefficients in the case of $P = 3$ and BPSK transmission. .	51
3.11	Derivation of coefficients in the case of $P = 2$ and 4-PAM transmission. .	52
3.12	MSE performances of the cluster-based estimation applied to quasi-static Rayleigh flat-fading channels in the case of $P = 1$	53
3.13	MSE performances of the cluster-based estimation applied to quasi-static Rayleigh flat-fading channels in the case of $P = 2$ and BPSK transmissions. .	54
3.14	MSE performances of the cluster-based estimation applied to quasi-static Rayleigh flat-fading channels.	55
3.15	Modulation scheme for DE-BPSK transmission.	57
3.16	Representation of DE-BPSK in Trellis diagram.	57

3.17	BER performances of GDMA-BPSK system employing cluster-based estimation with $N_t = 100$ over quasi-static Rayleigh flat-fading channels.	58
3.18	BER performances of GDMA-BPSK system employing cluster-based estimation with $N_t = 1000$ over quasi-static Rayleigh flat-fading channels.	58
3.19	BER performances of GDMA-4-PAM system employing cluster-based estimation with $N_t = 1000$ over quasi-static Rayleigh flat-fading channels.	59
3.20	Turbo processor: iterative demodulation and decoding.	60
3.21	Serial concatenation of differential encoding and an LDPC code represented in Tanner graph for DE-BPSK transmission.	61
3.22	BER performances of schemes that remove the phase ambiguity in LDPC-coded system over quasi-static Rayleigh flat-fading channel.	63
3.23	BLER performances of schemes that remove the phase ambiguity in LDPC-coded system over quasi-static Rayleigh flat-fading channel.	64
3.24	BLER performances of schemes that remove the phase ambiguity in LDPC-coded MC-DS-CDMA system over quasi-static frequency-selective Rayleigh fading channels.	65
3.25	BLER performances of (256,128) Polar-coded GDMA-SCD system employing cluster-based estimation over quasi-static Rayleigh flat-fading channels.	66
3.26	BLER performances of (1008,504) LDPC-coded GDMA-SCD system employing cluster-based estimation over quasi-static Rayleigh flat-fading channels.	66
3.27	BLER performances of (1008,504) LDPC-coded MC-DS-CDMA-GDMA system employing cluster-based estimation over quasi-static frequency-selective Rayleigh fading channels.	67
3.28	System model for asynchronous transmissions.	68
3.29	BLER performances of (1008,504) LDPC-coded MC-DS-CDMA-GDMA system employing cluster-based estimation over quasi-static frequency-selective Rayleigh fading channels with independent timing drifts.	69



3.30	Traversal of channel coefficients and the corresponding superimposed levels in the case of $m = 1$ and $P = 2$	70
3.31	BLER performances of transmissions over time-varying frequency-selective Rayleigh fading channels in (1008,504) LDPC-coded MC-DS-CDMA-GDMA system employing cluster-based estimation	71
4.1	Graphical representation of a four-edge-type MET-LDPC code	76
4.2	An encoder of DE-LDPC code for DE-BPSK transmission	83
4.3	Configuration of edge-types for DE-LDPC codes represented in MET framework for DE-BPSK transmission	83
4.4	Graphical representation of DE-LDPC code ensemble in MET framework for DE-BPSK transmission	84
4.5	BER and BLER performances of (12000,6000) LDPC codes over AWGN channel	89
4.6	BER performances of (6000,3000) LDPC codes with or without differential encoding over AWGN channel	90
4.7	BLER performances of (6000,3000) LDPC codes with or without differential encoding over AWGN channel	90
4.8	BLER performances of (1008,504) LDPC-coded MC-DS-CDMA system employing cluster-based estimation with $P = 1$ user over quasi-static frequency-selective Rayleigh fading channels	92
4.9	BLER performances of (1008,504) LDPC-coded MC-DS-CDMA-GDMA system employing cluster-based estimation with $P = 2$ users over quasi-static frequency-selective Rayleigh fading channels	92



List of Tables

2.1	Mapping rules for superimposed signal in the case of $m = 1$ and $P = 2$. . .	7
2.2	Mapping rules for superimposed signal in the case of $m = 1$ and $P = 3$. . .	10
3.1	Average numbers of iterations for different algorithms where $N_t = 100$ and $\bar{E}_b/N_0 = 5$ dB.	43
3.2	Average numbers of iterations for different algorithms where $N_t = 100$ and $\bar{E}_b/N_0 = 20$ dB.	43
4.1	Optimized degree distributions with a fixed set of degrees.	87
4.2	Optimized degree distributions for different d_v 's.	88



Chapter 1

Introduction

Multiple access techniques are critical topics in cellular mobile communications. In most of the multiple access systems, users are allowed to transmit signal simultaneously in the same bandwidth through different types of transmit resources, e.g., spreading sequences in code-division multiple access (CDMA), interleavers in interleave-division multiple access (IDMA), time-frequency resources in orthogonal-frequency division multiple access (OFDMA), etc. In non-orthogonal multiple access (NOMA), multiple users are superposed in the power domain. The number of users that can be served in a multiple access systems is usually limited due to the constraint of user-specific transmit resource in orthogonal multiple access schemes, and hence we introduce the gain-division multiple access (GDMA) [1] in this thesis to make the resource allocation more flexible. A schematic diagram for uplink transmission is provided in Fig. 1.1, where four user equipments (UEs) are transmitting signals with only three distinct resources. By exploiting the distinct amplitudes and phase shifts in channel coefficients caused by independent fading channels, P users are allowed to share the same transmit resource with multi-level

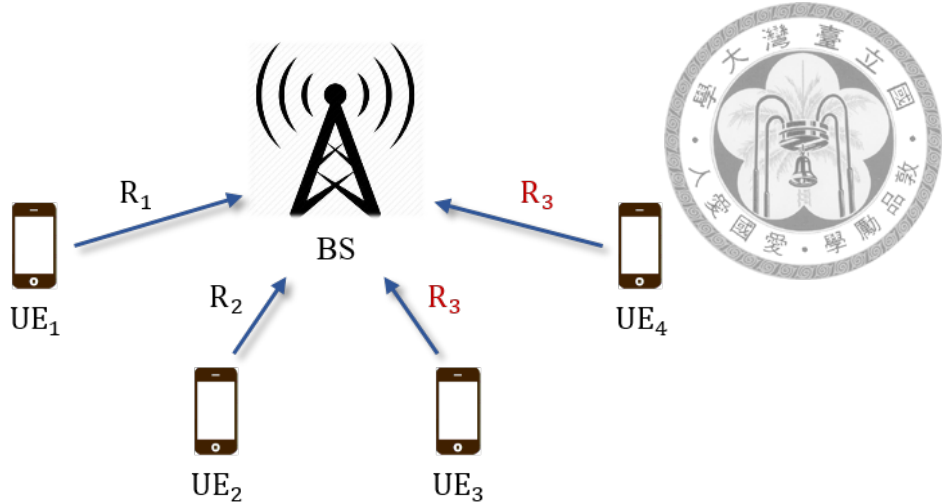


Figure 1.1: Schematic diagram for uplink transmission where the number of transmit resources is less than that of users.

detection technique in GDMA system. The detection scheme of GDMA is originated from the concept of physical layer network coding (PLNC), which coordinates transmissions among nodes and thus packet collisions in traditional wireless network can be eliminated [2].

Since the multi-level detection technique in GDMA system allows P users to share the same user-specific resource, each of the received symbols consisting of the signals transmitted from P users can be seen as a superimposed signal with 2^{mP} levels where m is the modulation order. By utilizing the geometrical configuration of received superimposed signal, we further apply clustering algorithms to estimate the scalar channels. Clustering is an unsupervised learning technique that involves the grouping of samples and aims to make the samples in the same group have similar properties while the samples in different groups have dissimilar properties. In [3], a local search algorithm was proposed to minimize the sum of squared distance between each sample and its closest centroid, which is usually referred to as



k-means algorithm. There are many research works in this topic [4] [5] [6] trying to improve the performances in terms of accuracy, convergence speed, etc. K-means algorithm classify samples into groups by iteratively pairing up each sample with closest matching centroid and then updating the centroids from the newly derived groups. If we can properly classify the received symbols into 2^{mP} groups, where the symbols corresponding to the same superimposed level are grouped together, the estimates of the levels can be attained through the average of the symbols in each group. The proposed scheme for cluster-based channel estimation is a kind of blind estimation, which results in high spectral efficiency since no additional pilot signal is needed for channel estimation. However, there is still an uncertain phase ambiguity in the estimates.

There is an inherent ambiguity problem typically in the estimates derived from blind estimations. A simple way to remove the phase ambiguity is to differentially encode (DE) the message but the bit error rate (BER) of DE-PSK is about twice the BER of PSK transmission. In order to alleviate the performance loss when the differential encoding is applied to remove the ambiguity, we represent the serial concatenation of low-density parity-check (LDPC) codes and differential encoding as multi-edge type (MET) LDPC codes [7]. In multi-edge framework, which is an unifying representation for graph-based codes, MET-LDPC codes are allowed to have multiple statistically equivalent classes of edges and thus a greater flexibility in code structure can be obtained. By using the MET density evolution (MET-DE) that has been widely used for designing MET-LDPC codes, one can

determine the asymptotic performance of belief propagation (BP) decoding for a given MET-LDPC code ensemble by iteratively tracking the probability density functions (PDFs) of messages passed along the edges in the corresponding Tanner graph. Therefore, our goal is to optimize the degree distributions of outer LDPC codes specifically when an inner differential encoding is cascaded to enhance the reliability in transmission for the system employing blind channel estimation.

The organization of this thesis is as follows. In Chapter 2, basic concepts of the GDMA technique are reviewed and the system models are also illustrated. The proposed cluster-based channel estimation for GDMA system is introduced in Chapter 3 including the clustering algorithms and the schemes to resolve the phase ambiguity problem. Moreover, the serial concatenation of outer LDPC codes and inner differential encoding is represented as MET-LDPC codes in Chapter 4, and the numerical results are provided to evaluate the contributions. Concluding remarks and future works are presented in Chapter 5.



Chapter 2

Gain-Division Multiple Access

In this chapter, we consider the scenario for uplink transmissions over independent fading channels and the gain-division multiple access (GDMA) with multi-level detection technique is reviewed for further discussions.

2.1 Detection Principle

A communication system in which P users are sharing the same transmit resource is considered, and the symbol timings of transmissions are assumed to be perfectly aligned. The block diagram of transmitters is shown in Fig. 2.1. The message bit sequence $\mathbf{d}_p = [d_p(1), d_p(2), \dots, d_p(k)]$ of user- p is encoded into the code-word $\mathbf{c}_p = [c_p(1), c_p(2), \dots, c_p(N_c)]$ by an (N_c, k) forward error-correction (FEC) code with code rate k/N_c , and the codeword \mathbf{c}_p is then passed to the modulator with order m to get the sequence of modulated symbols $\mathbf{x}_p = [x_p(1), x_p(2), \dots, x_p(N_c/m)]$. The signals of P users are transmitted to the receiver through the independent Rayleigh flat-fading channels, and each of the received symbols in sequence $\mathbf{r} =$

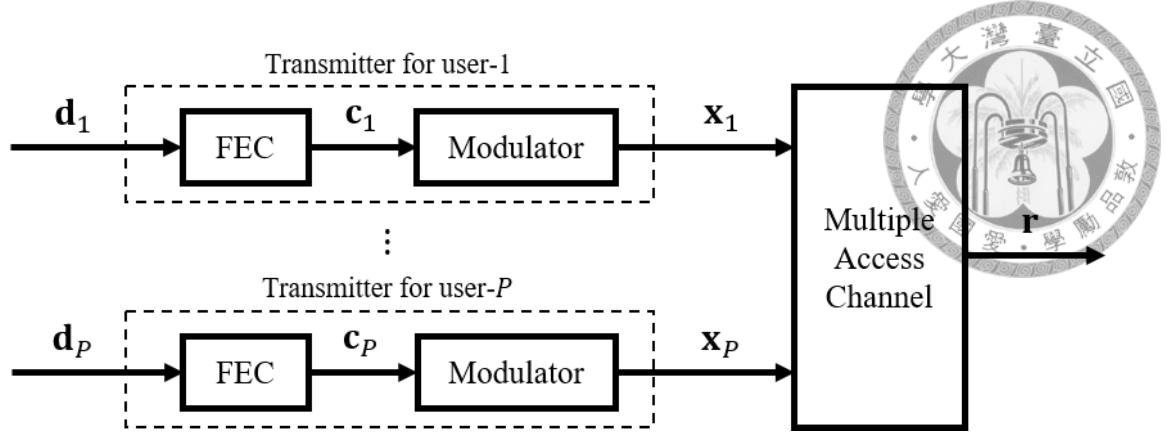


Figure 2.1: Transmitters of P users occupying the same resource.

$[r(1), r(2), \dots, r(N_c/m)]$ can be represented as

$$\begin{aligned}
 r(n) &= \sum_{p=1}^P h_p x_p(n) + w(n) \\
 &= s(n) + w(n),
 \end{aligned} \tag{2.1}$$

where h_p is the channel coefficient between user- p and the receiver, $w(n)$ is the complex additive white Gaussian noise (AWGN) and $s(n)$ is the superimposed symbol consisting of the signals transmitted from P users. There are 2^{mP} possible levels in each s , where we drop the symbol index n for brevity, and the levels are distinguishable due to the effect of independent fading channels.

We consider the case of $P = 2$ and the signals are BPSK-modulated ($m = 1$) for illustration, and the users are denoted as user-A and user-B. The mapping rules for codeword bits of two users and superimposed levels in this case are tabulated in Table 2.1, and the possible levels of s are denoted as $S[l]$ with $l \in \{0, 1, 2, 3\}$. In Fig. 2.2, a graphical example of the superimposed levels and the corresponding binary mappings (c_A, c_B) is provided when h_A and h_B are the channel coefficients

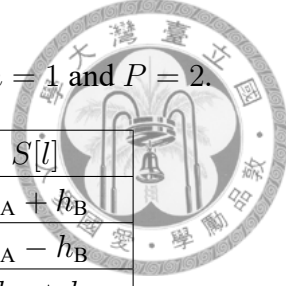


Table 2.1: Mapping rules for superimposed signal in the case of $m = 1$ and $P = 2$.

l	c_A	c_B	x_A	x_B	$S[l]$
0	0	0	1	1	$h_A + h_B$
1	0	1	1	-1	$h_A - h_B$
2	1	0	-1	1	$-h_A + h_B$
3	1	1	-1	-1	$-h_A - h_B$

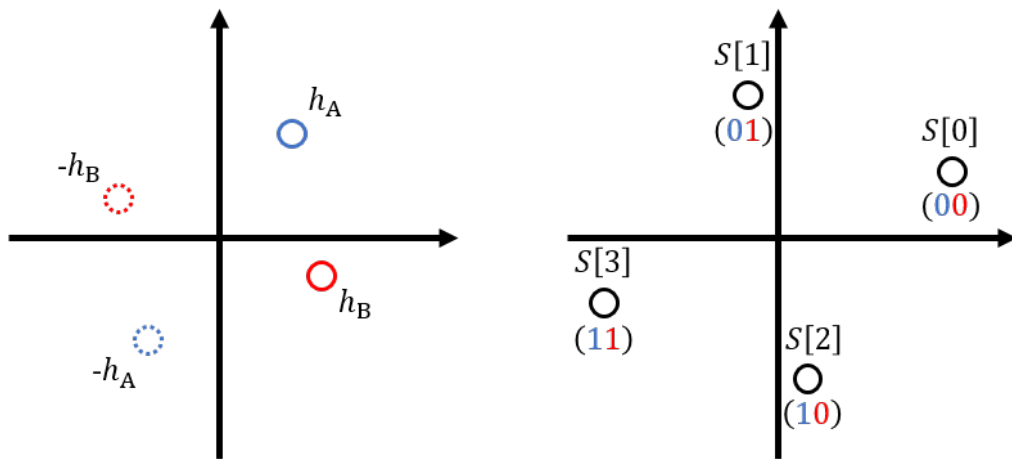


Figure 2.2: An example of superimposed levels in the case of $m = 1$ and $P = 2$.

of user-A and user-B respectively. Note that an accurate estimation of channel coefficients for all users is necessary to properly recognize the levels of superimposed signal. In this chapter we assume that the channel state information (CSI) can be perfectly recovered at the receiver, and thus we can derive all the possible levels of received symbol s for further detection.

The *a posteriori* probabilities (APPs) that s is the l -th level with $l \in \{0, 1, 2, 3\}$ given the received symbol r can be calculated by

$$\begin{aligned}
 p_l &= \Pr \{ s = S[l] | r \} \\
 &= \Pr \{ r | s = S[l] \} \cdot \frac{\Pr \{ s = S[l] \}}{\Pr \{ r \}}, \tag{2.2}
 \end{aligned}$$

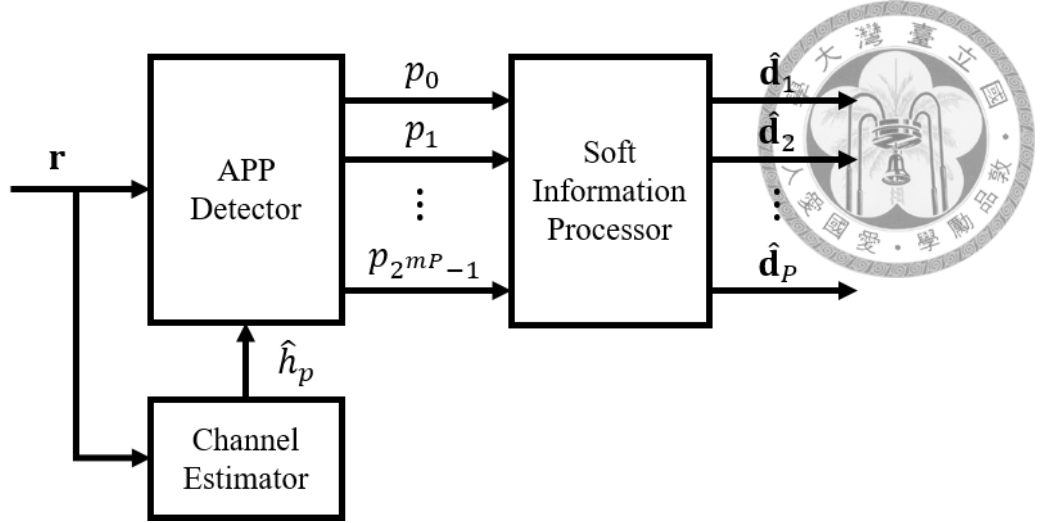


Figure 2.3: Multi-level receiver in GDMA system for recovering the messages of P users.

and

$$\Pr \{r|s = S[l]\} = \frac{1}{2\pi\sigma_w^2} \exp\left(-\frac{|r - S[l]|^2}{2\sigma_w^2}\right), \quad (2.3)$$

where $\Pr\{s = S[l]\}$ is the *a priori* probabilities of s and σ_w^2 is the variance of AWGN. According to the concept of physical layer network coding (PLNC), the APPs of codeword bits given the received symbol r can be obtained as

$$\begin{aligned} \Pr \{c_A = 0|r\} &= \Pr \{s = S[0]|r\} + \Pr \{s = S[1]|r\} = p_0 + p_1, \\ \Pr \{c_A = 1|r\} &= \Pr \{s = S[2]|r\} + \Pr \{s = S[3]|r\} = p_2 + p_3, \end{aligned} \quad (2.4)$$

and

$$\begin{aligned} \Pr \{c_B = 0|r\} &= \Pr \{s = S[0]|r\} + \Pr \{s = S[2]|r\} = p_0 + p_2, \\ \Pr \{c_B = 1|r\} &= \Pr \{s = S[1]|r\} + \Pr \{s = S[3]|r\} = p_1 + p_3. \end{aligned} \quad (2.5)$$

The APPs of codeword bits can be derived for multiple users with the observation

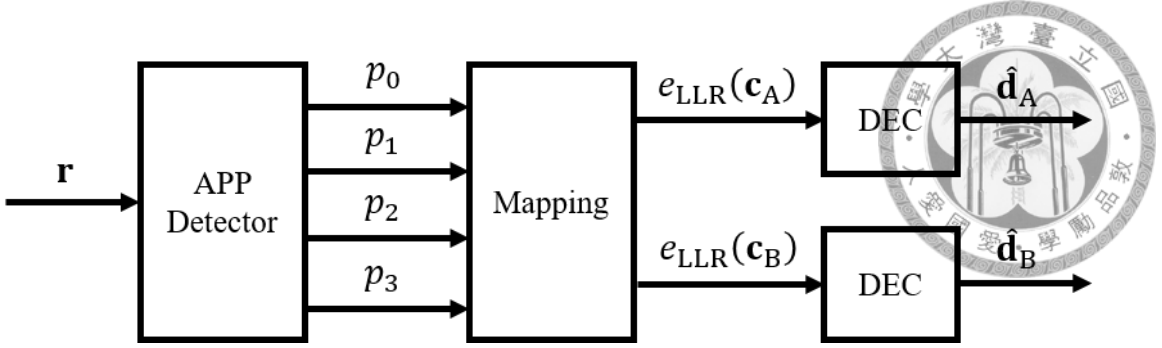


Figure 2.4: Separated channel decoding in the case of $m = 1$ and $P = 2$.

of received superimposed symbol as long as the CSI is available at the receiver, and this detection scheme was referred to as multi-level detection (MLDT) in [1]. Once the APPs of codeword bits are obtained, the corresponding log-likelihood ratios (LLRs) of codeword bits are given by

$$\begin{aligned} e_{\text{LLR}}(c_A) &= \ln \frac{\Pr\{c_A = 0|r\}}{\Pr\{c_A = 1|r\}} = \ln \frac{p_0 + p_1}{p_2 + p_3}, \\ e_{\text{LLR}}(c_B) &= \ln \frac{\Pr\{c_B = 0|r\}}{\Pr\{c_B = 1|r\}} = \ln \frac{p_0 + p_2}{p_1 + p_3}. \end{aligned} \quad (2.6)$$

The LLRs can be directly used for data detection or be further fed to the following soft information processor (SIP) when FEC coding is considered. The block diagram of multi-level receiver in GDMA system is shown in Fig. 2.3. The SIP can be implemented by using several decoders (DECs) and one for each user independently as shown in Fig. 2.4. If a low-density parity-check (LDPC) code is specifically employed for all users, a joint channel decoder proposed in [8] can be an alternative to implement the SIP and extract the messages of all users simultaneously. The implementation of SIP will be discussed in Sec. 2.3.

If the messages are transmitted without FEC coding, the decision rule with the

Table 2.2: Mapping rules for superimposed signal in the case of $m = 1$ and $P = 3$.

l	c_1	c_2	c_3	x_1	x_2	x_3	$S[l]$
0	0	0	0	1	1	1	$h_1 + h_2 + h_3$
1	0	0	1	1	1	-1	$h_1 + h_2 - h_3$
2	0	1	0	1	-1	1	$h_1 - h_2 + h_3$
3	0	1	1	1	-1	-1	$h_1 - h_2 - h_3$
4	1	0	0	-1	1	1	$-h_1 + h_2 + h_3$
5	1	0	1	-1	1	-1	$-h_1 + h_2 - h_3$
6	1	1	0	-1	-1	1	$-h_1 - h_2 + h_3$
7	1	1	1	-1	-1	-1	$-h_1 - h_2 - h_3$

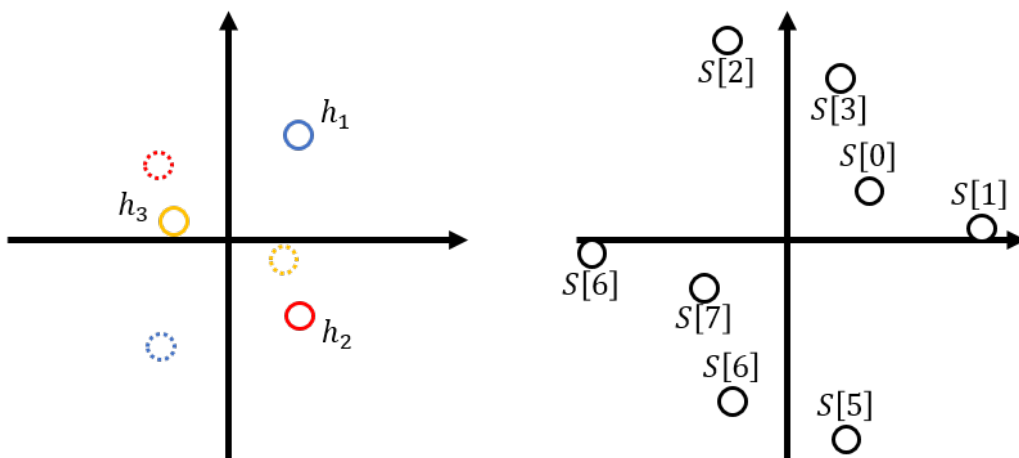


Figure 2.5: An example of superimposed levels in the case of $m = 1$ and $P = 3$.

APPs derived from multi-level detection is equivalent to finding the nearest neighbour of received symbol among all the levels and the corresponding decision region is dependent on the channel coefficients. A special case that $P = 2$ users are transmitting BPSK-modulated signals when the channel coefficients have the same amplitude and 90° difference in phases is equivalent to the transmission of QPSK-modulated signal and the message bits of two users are embedded in in-phase component and quadrature component, respectively.

The multi-level detection technique in GDMA system can be easily extended

to the system with $P > 2$ and/or $m > 1$. For example, in the case of $m = 1$ and $P = 3$, the mapping rules for codeword bits of users, denoted as user-1, user-2 and user-3, and superimposed levels are tabulated in Table 2.2. There are eight possible levels in each superimposed symbol s . Let p_l with $l \in \{0, 1, \dots, 7\}$ denote the APPs of s given in (2.2), the LLRs of codeword bits are

$$\begin{aligned} e_{\text{LLR}}(c_1) &= \ln \frac{\Pr\{c_1 = 0|r\}}{\Pr\{c_1 = 1|r\}} = \ln \frac{p_0 + p_1 + p_2 + p_3}{p_4 + p_5 + p_6 + p_7}, \\ e_{\text{LLR}}(c_2) &= \ln \frac{\Pr\{c_2 = 0|r\}}{\Pr\{c_2 = 1|r\}} = \ln \frac{p_0 + p_1 + p_4 + p_5}{p_2 + p_3 + p_6 + p_7}, \\ e_{\text{LLR}}(c_3) &= \ln \frac{\Pr\{c_3 = 0|r\}}{\Pr\{c_3 = 1|r\}} = \ln \frac{p_0 + p_2 + p_4 + p_6}{p_1 + p_3 + p_5 + p_7}. \end{aligned} \quad (2.7)$$

2.2 Bound of Error Rate

Since the signals are propagated through independent Rayleigh flat-fading channels in assumption, the channel coefficients $h_p = |h_p| \exp(j\theta_p)$ with $p \in \{1, 2, \dots, P\}$ are independent and identically distributed (i.i.d.), where θ_p is uniformly distributed in $[0, 2\pi)$ and $|h_p|$ is Rayleigh distributed with probability density function (PDF)

$$f_{|h_p|}(r) = \frac{2r}{\mathbb{E}[|h_p|^2]} \exp\left(-\frac{r^2}{\mathbb{E}[|h_p|^2]}\right). \quad (2.8)$$

Define $D_H(S[i], S[j])$ as the Hamming distance between the binary mappings of $S[i]$ and $S[j]$. Note that each of the superimposed levels is mapped from the bits of P users. Recall that the multi-level detection in GDMA system is equivalent to finding the nearest neighbour of received symbol among all the levels and the decision region is dependent on the channel coefficients. Therefore, the bit error rate

(BER) of uncoded transmissions in GDMA system, when the channel coefficients

h_p with $p \in \{1, 2, \dots, P\}$ are given, can be expressed as

$$\begin{aligned} P_{b|\{h_p\}} &= \sum_{i=0}^{2^{mP}-1} \sum_{j \neq i} \frac{D_H(S[i], S[j])}{mP} \Pr\{s = S[i] \cap \hat{s} = S[j]\} \\ &= \sum_{i=0}^{2^{mP}-1} \sum_{j \neq i} \frac{D_H(S[i], S[j])}{mP} \Pr\{s = S[i]\} \cdot \Pr\{\hat{s} = S[j] | s = S[i]\}, \quad (2.9) \end{aligned}$$

where \hat{s} is the decision of s at the receiver side. Moreover, we assume that the events of s being the l -th level with $l \in \{0, 1, \dots, 2^{mP} - 1\}$ have equally like probabilities, i.e., $\Pr\{s = S[l]\} = 2^{-mP}$ with $l \in \{0, 1, \dots, 2^{mP} - 1\}$. By replacing $\Pr\{\hat{s} = S[j] | s = S[i]\}$ in (2.9) with the pairwise error probability, a union bound of (2.9) can be written as

$$P_{b|\{h_p\}} \leq \sum_{i=0}^{2^{mP}-1} \frac{1}{2^{mP}} \sum_{j \neq i} \frac{D_H(S[i], S[j])}{mP} Q\left(\frac{|S[i] - S[j]|}{\sqrt{2N_0}}\right), \quad (2.10)$$

where $\sigma_w^2 = N_0/2$ is the variance of AWGN and $Q(x) = \frac{1}{\sqrt{2\pi}} \int_x^\infty \exp\left(-\frac{u^2}{2}\right) du$.

After weighting (2.10) with the PDFs of channel coefficients, we have an upper bound of BER in uncoded GDMA system over Rayleigh flat-fading channels

$$P_b \leq \mathbb{E}[P_{b|\{h_p\}}], \quad (2.11)$$

where $\mathbb{E}[\cdot]$ stands for the expected value.

Assuming that the transmitted symbols of each user have unit energy in average, and let $\bar{\gamma} = \frac{1}{N_0} \mathbb{E}[|h_p|^2]$ be the average of signal-to-noise ratio (SNR) per symbol over Rayleigh flat-fading channels. It is known that the average BER of (1) $P = 1$



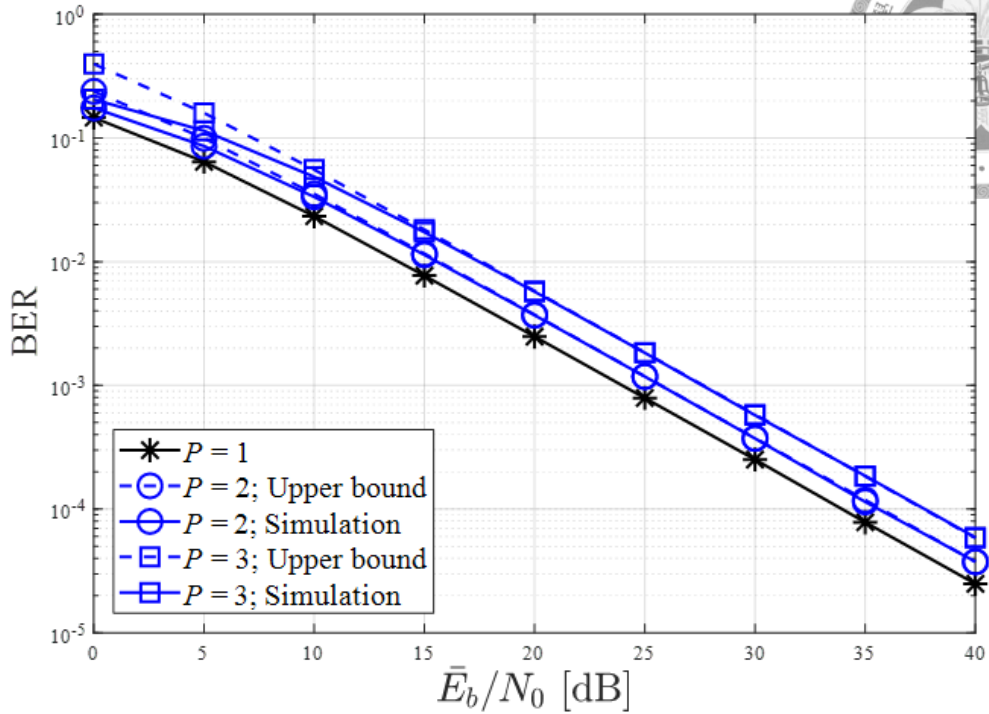
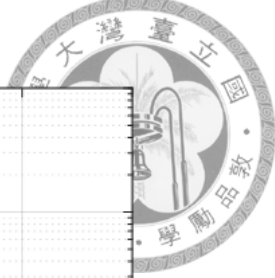


Figure 2.6: Upper bounds and exact BERs for BPSK transmissions.

case with BPSK transmission can be written as

$$P_b^{(1)} = \frac{1}{2} \left(1 - \sqrt{\frac{\bar{\gamma}}{1 + \bar{\gamma}}} \right). \quad (2.12)$$

The upper bounds of BERs for cases (2) $P = 2$ and (3) $P = 3$ with BPSK transmissions derived in [1] are

$$P_b^{(2)} \leq \frac{1}{2} \left(1 - \sqrt{\frac{\bar{\gamma}}{1 + \bar{\gamma}}} \right) + \frac{1}{2} \left(1 - \sqrt{\frac{2\bar{\gamma}}{1 + 2\bar{\gamma}}} \right), \quad (2.13)$$

and

$$P_b^{(3)} \leq \frac{1}{2} \left(1 - \sqrt{\frac{\bar{\gamma}}{1 + \bar{\gamma}}} \right) + \left(1 - \sqrt{\frac{2\bar{\gamma}}{1 + 2\bar{\gamma}}} \right) + \frac{1}{2} \left(1 - \sqrt{\frac{3\bar{\gamma}}{1 + 3\bar{\gamma}}} \right). \quad (2.14)$$

Moreover, the upper bounds of BERs in the case of $P = 2$ with (4) QPSK and (5)



4-PAM transmissions are derived as

$$P_b^{(4)} \leq \frac{1}{2} \left(1 - \sqrt{\frac{\bar{\gamma}/2}{1 + \bar{\gamma}/2}} \right) + \frac{3}{2} \left(1 - \sqrt{\frac{\bar{\gamma}}{1 + \bar{\gamma}}} \right) \\ + \frac{3}{2} \left(1 - \sqrt{\frac{3\bar{\gamma}/2}{1 + 3\bar{\gamma}/2}} \right) + \frac{1}{2} \left(1 - \sqrt{\frac{2\bar{\gamma}}{1 + 2\bar{\gamma}}} \right), \quad (2.15)$$

and

$$P_b^{(5)} \leq \frac{3}{8} \left(1 - \sqrt{\frac{\bar{\gamma}E_0}{1 + \bar{\gamma}E_0}} \right) + \frac{9}{16} \left(1 - \sqrt{\frac{2\bar{\gamma}E_0}{1 + 2\bar{\gamma}E_0}} \right) + \frac{1}{2} \left(1 - \sqrt{\frac{4\bar{\gamma}E_0}{1 + 4\bar{\gamma}E_0}} \right) \\ + \frac{9}{8} \left(1 - \sqrt{\frac{5\bar{\gamma}E_0}{1 + 5\bar{\gamma}E_0}} \right) + \frac{1}{2} \left(1 - \sqrt{\frac{8\bar{\gamma}E_0}{1 + 8\bar{\gamma}E_0}} \right) + \frac{1}{8} \left(1 - \sqrt{\frac{9\bar{\gamma}E_0}{1 + 9\bar{\gamma}E_0}} \right) \\ + \frac{3}{8} \left(1 - \sqrt{\frac{10\bar{\gamma}E_0}{1 + 10\bar{\gamma}E_0}} \right) + \frac{3}{8} \left(1 - \sqrt{\frac{13\bar{\gamma}E_0}{1 + 13\bar{\gamma}E_0}} \right) + \frac{1}{16} \left(1 - \sqrt{\frac{18\bar{\gamma}E_0}{1 + 18\bar{\gamma}E_0}} \right), \quad (2.16)$$

where the constellation of transmitted signal used in 4-PAM transmission is configured as $\{-3\sqrt{E_0}, -\sqrt{E_0}, \sqrt{E_0}, 3\sqrt{E_0}\}$.

The theoretical bounds and simulated results are both shown in Fig. 2.6 and 2.7. When the number of users is increased by one, the required SNR for a specific error rate is increased of 1.8 dB, 4 dB and 4.6 dB in GDMA system with BPSK, 4-PAM and QPSK transmissions respectively. If the transmissions are over independent fading channels, the superimposed signals can be further separated in GDMA system by exploiting the distinct channel coefficients without requiring additional user-specific resources. Thus, the GDMA technique can be used for increasing the number of users in a multiple access system or a solution to user collision.

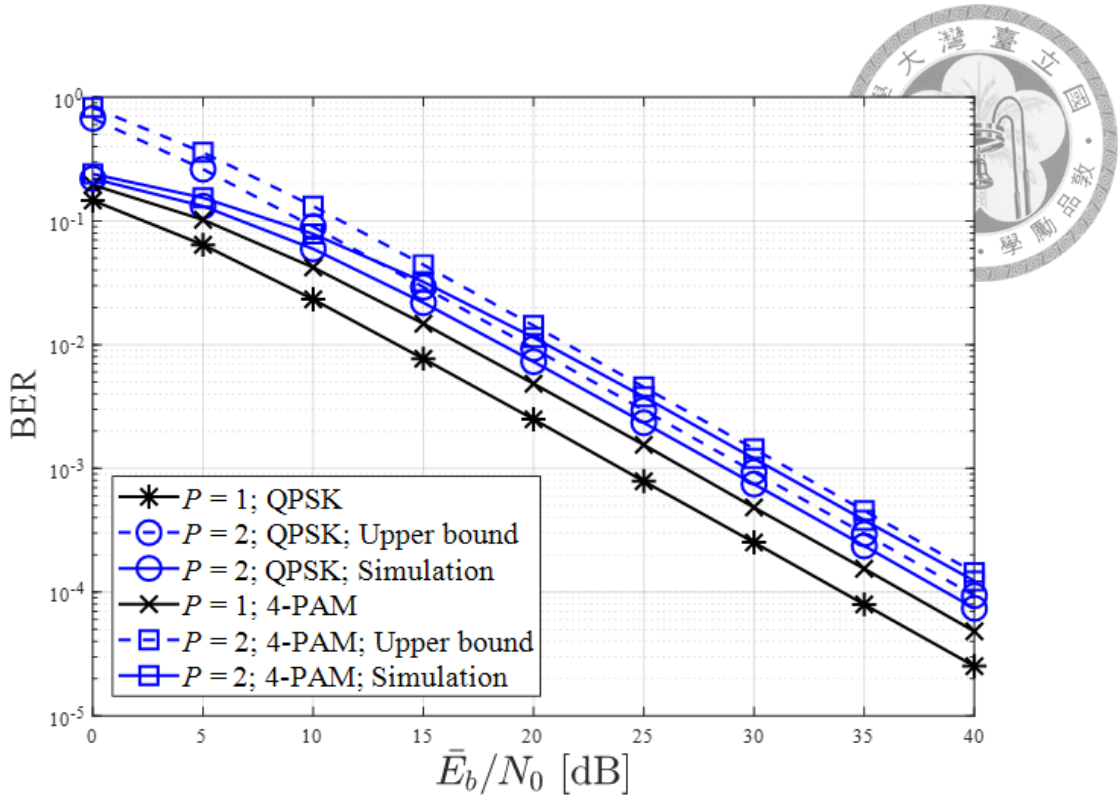


Figure 2.7: Upper bounds and exact BERs in the case of $m = 2$.

2.3 Multi-Level Receiver with Error-Correcting Codes

In this section, implementation flow of soft information processor (SIP) in multi-level receiver is discussed and the throughput performances of GDMA system employing rateless codes are also provided.

2.3.1 Joint Channel Decoding

A straightforward method to construct the SIP in GDMA system is called separated channel decoding (SCD) as shown in Fig. 2.4 To recover the messages of P users in GDMA-SCD system, the APPs of codeword bits are first attained and then be fed to the following decoders independently for each user. Note that there is no exchange of informations between collided users in GDMA-SCD scheme.

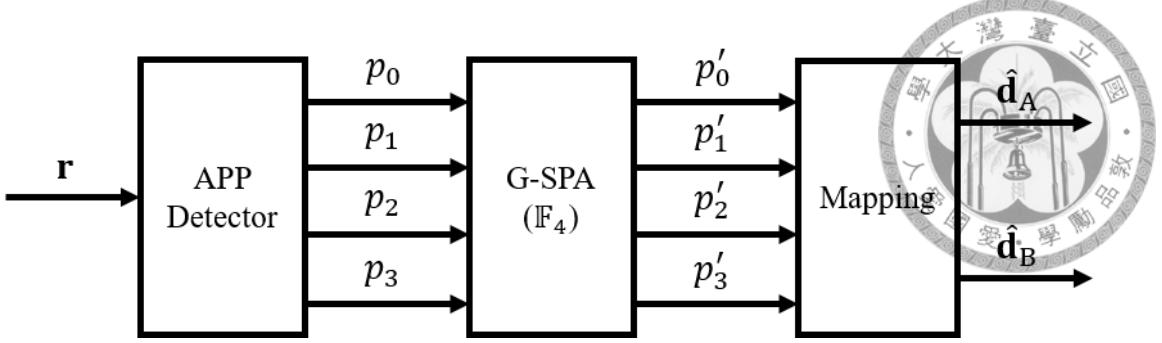


Figure 2.8: Joint channel decoding in the case of $m = 1$ and $P = 2$.

Assuming that the same binary LDPC code is employed for P users, an alternative to implement the SIP is shown in Fig. 2.8 in the case of $P = 2$ and BPSK transmission, which was originally called generalized joint channel decoding and physical-layer network coding (G-JCNC) in [8]. The G-JCNC was proposed to combine the soft decoding of LDPC codes and the physical-layer network coding (PLNC), and here we take advantage of joint channel decoding (JCD) to extract the messages of P users simultaneously. The APPs of each symbol $s(n)$, p_l with $l \in \{0, 1, \dots, 2^{mP} - 1\}$, are sent to a non-binary decoder using generalized SPA (G-SPA), and the decoding is performed with respect to $\mathbb{F}_{2^{mP}}$. The procedure of G-SPA in the case of $P = 2$ and BPSK transmission is described as follows.

Messages and Initialization

An LDPC code can be represented as a bipartite graph, called Tanner graph, defined by the parity-check matrix with two kinds of nodes: check nodes and variable nodes. The G-SPA iteratively determines the APPs of the symbol $s(n)$ with $n \in \{1, 2, \dots, N_c\}$ over the Tanner graph [9]. The four possible levels in each $s(n)$ are shown in Table 2.1. The message passed through the edges in the correspond-

ing Tanner graph are represented by probability vector $\mathbf{p} = [p_0 \ p_1 \ p_2 \ p_3]$ where p_i is the probability that the value of variable $s(n)$ is $S[l]$ with $l \in \{0, 1, 2, 3\}$, and $p_0 + p_1 + p_2 + p_3 = 1$ holds. The initial message of variable node $s(n)$ given the received symbol $r(n)$ is $p_l = \Pr \{s(n) = S[l] | r\}$ with $l \in \{0, 1, 2, 3\}$ given in (2.2).

The message updating rules at variable nodes and check nodes within the G-SPA are the same as that discussed in [9], and the update functions are defined as VAR and CHK for variable nodes and check nodes respectively. The discussion is restricted to nodes of degree three and the messages from the nodes with degree greater than three can be calculated by

$$\begin{aligned} \text{VAR}(\mathbf{p}, \mathbf{q}, \dots) &= \text{VAR}(\mathbf{p}, \text{VAR}(\mathbf{q}, \text{VAR}(\dots, \dots))), \\ \text{CHK}(\mathbf{p}, \mathbf{q}, \dots) &= \text{CHK}(\mathbf{p}, \text{CHK}(\mathbf{q}, \text{CHK}(\dots, \dots))), \end{aligned} \quad (2.17)$$

where \mathbf{p} and \mathbf{q} denote the corresponding input messages derived from variable nodes or check nodes. The functions of VAR and CHK at the nodes of degree three are illustrated in Fig. 2.9, and the circles and squares represent the variable nodes and check nodes respectively.

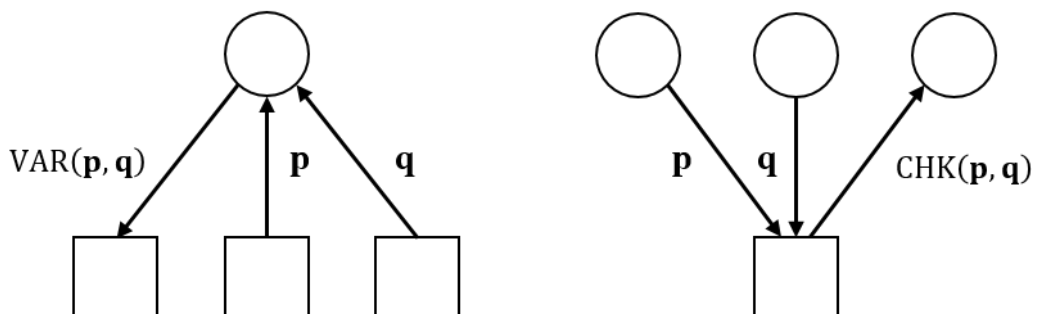


Figure 2.9: The message passing algorithm along the edges in factor graph.



Output Message of Variable Nodes

When the two input messages $\mathbf{p} = [p_0 \ p_1 \ p_2 \ p_3]$ and $\mathbf{q} = [q_0 \ q_1 \ q_2 \ q_3]$ arrive at the variable node $s(n)$, the probability that $s(n) = S[l]$ with $l \in \{0, 1, 2, 3\}$ is given by

$$\begin{aligned}\Pr\{s(n) = S[l]|\mathbf{p}, \mathbf{q}\} &= \frac{\Pr\{\mathbf{p}, \mathbf{q}|s(n) = S[l]\}\Pr\{s(n) = S[l]\}}{\Pr\{\mathbf{p}, \mathbf{q}\}} \\ &= \frac{\Pr\{s(n) = S[l]|\mathbf{p}\}\Pr\{s(n) = S[l]|\mathbf{q}\}\Pr\{\mathbf{p}\}\Pr\{\mathbf{q}\}}{\Pr\{\mathbf{p}, \mathbf{q}\}} \\ &= \beta p_l q_l,\end{aligned}\tag{2.18}$$

where

$$\beta = \frac{\Pr\{\mathbf{p}\}\Pr\{\mathbf{q}\}}{\Pr\{\mathbf{p}, \mathbf{q}\}} = \frac{1}{p_0 q_0 + p_1 q_1 + p_2 q_2 + p_3 q_3},\tag{2.19}$$

is a normalization factor. Therefore, the output message of variable node $s(n)$ is

$$\text{VAR}(\mathbf{p}, \mathbf{q}) = \beta [p_0 q_0 \ p_1 q_1 \ p_2 q_2 \ p_3 q_3].\tag{2.20}$$

Output Message of Check Nodes

A specific parity-check equation is satisfied if the \mathbb{F}_4 sum of the connected quaternary symbols in the corresponding Tanner graph is equal to zero, i.e., $s(n) \oplus s(n_1) \oplus s(n_2) = 0$. Assuming that the two input messages derived from the variable nodes $s(n_1)$ and $s(n_2)$ are $\mathbf{p} = [p_0 \ p_1 \ p_2 \ p_3]$ and $\mathbf{q} = [q_0 \ q_1 \ q_2 \ q_3]$, respectively. The probability that the parity-check equation is satisfied under the assumption



that $s(n) = S[0]$ is

$$\begin{aligned}
 \Pr\{s(n) = S[0]|\mathbf{p}, \mathbf{q}\} &= \Pr\{s(n_1) = S[0], s(n_2) = S[0]|\mathbf{p}, \mathbf{q}\} \\
 &\quad + \Pr\{s(n_1) = S[1], s(n_2) = S[1]|\mathbf{p}, \mathbf{q}\} \\
 &\quad + \Pr\{s(n_1) = S[2], s(n_2) = S[2]|\mathbf{p}, \mathbf{q}\} \\
 &\quad + \Pr\{s(n_1) = S[3], s(n_2) = S[3]|\mathbf{p}, \mathbf{q}\} \\
 &= p_0 q_0 + p_1 q_1 + p_2 q_2 + p_3 q_3. \tag{2.21}
 \end{aligned}$$

Similarly we can have

$$\begin{aligned}
 \Pr\{s(n) = S[1]|\mathbf{p}, \mathbf{q}\} &= p_0 q_1 + p_1 q_0 + p_2 q_3 + p_3 q_2, \\
 \Pr\{s(n) = S[2]|\mathbf{p}, \mathbf{q}\} &= p_0 q_2 + p_2 q_0 + p_1 q_3 + p_3 q_1, \\
 \Pr\{s(n) = S[3]|\mathbf{p}, \mathbf{q}\} &= p_0 q_3 + p_3 q_0 + p_1 q_2 + p_2 q_1. \tag{2.22}
 \end{aligned}$$

Finally, the message out of one check node equals

$$\text{CHK}(\mathbf{p}, \mathbf{q}) = \begin{bmatrix} p_0 q_0 + p_1 q_1 + p_2 q_2 + p_3 q_3 \\ p_0 q_1 + p_1 q_0 + p_2 q_3 + p_3 q_2 \\ p_0 q_2 + p_2 q_0 + p_1 q_3 + p_3 q_1 \\ p_0 q_3 + p_3 q_0 + p_1 q_2 + p_2 q_1 \end{bmatrix}^T. \tag{2.23}$$

Finalization and Symbol-to-Bit Mapping

The decoding algorithm is stopped if all parity-check equations are fulfilled or the maximum number of iterations is reached. Otherwise, the process proceed

with further iteration until one of the conditions is satisfied. At the end of the decoding algorithm, the G-SPA generates the APP vector $\mathbf{p} = [p_0 \ p_1 \ p_2 \ p_3]$ with $p_i = \Pr\{s(n) = S[l]|r\}$ for each symbol $s(n)$ with $n \in \{1, 2, \dots, N_c\}$ and the symbol-to-bit mapping is done by (2.6). The combination of multi-level detection and G-SPA is referred to as GDMA-JCD scheme in this thesis. The G-SPA with higher-order modulation scheme was investigated in [10].

Simulation Results

The block error rate (BLER) performances of GDMA-SCD scheme using a (256,128) rate-1/2 Polar code [11] over quasi-static Rayleigh flat-fading channels are provided in Fig. 2.10. The Polar code construction, a ranking algorithm to

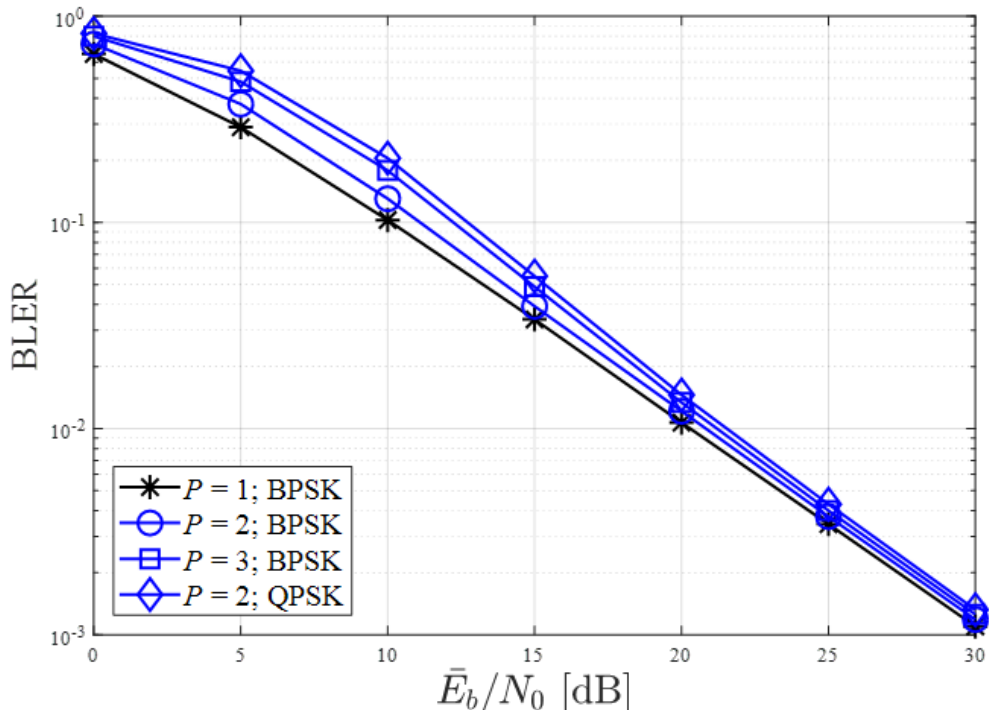


Figure 2.10: BLER performances of (256, 128) Polar-coded GDMA-SCD system over quasi-static Rayleigh flat-fading channels.

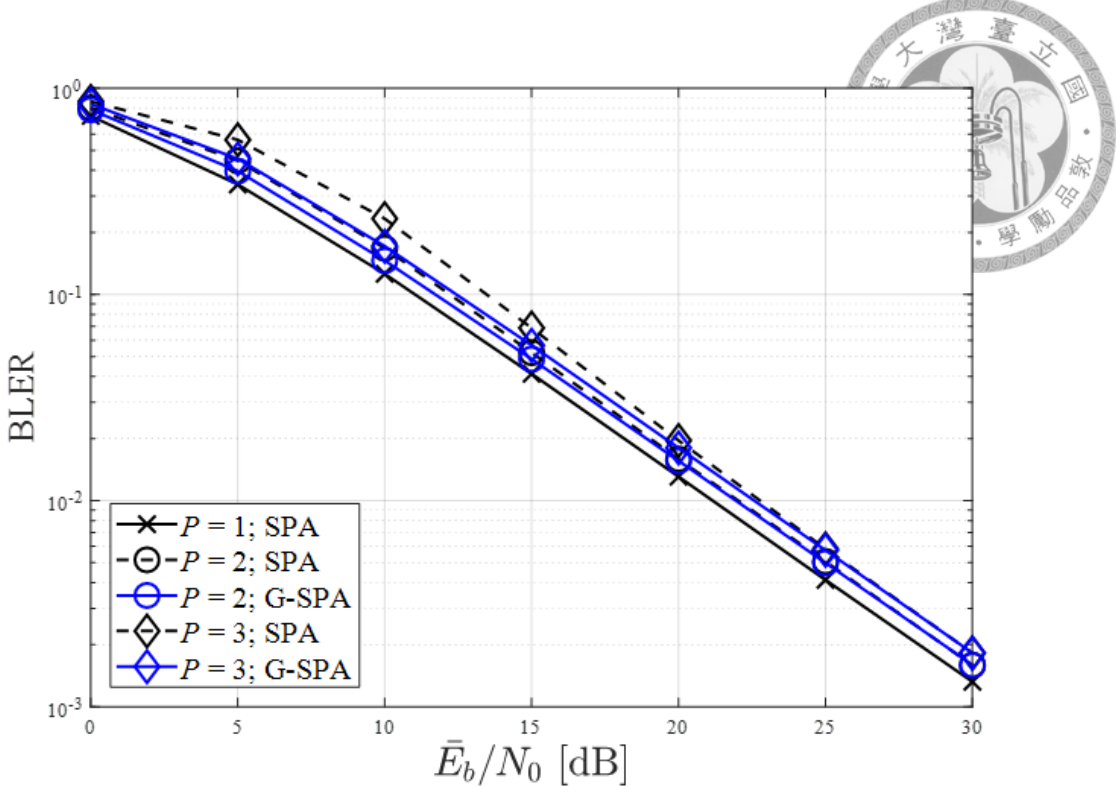


Figure 2.11: BLER performances of (1008, 504) LDPC-coded GDMA systems over quasi-static Rayleigh flat-fading channels.

distinguish the reliabilities of input bit-channels for the arrangement of message bits and frozen bits, employed here is the piecewise linear approximation proposed in [1]. The decoding algorithm is successive cancellation list (SCL) decoding [12] and list size is set to 32. In the case of $P = 2$ and QPSK transmission, bit-interleaving is applied to codeword bits after Polar encoding to overcome the effect of non-uniform reliabilities of output bit-channels. From the simulations shown in Fig. 2.10, one can see that the performance loss caused by increasing the number of users in GDMA system is narrower than that of the system without FEC coding as shown in Fig. 2.6 and 2.7.

The BLER performances of GDMA-JCD and GDMA-SCD systems using a (1008, 504) rate-1/2 binary (3,6)-regular LDPC code with BPSK transmissions over

quasi-static Rayleigh flat-fading channels are provided in Fig. 2.11. The maximum number of decoding iterations is set to 50 for both SPA and G-SPA. In the transmissions over block flat-fading channels, the GDMA-JCD scheme outperforms the GDMA-SCD scheme in low-SNR region and the performances of two schemes converge to each other in high-SNR region.



2.3.2 Throughput Performance of Rateless Coding

In [1], the average capacity of GDMA system over Rayleigh flat-fading channels in the case of $P = 2$ and BPSK transmission was derived. In this section, we simulate the throughput performances of GDMA system employing rateless codes. Fountain codes [13], originally proposed for the transmission over erasure channels, form a class of rateless codes. Luby Transform (LT) codes [14] are the first class of efficient Fountain codes and also a type of low-density generator matrix (LDGM) codes which can generate limitless number of codeword symbols with fixed number of message bits. To mitigate the error floor problem over noisy channels and also permit efficient encoding and decoding, an LT code is concatenated with an outer code to form a Raptor code [15]. In the outer code, called precode, a high-rate LDPC code is usually considered.

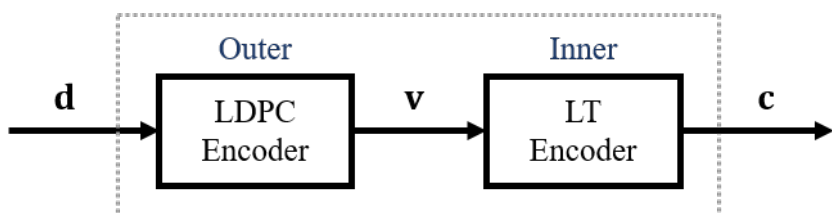


Figure 2.12: An encoder of a Raptor code.

Raptor codes can be specified by three parameters $(k, V, \Omega(x))$, where k is the input number of message bits, V is the precode with code length N_i and $\Omega(x)$ is the polynomial of output check node degree distribution. The degree distribution $\Omega(x)$ is in the form of $\Omega(x) = \sum_d \Omega_d x^d$ where Ω_d represents the probability that an output check node has degree d . An example of a Raptor code presented in Tanner graph is provided in Fig. 2.13, where m is an arbitrary code length and the connection of edges between intermediate check nodes and input nodes is defined by the parity-check matrix of LDPC code. Note that the codeword \mathbf{v} and \mathbf{c} in Fig. 2.12 are represented by input nodes and output nodes respectively. An important property is that universal Raptor codes do not exist on general binary memoryless symmetric (BMS) channels, and the degree distribution with the throughput close to the

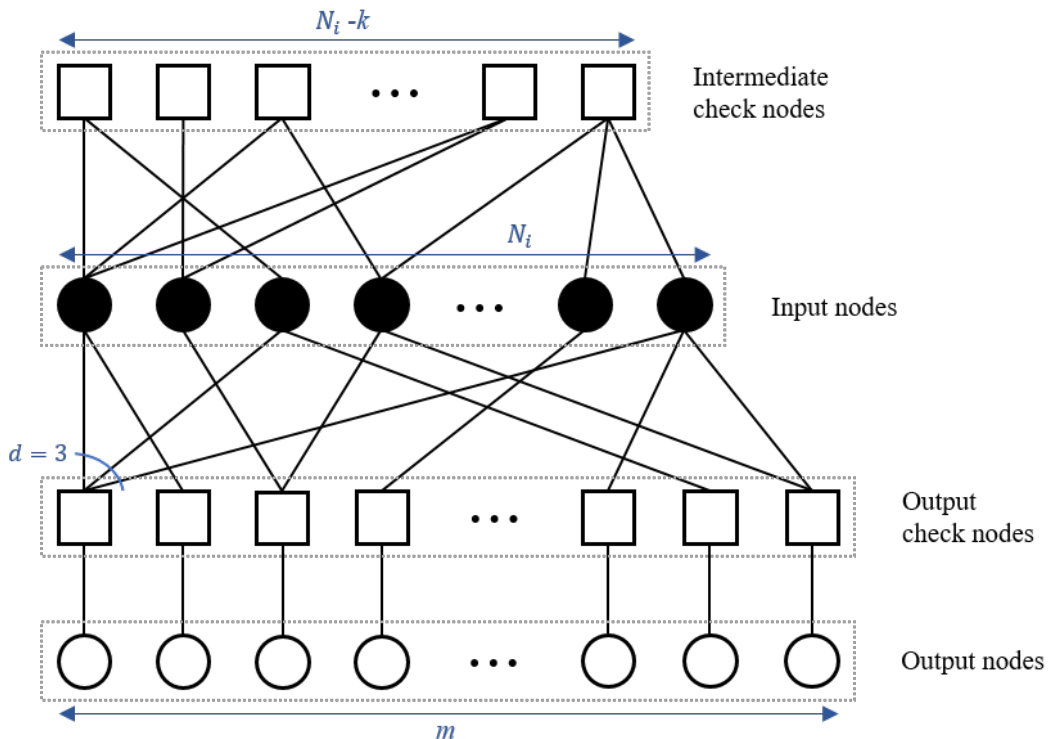


Figure 2.13: An example of a Raptor code represented in Tanner graph.

capacity can be specifically found for a designed SNR γ_d in AWGN channel.

In [16], a multi-edge representation of Raptor codes was investigated. The traditional design methods for Raptor codes are based on extrinsic information transfer (EXIT) chart analysis or Gaussian approximation, and the analyses are mainly focused on tandem decoding. In tandem decoding, the LT component is decoded first and the soft information is then sent to the LDPC component. However, the assumption of symmetric Gaussian distribution for the messages passed on the edges in the Tanner graph may not be accurate particularly at low rates and with punctured variable nodes, which is exactly the case for Raptor codes. Therefore, the multi-edge type density evolution (MET-DE) leads to better accuracy in the prediction of Raptor code ensemble compared to other approximate algorithms and the Raptor codes optimized in multi-edge framework result in good performances especially in low-SNR region. In addition, the Raptor codes can be specifically designed for joint decoding in multi-edge representation. In the joint decoding, one decoding iteration consists of L_{lt} decoding iterations on the LT code and L_{ldpc} decoding iterations on the LDPC code. It was shown in [16] that the joint decoding always gives better rate efficiency compared to the tandem decoding.

Here we consider the output check node degree distribution given in Table V of [16] in the simulations using non-systematic code. Besides, the adaptive Raptor code proposed in [17] is also considered in the simulations using systematic code. Adaptive Raptor codes consist of distinct degree distributions for distinct designed SNRs, and the distribution used in the encoding is dependent on the num-

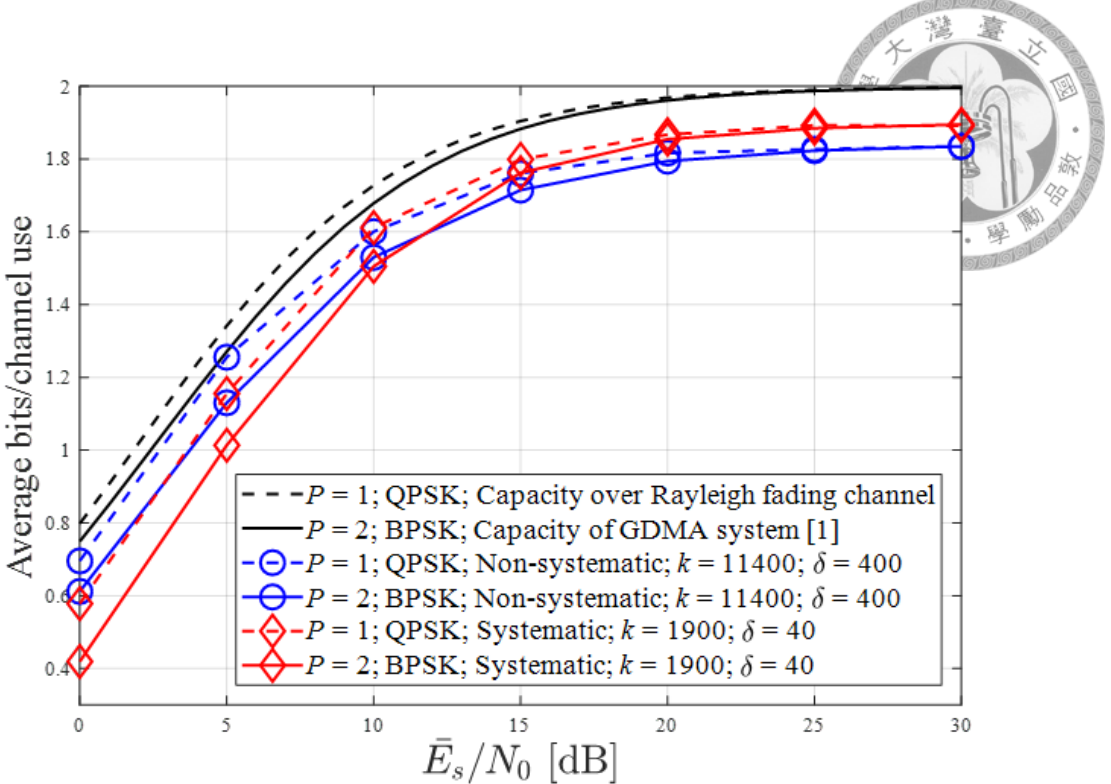


Figure 2.14: Throughput performances of Raptor-coded GDMA-SCD system over quasi-static Rayleigh flat-fading channels.

ber of output symbols. In Fig. 2.14, the throughput performances of Raptor-coded GDMA-SCD system over quasi-static Rayleigh flat-fading channels are provided. In simulations, the incremental redundancy hybrid automatic repeat-request (IR-HARQ) scheme is considered and the Raptor encoder continually sends codeword symbols until it receives the acknowledgement (ACK) sent from the receiver. In the first decoding attempt, the receiver decodes the received sequence after received N_i symbols. Except for the first attempt, the Raptor decoder collects another δ symbols if the decoding is not successful. The receiver checks for errors in the recovered message by checking if all the parity-check equations of the LDPC code are satisfied. The decoding scheme considered in simulations is the joint decoding with $L_{lt} = L_{ldpc} = 1$ and the maximum numbers of decoding iterations are set to

30 and 300 for systematic and non-systematic Raptor codes respectively. In the precode, rate-0.95 regular LDPC codes are considered. Moreover, we additionally put a constraint on the code rate of Raptor encoder during the transmission, which means that once the code rate k/m is less than 1/8, the block that is still not successfully decoded will be directly discard and zero throughput is then achieved instantaneously.

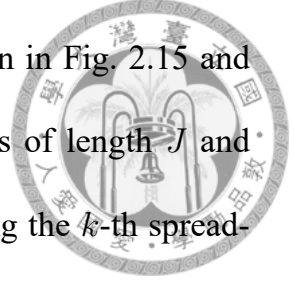


2.4 System Examples

The GDMA concept was introduced in previous sections, and the messages of multiple collided users can be recovered by using multi-level detection technique. In this section, we further apply the GDMA technique to other systems, including multi-carrier system and multi-antenna system, to see the contributions.

2.4.1 Multi-Carrier DS-CDMA

Recall that GDMA technique can be easily combined with other multiple access systems since the multi-level detection does not require additional user-specific resources. By assigning distinct spreading sequences to users, a direct-sequence code-division multiple access (DS-CDMA) system can accommodate multiple users in the same bandwidth. The combination of DS-CDMA scheme and multi-carrier transmission forms the system called multi-carrier DS-CDMA (MC-DS-CDMA) system. Here we further allow P users to occupy the same spreading sequence to construct the MC-DS-CDMA-GDMA system.



The transceiver of MC-DS-CDMA-GDMA system is shown in Fig. 2.15 and 2.16. Assuming that there are K distinct spreading sequences of length J and each of the sequences is shared by P users. The p -th user using the k -th spreading sequence is denoted as user- (k, p) and the total number of users in system is KP . The message bit sequence $\mathbf{d}_{k,p}$ of user- (k, p) , after FEC coding and modulation mapping with order m , is turned into the sequence of modulated symbols $\mathbf{x}_{k,p} = [x_{k,p}(1), x_{k,p}(2), \dots, x_{k,p}(N_c/m)]$ and then be processed in block-by-block manner with length Q for the orthogonal-frequency division multiplexing (OFDM) transmission. For $q \in \{1, 2, \dots, Q\}$, the modulated symbol $x_{k,p}(iQ+q)$ is spread by the sequence $\mathbf{s}_k = [s_k(1), s_k(2), \dots, s_k(J)]$ to obtain $\mathbf{X}_{k,p}^q(i) = x_{k,p}(iQ + q)\mathbf{s}_k = [X_{k,p}^q(i, 1), X_{k,p}^q(i, 2), \dots, X_{k,p}^q(i, J)]$, where $i \in \{1, 2, \dots, N/(mQ)\}$. For each i , the frequency domain signal $[X_{k,p}^1(i, j), X_{k,p}^2(i, j), \dots, X_{k,p}^Q(i, j)]$ is fed to the Q -point inverse fast Fourier transform (IFFT) to get the time domain signal where $j \in \{1, 2, \dots, J\}$. The cyclic prefix (CP) is inserted and the number of symbols in CP is equal to channel order to avoid inter-symbol interference (ISI) and inter-carrier interference (ICI).

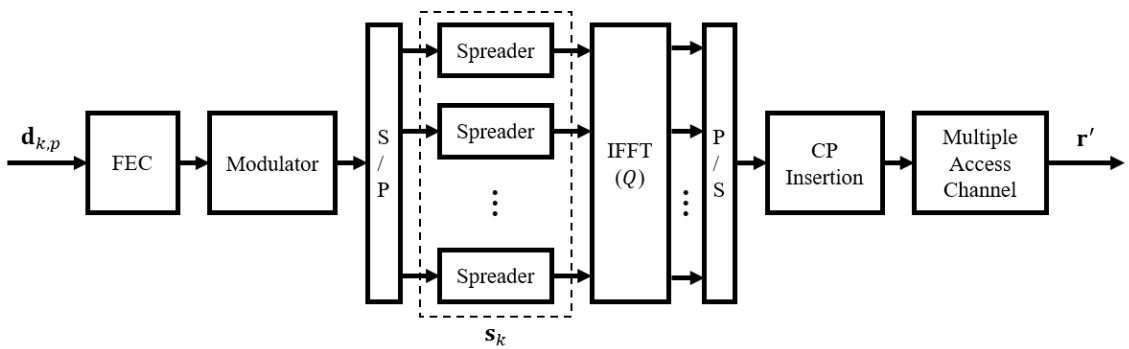


Figure 2.15: Transmitter of user- (k, p) in MC-DS-CDMA-GDMA system.

At the receiver side, after CP removal and the Q -point FFT, the frequency domain received signal propagated through the q -th sub-channel can be represented as $\mathbf{R}^q(i) = [R^q(i, 1), R^q(i, 2), \dots, R^q(i, J)]$ and

$$R^q(i, j) = \sum_{k=1}^K \sum_{p=1}^P H_{k,p}^q X_{k,p}^q(i, j) + W(i, j), \quad (2.24)$$

where $H_{k,p}^q$ is the channel coefficient of user- (k, p) on the q -th sub-channel in the frequency domain and $W(i, j)$ is the complex AWGN. The sequence $\mathbf{R}^q(i)$ of length J is then despread for each i and the signal after passing through the k -th correlator is obtained as

$$R_k^q(i) = \frac{1}{J} \sum_{j=1}^J R^q(i, j) s_k(j). \quad (2.25)$$

Here we employ the Hadamard code as spreading sequences. When the chips are perfectly aligned, the Hadamard sequences are orthogonal to each others. Therefore, the interferences from the signals spread by different spreading sequences can be totally eliminated due to the orthogonality. The signal after passing through the

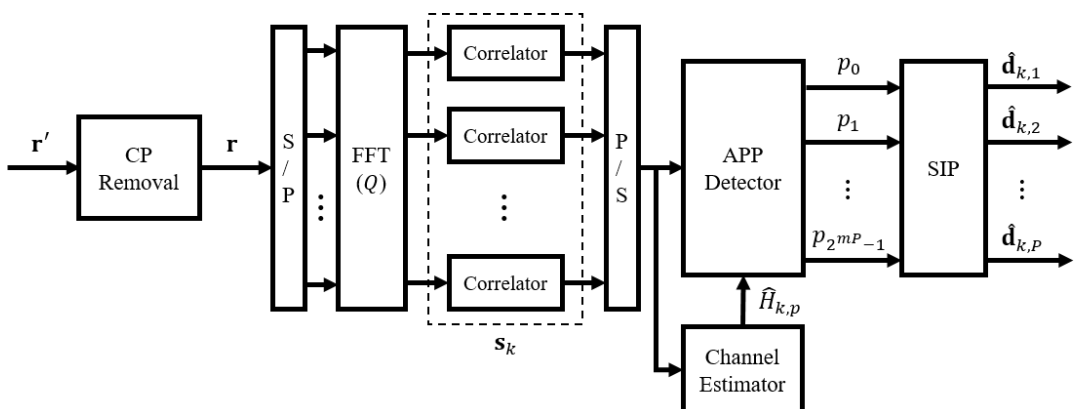


Figure 2.16: Multi-level receiver in MC-DS-CDMA-GDMA system for recovering the signals using the k -th spreader.

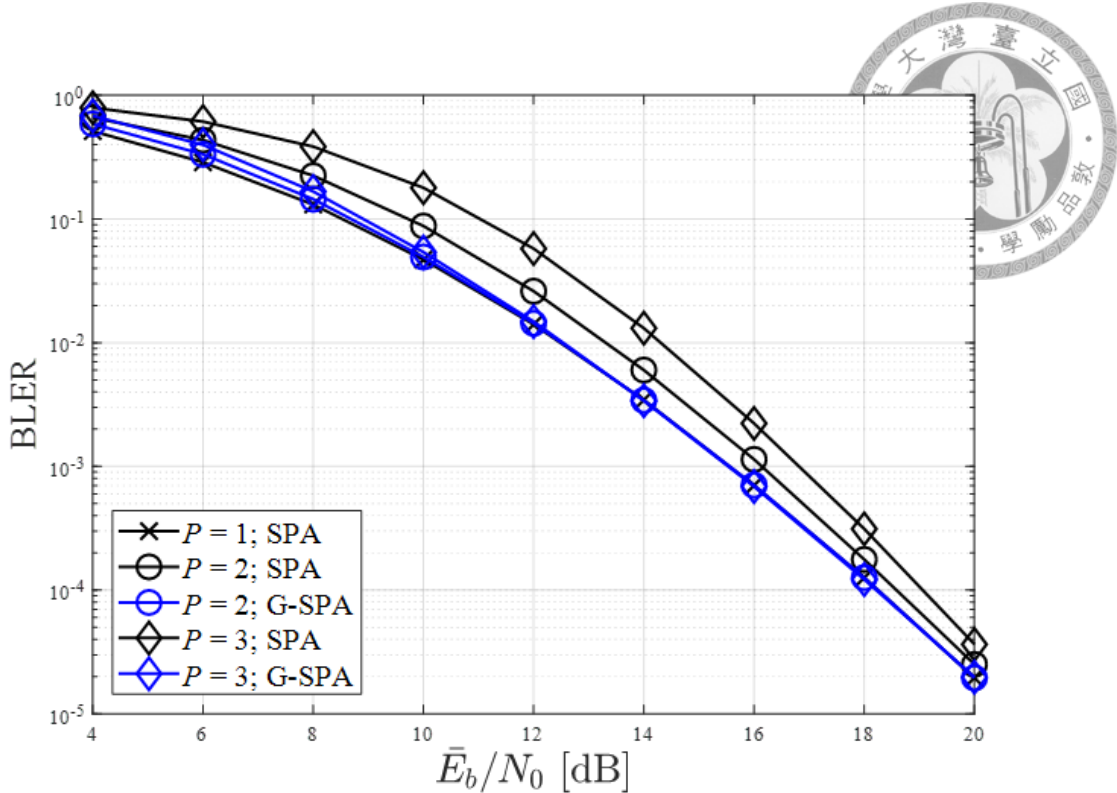


Figure 2.17: BLER performances of (1008,504) LDPC-coded MC-DS-CDMA-GDMA system over quasi-static frequency-selective Rayleigh fading channels.

k -th correlator when Hadamard sequences are employed can be written as

$$\begin{aligned}
 R_k^q(i) &= \frac{1}{J} \sum_{j=1}^J R^q(i, j) s_k(j) \\
 &= \sum_{p=1}^P H_{k,p}^q x_{k,p}(iQ + q) + \frac{1}{J} \sum_{j=1}^J W(i, j),
 \end{aligned} \tag{2.26}$$

where the despread signal consist of the channel noise and the signals transmitted from P users sharing the same spreading sequence, and the messages of P users can be recovered by using the multi-level detection technique. Because of the orthogonality of Hadamard sequences, the MC-DS-CDMA-GDMA system can be seen as an OFDM-GDMA system with P users occupying the same time-frequency resources when the chip timings are perfectly aligned.

The BLER performances of MC-DS-CDMA-GDMA system are provided in Fig. 2.17. A (3,6)-regular (1008,504) LDPC code with 100 maximum decoding iterations is used. The signals are propagated through independent five-tap Rayleigh fading channels with exponentially decayed power in taps. When the Hadamard code is employed, where $K = J = Q = 16$ in simulations, it is interesting to see that the BLER performances of $P = 2$ and $P = 3$ cases are converge to that of $P = 1$ case. In the transmissions of OFDM-GDMA-JCD system over frequency selective channels, we can make the number of active users in a multiple access system become P times greater than that of it originally have without performance degradation.

2.4.2 Alamouti Space-Time Scheme

The Alamouti scheme [18] is the first space-time block code to provide full transmit diversity. Here we allow P users to transmit signals simultaneously with the same Alamouti code to form the space-time coded GDMA (STC-GDMA) system. The receiver has one antenna and each of the transmitters has two antennas. The block diagrams of STC-GDMA transceiver are shown in Fig. 2.18 and 2.19.

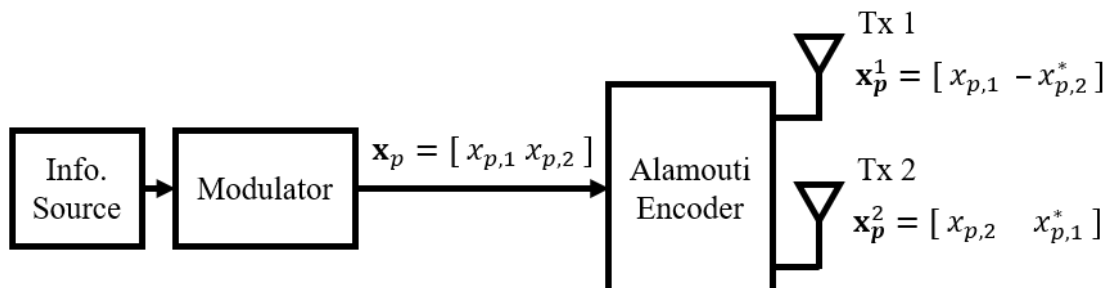


Figure 2.18: Alamouti space-time transmitter of user- p .

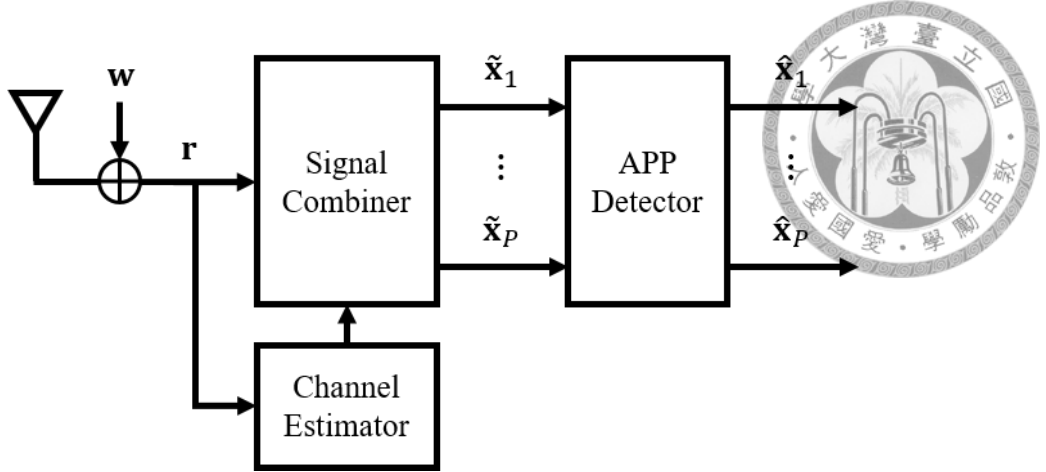


Figure 2.19: Multi-level receiver in STC-GDMA system for recovering the messages of P users.

Assuming that there are $P = 2$ users in system and the signals transmitted from different users collide in the same resource. The received signals $\mathbf{r} = [r_1, r_2]$ in two consecutive symbol intervals are

$$\begin{aligned} r_1 &= h_{A,1}x_{A,1} + h_{A,2}x_{A,2} + h_{B,1}x_{B,1} + h_{B,2}x_{B,2} + w_1, \\ r_2 &= h_{A,2}x_{A,1}^* + h_{A,1}x_{A,2}^* + h_{B,2}x_{B,1}^* + h_{B,1}x_{B,2}^* + w_2. \end{aligned} \quad (2.27)$$

Let $\{h_{A,1}, h_{A,2}\}$ and $\{h_{B,1}, h_{B,2}\}$ be the channel coefficients of user-A and user-B from the first and second transmit antennas to the receive antenna, respectively. If the channel coefficients can be perfectly recovered at the receiver, the signal combiner can further exploit the orthogonality of the transmitted sequences from the two transmit antennas. However, the orthogonality is only available for the symbols transmitted from the same user and hence the interferences from different users cannot be eliminated. In the situation that P users collide together in the same resource of STC system, we can use the multi-level detection technique as a solution to recover the messages.

The noise-free case is considered for brevity in illustration. By using the channel coefficients of user-A $\{h_{A,1}, h_{A,2}\}$ as the channel state information (CSI), the output decision statistics $\tilde{\mathbf{x}}_A = [\tilde{x}_{A,1}, \tilde{x}_{A,2}]$ of the signal combiner can be written as

$$\begin{aligned}
\tilde{x}_{A,1} &= h_{A,1}^* r_1 + h_{A,2} r_2^* \\
&= (|h_{A,1}|^2 + |h_{A,2}|^2) x_{A,1} \\
&\quad + (h_{A,1}^* h_{B,1} + h_{A,2} h_{B,2}^*) x_{B,1} + (h_{A,1}^* h_{B,2} - h_{A,2} h_{B,1}^*) x_{B,2}, \\
\tilde{x}_{A,2} &= h_{A,2}^* r_1 - h_{A,1} r_2^* \\
&= (|h_{A,1}|^2 + |h_{A,2}|^2) x_{A,2} \\
&\quad + (h_{A,2}^* h_{B,1} - h_{A,1} h_{B,2}^*) x_{B,1} + (h_{A,2}^* h_{B,2} + h_{A,1} h_{B,1}^*) x_{B,2}. \tag{2.28}
\end{aligned}$$

Similarly, by using the channel coefficients of user-B $\{h_{B,1}, h_{B,2}\}$ as the CSI, the output decision statistics $\tilde{\mathbf{x}}_B = [\tilde{x}_{B,1}, \tilde{x}_{B,2}]$ of the signal combiner can be written as

$$\begin{aligned}
\tilde{x}_{B,1} &= h_{B,1}^* r_1 + h_{B,2} r_2^* \\
&= (|h_{B,1}|^2 + |h_{B,2}|^2) x_{B,1} \\
&\quad + (h_{B,1}^* h_{A,1} + h_{B,2} h_{A,2}^*) x_{A,1} + (h_{B,1}^* h_{A,2} - h_{B,2} h_{A,1}^*) x_{A,2}, \\
\tilde{x}_{B,2} &= h_{B,2}^* r_1 - h_{B,1} r_2^* \\
&= (|h_{B,1}|^2 + |h_{B,2}|^2) x_{B,2} \\
&\quad + (h_{B,2}^* h_{A,1} - h_{B,1} h_{A,2}^*) x_{A,1} + (h_{B,2}^* h_{A,2} + h_{B,1} h_{A,1}^*) x_{A,2}. \tag{2.29}
\end{aligned}$$

There are four decision statistics, $\tilde{x}_{A,1}$, $\tilde{x}_{A,2}$, $\tilde{x}_{B,1}$ and $\tilde{x}_{B,2}$, and each can be seen as an eight-level superimposed signal if the signals are BPSK-modulated. The decision

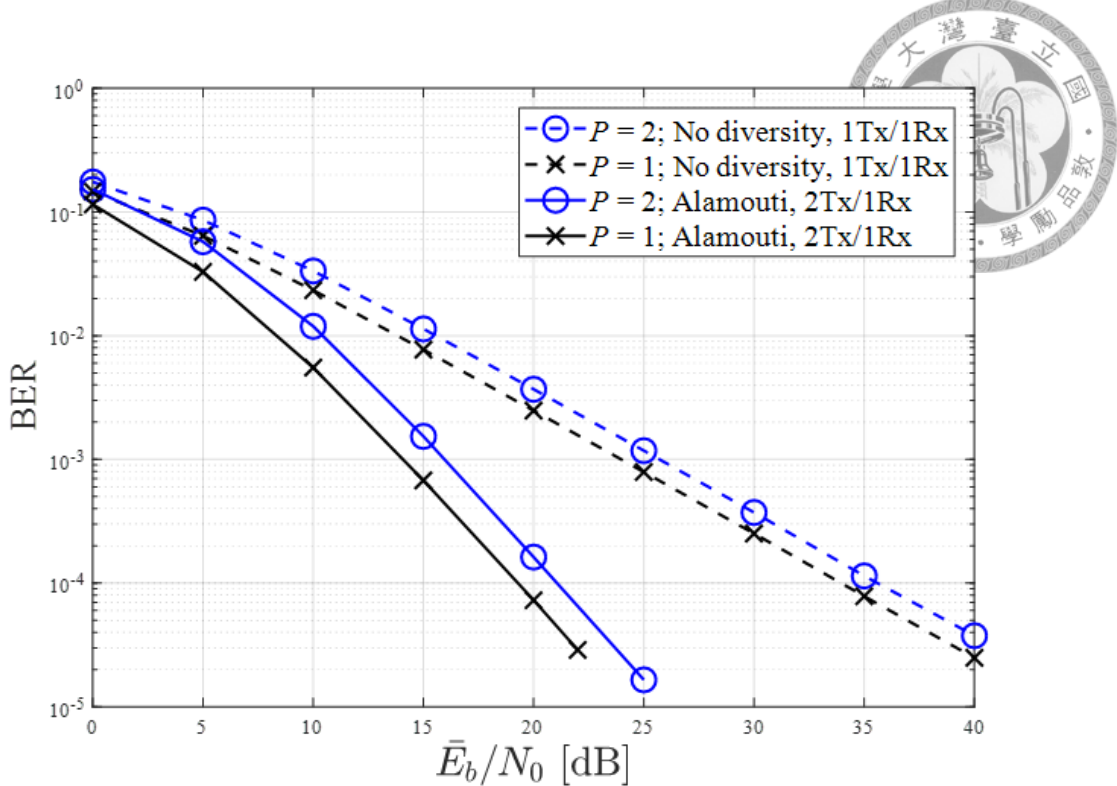


Figure 2.20: BER performances of STC-GDMA system over quasi-static Rayleigh flat-fading channels.

statistics can be further detected by using the multi-level detection as long as the CSI is available at the receiver. For example, the decision statistic $\tilde{x}_{A,1}$ can be formulated as $\tilde{x}_{A,1} = h'_1 x_{A,1} + h'_2 x_{B,1} + h'_3 x_{B,2}$, where h'_i with $i \in \{1, 2, 3\}$ is the equivalent channel coefficients, and the bit LLRs of $x_{A,1}$, $x_{B,1}$ and $x_{B,2}$ can then be derived from (2.7) with the observation of $\tilde{x}_{A,1}$. Similarly, the multi-level detection can be applied to each of the decision statistics to attain the LLRs of message bits. The BER performances of the STC-GDMA system are shown in Fig. 2.20 and the cost of increasing the number of users from $P = 1$ to $P = 2$ is the increase of required SNR by 2 dB.



Chapter 3

Cluster-Based Channel Estimation

In Chapter 2, we reviewed the concept of GDMA technique. When the transmissions of multiple users are over independent fading channels, the signals can be further separated by exploiting the distinct channel coefficients without requiring user-specific resources. The requirement for applying multi-level detection in GDMA system is that the channel coefficients need to be recovered accurately at the receiver to construct all the possible levels of superimposed signal. Because of the existence of channel noise, received signals within a block that the channel re-

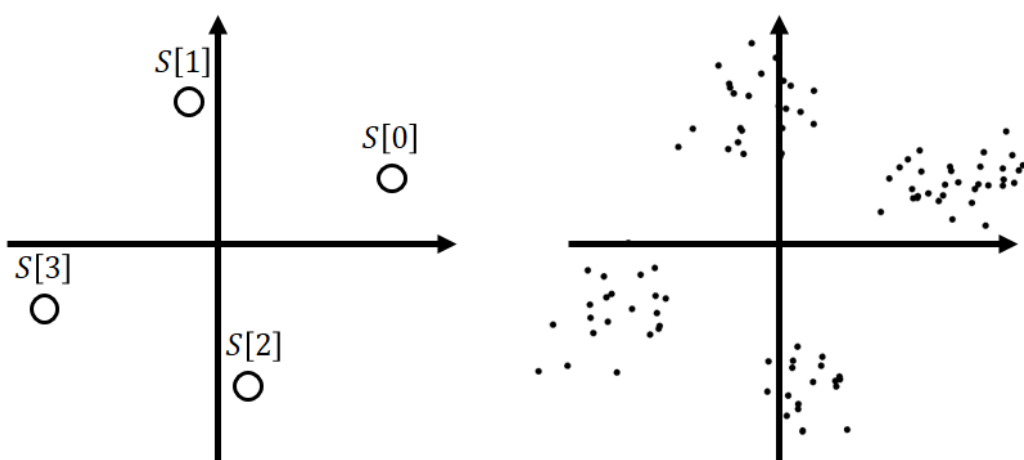


Figure 3.1: Superimposed levels and the corresponding received signals in the case of $m = 1$ and $P = 2$.

mains unchanged are two-dimensional Gaussian distributed with mean $S[l]$ where $l \in \{0, 1, \dots, 2^{mP} - 1\}$ according to the messages of P users.



If we can somehow classify the received symbols into 2^{mP} groups, where the symbols corresponding to the same superimposed level are grouped together, the estimates of the levels can be attained through the average of the symbols in each group. In this chapter, we assume that the fading coefficients are constant across a block of N_t consecutive symbols. An example of the received signals with $N_t = 100$ in the case of $m = 1$ and $P = 2$ is shown in Fig. 3.1. Therefore, we utilize the clustering algorithm to classify the received symbols and blindly estimate the channel coefficients of P users. Clustering is an unsupervised learning technique that involves the grouping of training samples and, ideally, the samples in the same group have similar features, whereas the samples in different groups have dissimilar features. Note that the clustering technique in the proposed scheme takes the signals carrying messages as the input training samples and thus high spectral efficiency, along with an inevitable ambiguity in estimate, can be attained since the estimation does not require additional pilot signal. In [19], the clustering algorithm was employed to estimate the unknown initial phase in the transmission of angle differential quadrature amplitude modulation (ADQAM) system.

3.1 K-Means Algorithm

One of the most popular clustering techniques is k-means algorithm [3] which aims to minimize the sum of squared distances between each sample and its closest

centroid. In k-means problem, it is desirable to choose a set of centroids S such that the following function can be minimized.

$$\phi = \sum_{x \in X} \min_{s \in S} \|x - s\|^2, \quad (3.1)$$

where X is the set of training vectors and ϕ is the corresponding distortion. Therefore, k-means algorithm classify the samples into groups by iteratively pairing up each sample with closest centroid and then updating the centroids from the newly derived groups.

For the purpose of channel estimation in GDMA system, all the levels should be distinguished and thus the number of groups to be classified is set to 2^{mP} in the clustering. The steps of k-means algorithm are organized as follows.

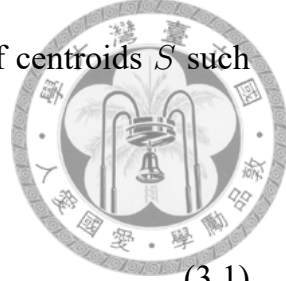
Step 1) Randomly pick the initial centroids from the symbols in received sequence.

Step 2) Classify the received symbols into 2^{mP} groups by applying the nearest-neighbour rule with respect to the current centroids.

Step 3) Recompute the centroids by averaging the symbols in each group.

Step 4) Return to Step 2 until the centroids no longer change.

The required number of iterations for clustering algorithms cannot be predicted ahead of time. In addition, the random seeding in the initial step of k-means may yield different grouping results in different runs of the algorithm. An example of k-means clustering is provided in Fig. 3.2 and the algorithm is terminated after



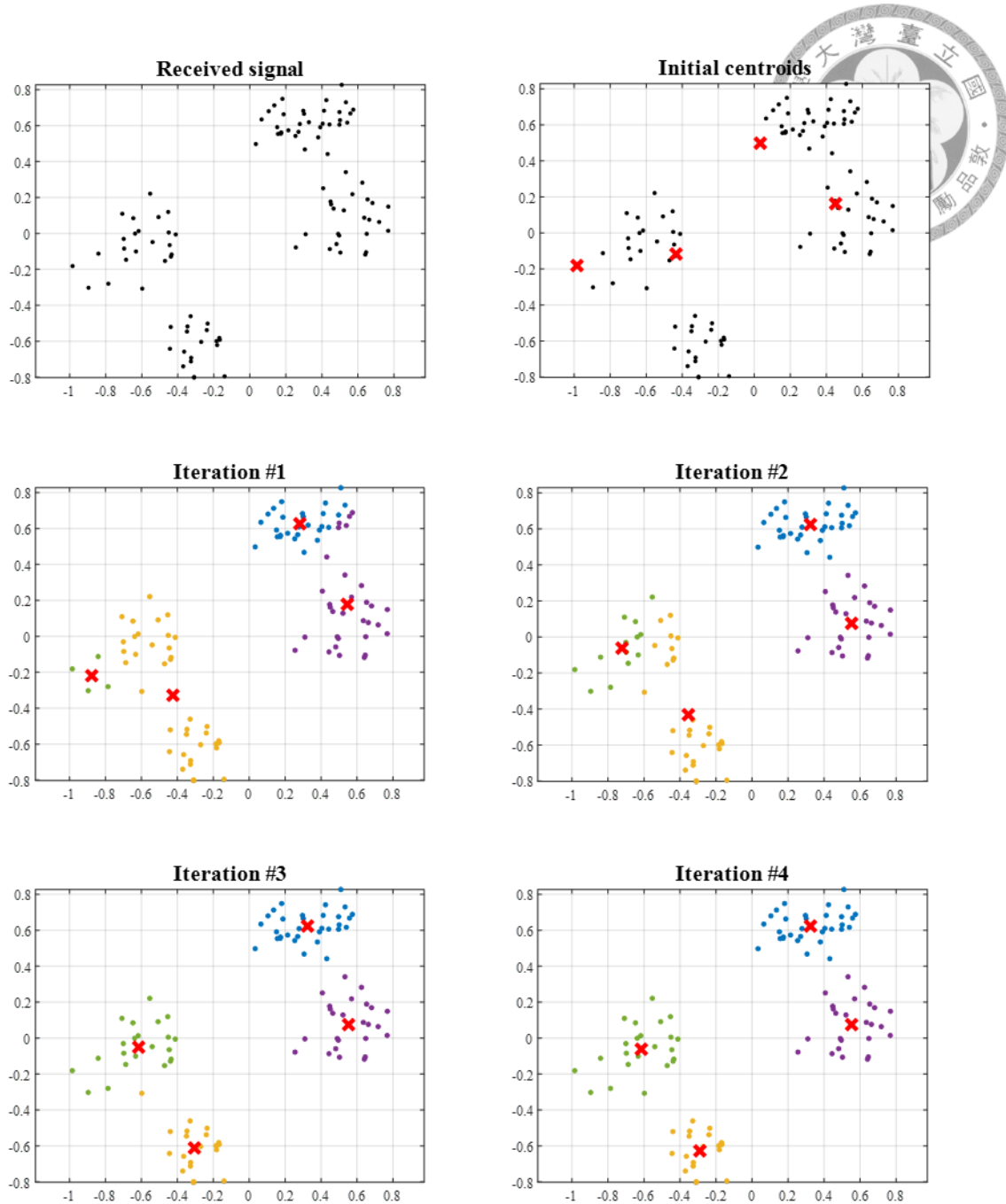


Figure 3.2: An example of k-means algorithm and the resultant centroids.

the forth iteration. The four different colors in Fig. 3.2 represent the samples in different groups.

In the k-means algorithm, the most crucial task is to select an acceptable initial centroids in the neighbourhood of the correct solution since it can only find local

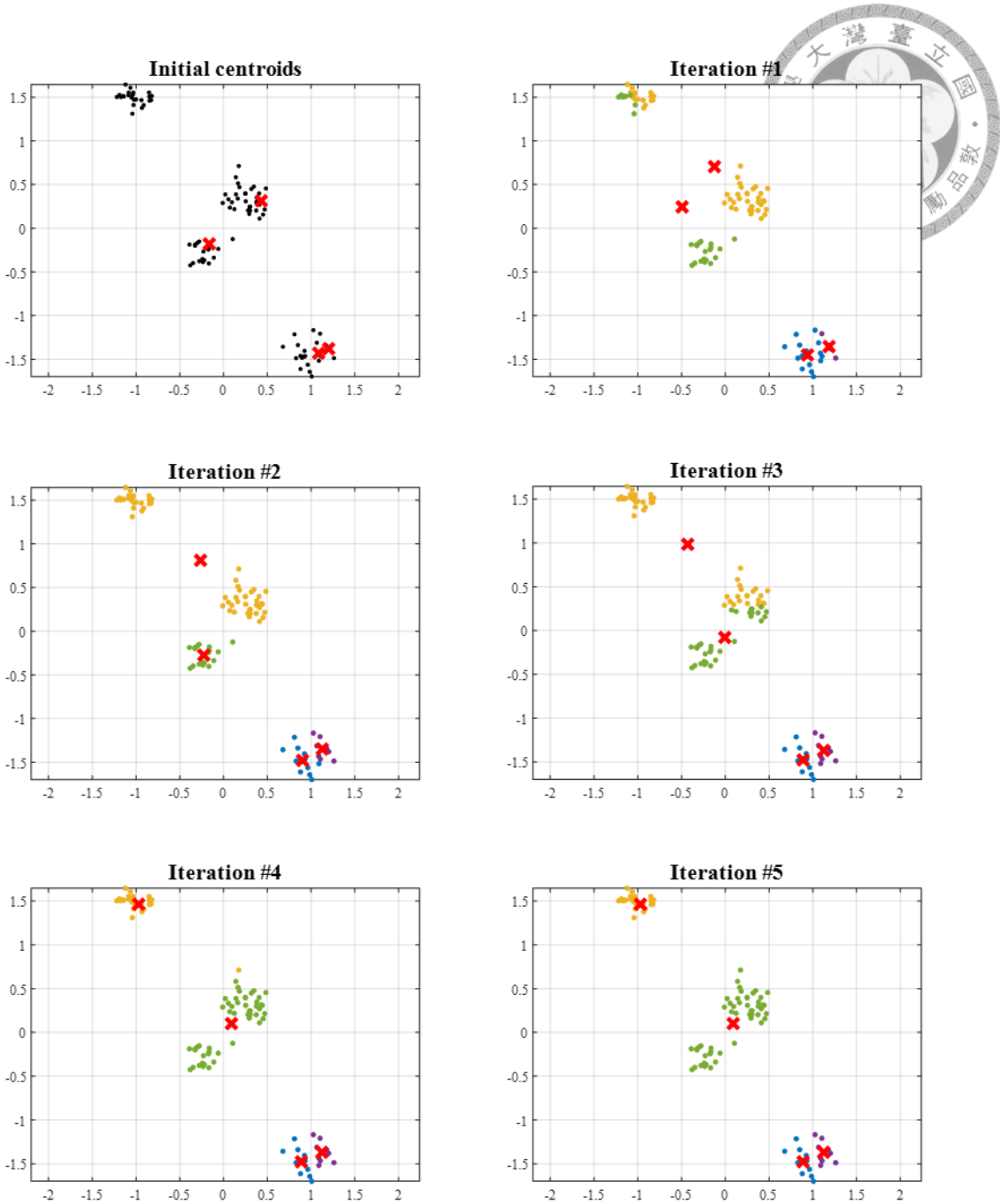
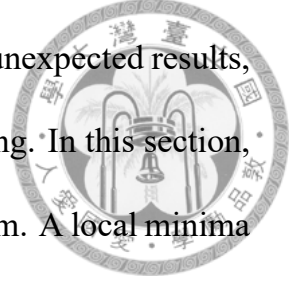


Figure 3.3: A local minima found by k-means algorithm.

minimum. However, the constellations of transmitted signals in consideration are symmetric, and thus we can detect the case of local minimum by checking whether the average of the resultant centroids is significantly deviated from the origin and repeat the algorithm with different initial seeding until the symmetric condition is

satisfied. Although we have the protective mechanism to avoid unexpected results, the latency caused by the ad-hoc methodology is still unsatisfying. In this section, we consider some of the improved methods for k-means algorithm. A local minima found by k-means is provided in Fig. 3.3.



3.1.1 The LBG Algorithm

The Linde – Buzo – Gray (LBG) algorithm [4], sometimes referred to as generalized Lloyd algorithm (GLA), is a technique to design vector quantizer and a so-called "splitting" method is employed to select the initial centroids for the following k-means clustering. The steps of LBG algorithm are organized as follows.

Step 1) Split the origin into two close points ϵ and $-\epsilon$ and hence the set of initial centroids $S = \{\epsilon, -\epsilon\}$ with size $M = 2$ is obtained.

Step 2) Classify the received symbols into M groups, based on the current centroids S , by applying the nearest-neighbor rule and compute the centroid ρ_i of each group with $i \in \{1, 2, \dots, M\}$.

Step 3) Split ρ_i into two close points $q_{2i-1} = \rho_i + \epsilon$ and $q_{2i} = \rho_i - \epsilon$ with $i \in \{1, 2, \dots, M\}$ and the set of new centroids $S = \{q_i | i = 1, 2, \dots, 2M\}$ is obtained.

Step 4) Replace M by $2M$ and return to Step 2 until $M = 2^{mP}$.

Step 5) Proceed with the standard k-means clustering.

An example of the quantization region designed by the LBG algorithm is provided

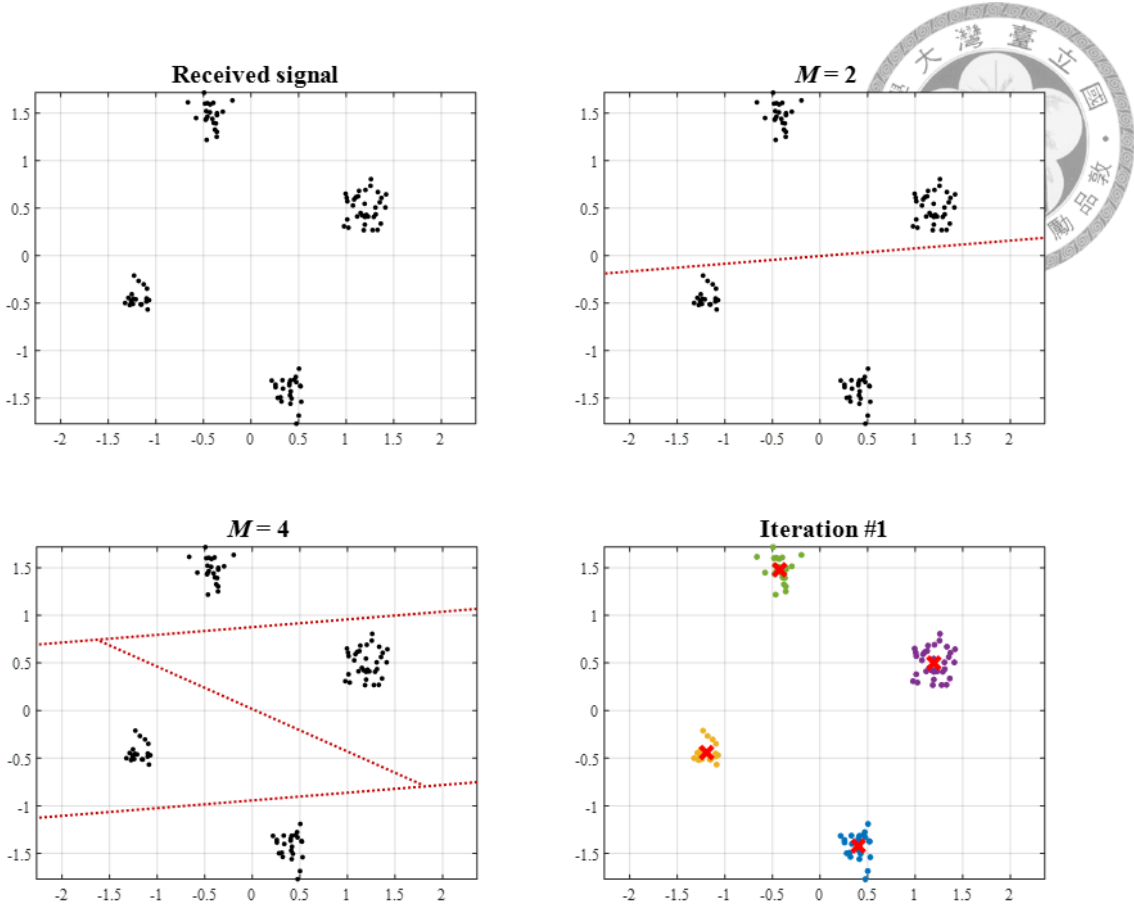


Figure 3.4: An example of the quantization region designed by the LBG algorithm.

in Fig. 3.4, where the samples are divided into $M = 4$ partitions for the following clustering and only one iteration is needed to finish the k-means algorithm. In the LBG algorithm, a fixed perturbation vector ϵ with an ultimately small distance from the origin needs to be determined at first. An example of splitting is provided in Fig. 3.5 where θ_s is a uniformly distributed random variable in $(0, 2\pi]$ and is determined in each run of the algorithm.

If the symmetric condition is not fulfilled, the LBG algorithm is repeated with another splitting direction to avoid the case of local minima. However, the point to be split is derived by averaging the samples in each group as shown in Step 3 and thus the LBG algorithm is highly dependent on the accuracy of training samples.

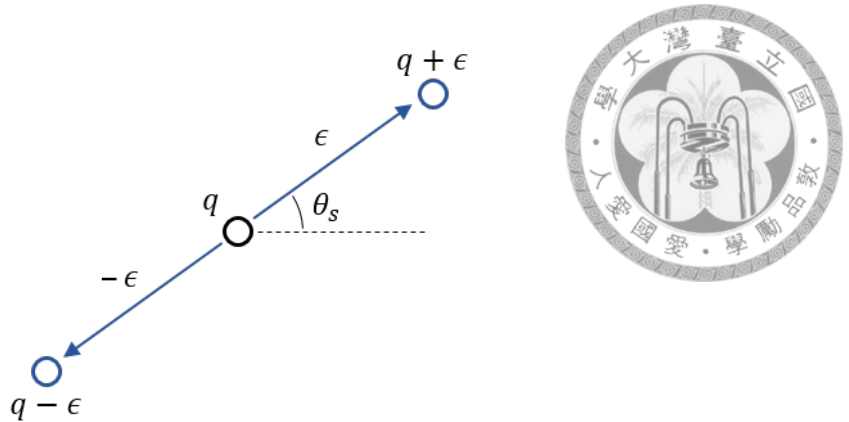


Figure 3.5: Splitting from q to get $q + \epsilon$ and $q - \epsilon$ with a perturbation vector ϵ .

In Fig. 3.6, an example is provided for the case that the resultant centroids found by the LBG algorithm is stuck into the local minima regardless of the selection of

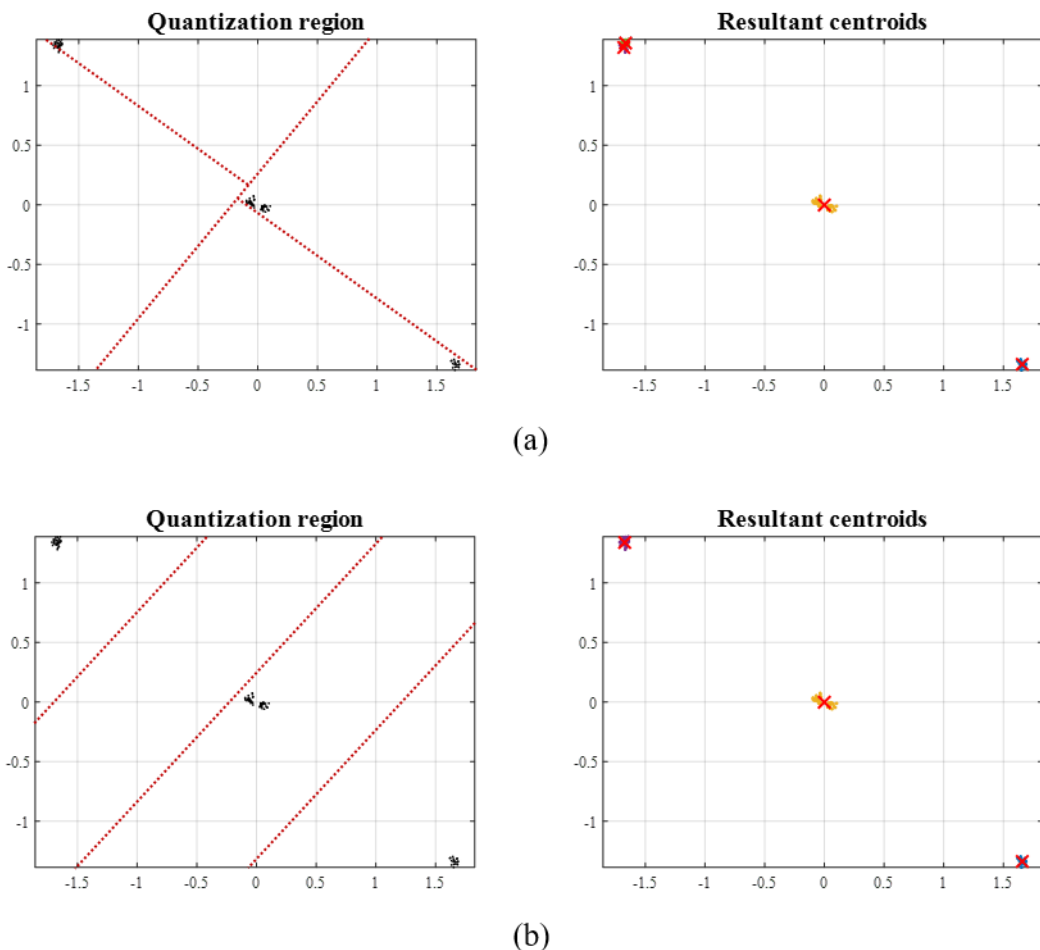


Figure 3.6: An example of local minimums found by the LBG algorithm

θ_s in perturbation vector ϵ , and Fig. 3.6(a) and Fig. 3.6(b) present the two different quantization regions designed by the LBG algorithm with the same set of training samples. Moreover, the LBG algorithm is more likely to have local minimum as a solution when the SNR is higher. The situation shown in Fig. 3.6 makes the LBG algorithm unreliable to the following estimation and also wastes the effort in the process. When the clustering algorithm needs to be restarted for another trial, it is preferred to select the initial centroids as random as possible.

3.1.2 K-Means++ Algorithm

The k-means++ algorithm was proposed in [5] to choose the initial centroids for the following k-means clustering, which can be seen as a generalization of standard k-means algorithm. The concept of k-means++ algorithm is to randomly select the initial centroids as sparse as possible. Note that the randomness is reserved in the initialization and thus k-means++ might not be as dependent on the accuracy of training samples as the LBG algorithm. Let $D(r)$ denote the distance from a received symbol r to the closest centroid we have already chosen. The steps of k-means++ algorithm are organized as follows.

Step 1) Pick the first centroid q_1 uniformly at random from the symbols in received sequence and set $i = 1$.

Step 2) Pick the next centroid q_{i+1} from the remaining symbols with probability proportional to $D^2(r)$ and replace i by $i + 1$.

Step 3) Return to Step 2 until $i = 2^{mP}$.

Step 4) Proceed with the standard k-means clustering.



The k-means++ outperforms the standard k-means in terms of accuracy and convergence speed. Moreover, the situation that the initialization always leads to local minimum as shown in Fig. 3.6 will not happen with k means++ due to the randomness in the selection of initial centroids with weighted probabilities.

Since the number of iterations for clustering cannot be predicted ahead of time, the required number of iterations for each algorithm is simulated in Table 3.1 and 3.2 to evaluate the time complexity. Recall that the algorithm is repeated until the final centroids meet the symmetric condition, and thus the iterations of each retrial will be accumulated. From the simulations, one can observe that both the LBG algorithm and k-means++ algorithm can achieve better convergence speed compared to the standard k-means algorithm using random seeding.

Table 3.1: Average numbers of iterations for different algorithms where $N_t = 100$ and $\bar{E}_b/N_0 = 5$ dB.

	K-means	LBG	K-means++
BPSK/ $P = 1$	71.48	61.68	65.17
BPSK/ $P = 2$	113.70	93.71	96.09
4-PAM/ $P = 2$	95.76	58.73	59.42

Table 3.2: Average numbers of iterations for different algorithms where $N_t = 100$ and $\bar{E}_b/N_0 = 20$ dB.

	K-means	LBG	K-means++
BPSK/ $P = 1$	2.62	2.25	2.12
BPSK/ $P = 2$	9.25	2.92	2.75
4-PAM/ $P = 2$	95.80	29.28	10.58



3.1.3 Gaussian Mixture Model

Clustering techniques can be categorized into two types: soft clustering and hard clustering. In hard clustering, each sample is assigned to exactly one group by applying nearest neighbor rule. However, when the samples produced from different sources are highly overlapped, it is hard to tell which group the sample belongs to in overlapped area. In Fig. 3.7, there are two sources producing samples with two-dimensional Gaussian distribution and the means are denoted as red dots. The red crosses are the resultant centroids, and the colors indicate the groups classified by hard clustering in Fig. 3.7. In fact, the samples in Fig. 3.7 are the received symbols in BPSK-modulated transmission of $P = 1$ user, and the SNR is relatively low such that the disturbance of channel noise makes the two levels hard to be distinguished and also decrease the accuracy in the estimation.

One of the solutions to overcome the problem of overlapped sources is soft clustering, which classify samples in the probability domain. In soft clustering, each sample can simultaneously belong to multiple groups but with different levels

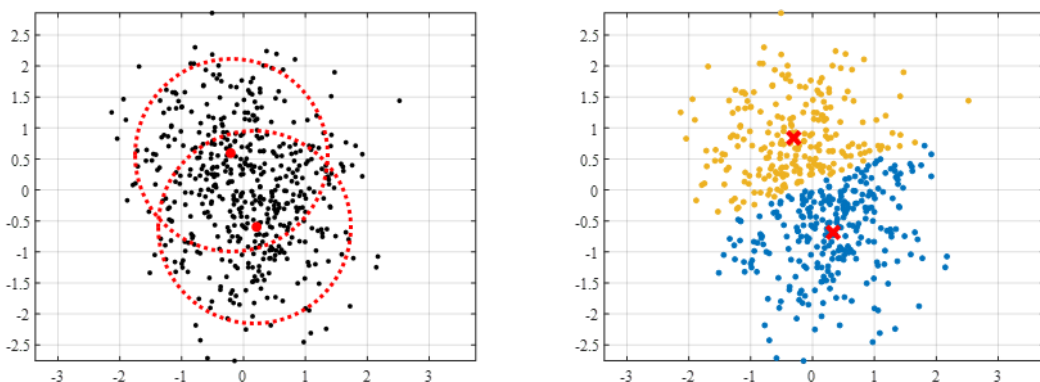


Figure 3.7: Grouping result of hard clustering by applying nearest neighbor rule.

of belief and thus the sources may overlap with each others. Gaussian mixture model (GMM) is a way to implement soft clustering and it assumes that the samples produced from different sources are Gaussian distributed with different parameters, i.e., means and covariances. Therefore, the problem of clustering is converted into the optimization of parameters for Gaussian components in GMM.

The expectation-maximization (EM) algorithm [6] is usually used to discover the parameters of Gaussian components in GMM. Following we give an example in Fig. 3.8 to illustrate the EM algorithm. Assuming that there are two one-dimensional sources, denoted as source-A and source-B, with parameters (μ_A, σ_A^2) and (μ_B, σ_B^2) as means and variances respectively, and the samples produced from different sources are distinguished by different colors as shown in Fig. 3.8(a). Note that the distributions of the samples from different sources are arbitrary. If we have the estimates of parameters $(\tilde{\mu}_A, \tilde{\sigma}_A^2)$ and $(\tilde{\mu}_B, \tilde{\sigma}_B^2)$ for the distributions of two sources but the assignments of samples are unknown as shown in Fig. 3.8(b), we can guess whether the sample is more likely to be source-A or source-B. The probability that sample x_i belongs to source-A is

$$\Pr(A|x_i) = \frac{f(x_i|A)\Pr(A)}{f(x_i|A)\Pr(A) + f(x_i|B)\Pr(B)}, \quad (3.2)$$

where $\Pr(A)$ is the occurrence probability of source-A. In GMM, the sources are assumed to be Gaussian distributed and thus

$$f(x_i|A) = \frac{1}{\sqrt{2\pi\tilde{\sigma}_A^2}} \exp\left(-\frac{(x_i - \tilde{\mu}_A)^2}{2\tilde{\sigma}_A^2}\right). \quad (3.3)$$

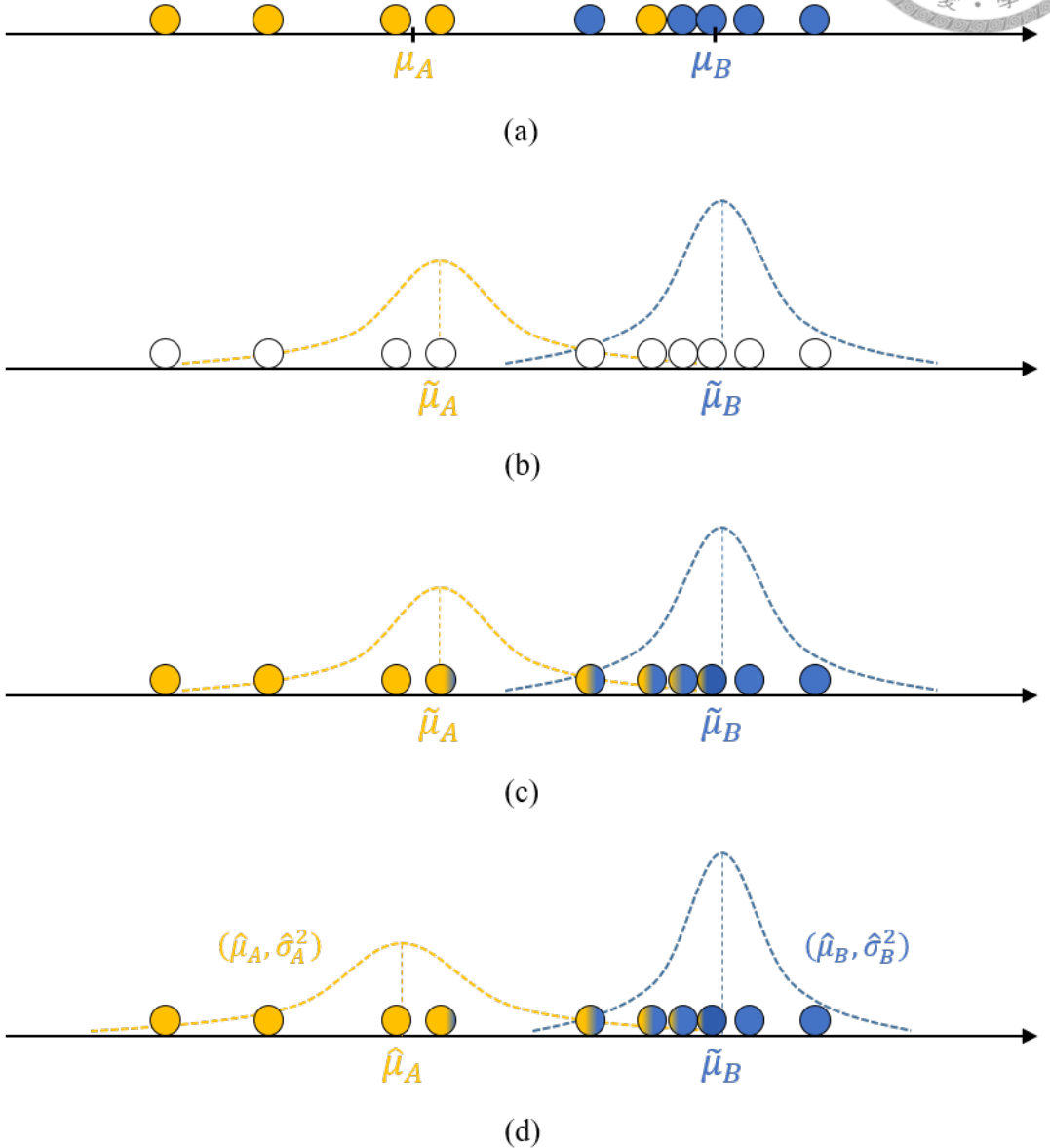
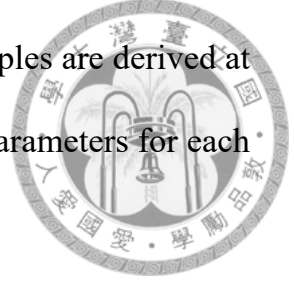


Figure 3.8: An example of EM clustering with GMM.

Similarly we can have the probability that sample x_i belongs to source-B with estimates $(\tilde{\mu}_B, \tilde{\sigma}_B^2)$, and the soft assignment of sample x_i is derived as two probabilities: $f(x_i|A)$ and $f(x_i|B)$. Accordingly, the soft assignments of all samples can be obtained and then be represented by the proportion of two colors in each sample

in Fig. 3.8(c). On the other hand, if the soft assignments of samples are derived at first, we can have the maximum likelihood (ML) estimates of parameters for each Gaussian component. The ML estimates for source-A are



$$\hat{\mu}_A = \frac{1}{N_A} \sum_i x_i \Pr(A|x_i), \quad (3.4)$$

and

$$\hat{\sigma}_A^2 = \frac{1}{N_A} \sum_i (x_i - \hat{\mu}_A)^2 \Pr(A|x_i), \quad (3.5)$$

where $N_A = \sum_i \Pr(A|x_i)$. The occurrence probability is also updated as $\Pr(A) = N_A/N_t$ with N_t being the number of samples. Similarly we can have the ML estimates $(\hat{\mu}_B, \hat{\sigma}_B^2)$ and also the occurrence probability $\Pr(B) = N_B/N_t$ with $N_B = \sum_i \Pr(B|x_i)$ for source-B. The distributions of two components are updated by newly derived parameters as shown in Fig. 3.8(d). The steps in Fig. 3.8(c) and Fig. 3.8(d) therefore form an iterative optimization algorithm to find the optimal parameters for Gaussian components in GMM.

Obviously the assumption of Gaussian components in GMM is suitable for the clustering of received symbols, since the channel noise is exactly Gaussian distributed. In addition, only the means of components need to be concerned since the variances of every Gaussian components are equal to the variance of channel noise and the occurrence probabilities are equally like as stated previously. The steps of EM clustering with GMM for the received signals in GDMA system are organized as follows.



Step 1) Initially set the occurrence probability $\Pr(i) = 2^{-mP}$ and the covariance matrix of Gaussian distribution is $\Sigma_i = \sigma_w^2 \mathbf{I}_2$, where σ_w^2 is the variance of channel noise and \mathbf{I}_2 is a two-by-two unit matrix, for each component i with $i \in \{1, 2, \dots, 2^{mP}\}$.

Step 2) Proceed with k-means clustering and the resultant centroids are configured as the initial means of Gaussian components.

Step 3) Compute the soft assignment of each received symbol $r(n)$ by

$$\Pr(i|r(n)) = \frac{\mathcal{CN}(r(n)|\mu_i, \Sigma_i)}{\sum_{j=1}^{2^{mP}} \mathcal{CN}(r(n)|\mu_j, \Sigma_j)}, \quad (3.6)$$

where $i \in \{1, 2, \dots, 2^{mP}\}$ and \mathcal{CN} denotes the PDF of complex Gaussian distribution.

Step 4) Derive the ML estimate of mean for component i with

$$\mu_i = \frac{1}{N_i} \sum_{n=1}^{N_t} r(n) \Pr(i|r(n)), \quad (3.7)$$

where $i \in \{1, 2, \dots, 2^{mP}\}$ and $N_i = \sum_{n=1}^{N_t} \Pr(i|r(n))$.

Step 4) Return to Step 3 until the means no longer change.

The procedure of EM clustering is quite similar to that of the k-means algorithm, and it also needs the initialization of the parameters. Here we directly use the centroids derived from the k-means++ algorithm to be the initial means of Gaussian components in GMM as stated in Step 2. After the EM clustering, the means of components become the resultant centroids.

3.2 Derivation of Channel Coefficients



We can classify the received symbols into 2^{mP} groups by the clustering techniques introduced in Sec. 3.1, and the centroids of groups are the estimates of superimposed levels. Recall that the fading coefficients are constant across a block of N_t consecutive symbols and the occurrence probabilities of superimposed levels are equally like in assumption. By using the geometrical configuration of the superimposed signal, we can further estimate the channel coefficients of P users from the resultant centroids. In this section, ideal clustering that the centroids are exactly equal to superimposed levels is assumed to illustrate the procedure clearly.

When there is only $P = 1$ user transmitting signal in system, the channel coefficient can be easily found by comparing the centroids to the constellation of transmitted signal. However, since the clustering takes the signals that carry messages as the training samples, there is an uncertain phase ambiguity needs to be

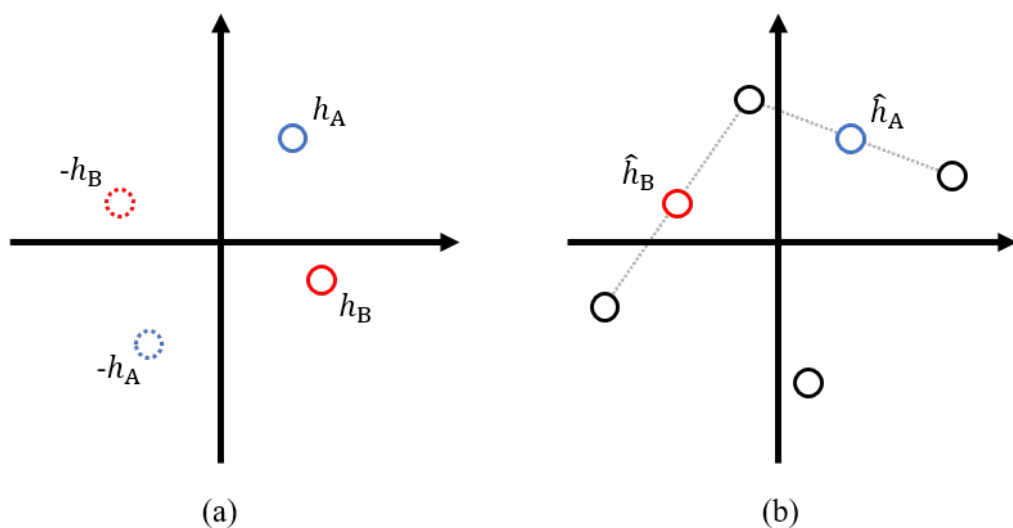


Figure 3.9: Derivation of coefficients in the case of $P = 2$ and BPSK transmission.

resolved. The schemes to remove the ambiguity will be discussed in Sec. 3.3. The channel coefficients of $P = 2$ users are shown in Fig. 3.9(a), and the black circles in Fig. 3.9(b) are the centroids of received signals. The two midpoints, \hat{h}_A and \hat{h}_B , on the edges formed by connecting three of the centroids are the channel coefficients of users with an uncertain phase offset.

In the case of $P = 3$ and BPSK transmissions, the channel coefficients of users are shown in Fig. 3.10(a), and the black circles in Fig. 3.10(b) are the centroids of received signals. To find the coefficients, the first step is to pair the centroids with the sum of each pair is equal to zero. In Fig. 3.10(c), pair A, B, C and D are found, and the order of pairs is arbitrary. After the pairing, centroids (A,D) and (B,C) form two parallelograms, respectively, and then we can have the channel coefficient of user-1 by finding the overlapped midpoints on the edges of the two parallelograms as shown in Fig. 3.10(d). Similarly, the overlapped midpoints on the edges of the parallelograms formed by centroids (A,C) and (B,D), respectively, are the channel coefficient of user-2 as shown in Fig. 3.10(e). Finally, the overlapped midpoints on the edges of the parallelograms formed by centroids (A,B) and (C,D), respectively, are the channel coefficient of user-3 as shown in Fig. 3.10(f). All the estimates has an uncertain phase offset.

Besides the cases of BPSK transmissions, the channel coefficients of $P = 2$ users are shown in Fig. 3.11(a) and the black circles in Fig. 3.11(b) are the centroids of received signals with 4-PAM transmissions. It is sufficient to attain the coefficients of users with only three of the corners, e.g., centroids c_1 , c_2 and c_3 in

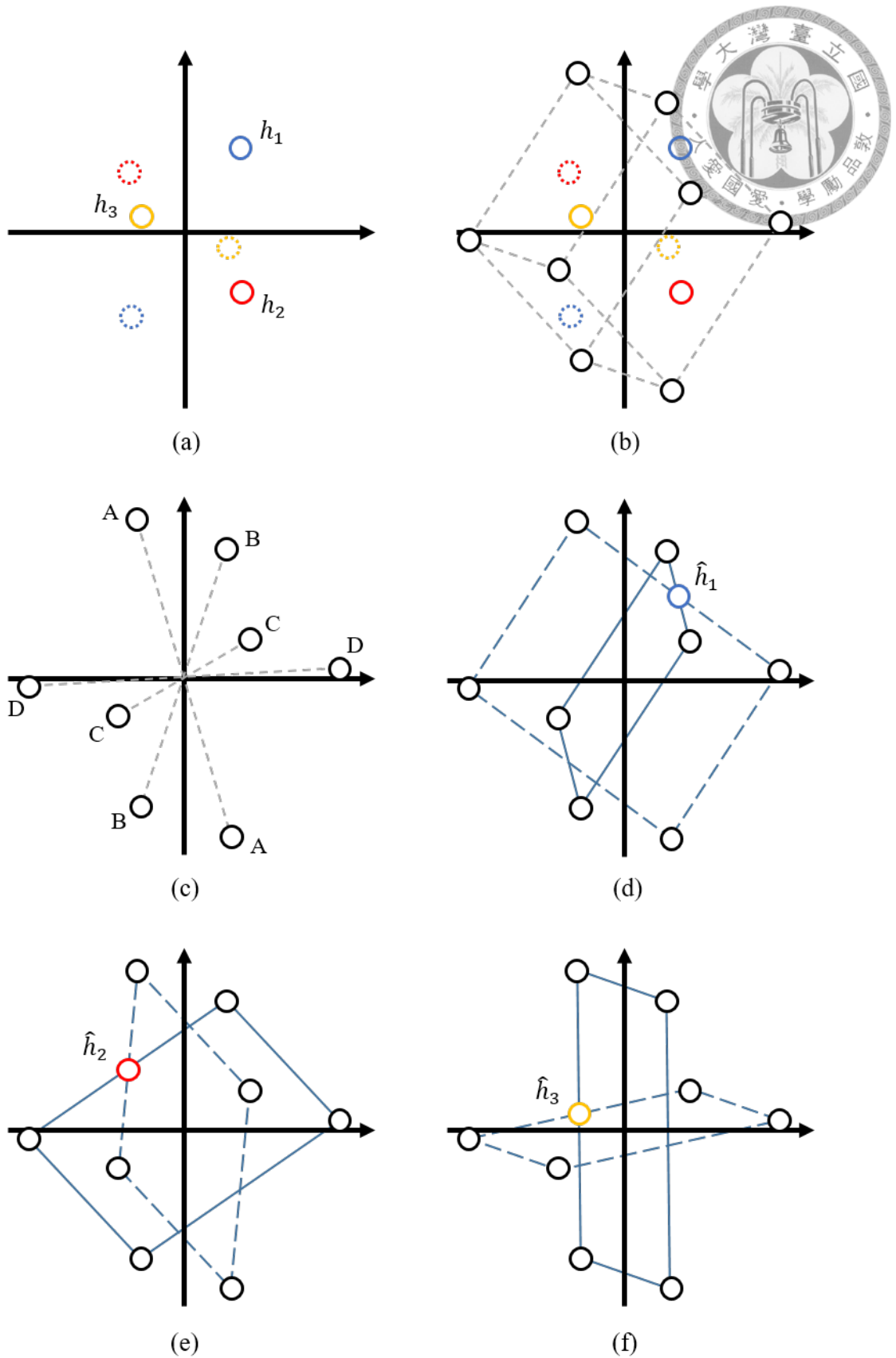


Figure 3.10: Derivation of coefficients in the case of $P = 3$ and BPSK transmission.

Fig. 3.11(c). To find the corners, first we pick the two, c_1 and c_2 in Fig. 3.11(c), with the largest distances from the origin. Once we find c_1 and c_2 , the centroid with the largest perpendicular distance from the line formed by connecting c_1 and c_2 is the third corner c_3 . The two midpoints, h'_A and h'_B , on the edges formed by connecting c_1 , c_2 and c_3 are the channel coefficients of users after normalized by $\sqrt{3E_0}$ if the constellation of 4-PAM is $\{-3\sqrt{E_0}, -\sqrt{E_0}, \sqrt{E_0}, 3\sqrt{E_0}\}$. The methodology used here is applicable to 2^m -PAM with arbitrary order m .

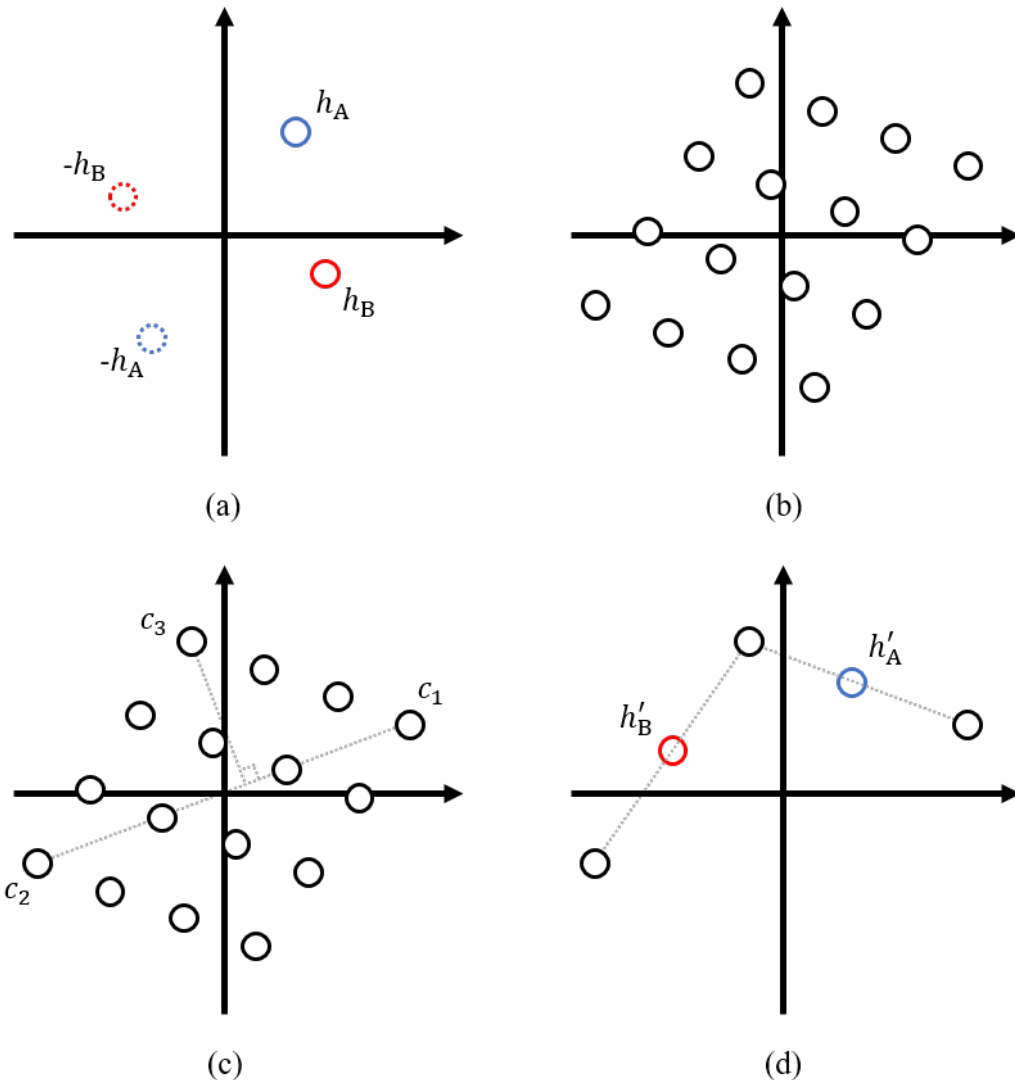


Figure 3.11: Derivation of coefficients in the case of $P = 2$ and 4-PAM transmission.

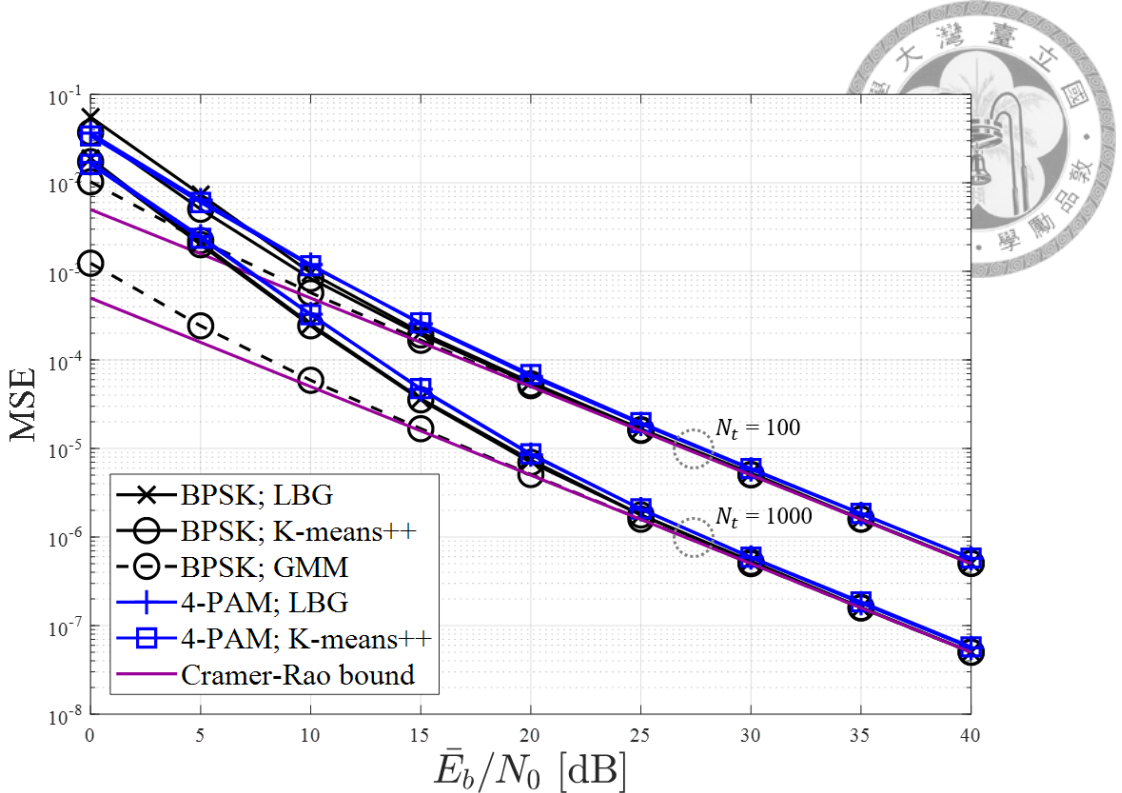


Figure 3.12: MSE performances of the cluster-based estimation applied to quasi-static Rayleigh flat-fading channels in the case of $P = 1$.

The mean-squared error (MSE) performances are simulated in Fig. 3.12-3.14 to evaluate the performances of cluster-based estimation applied to Rayleigh flat-fading channels and the MSE is defined as

$$\text{MSE}(h, \hat{h}) = \frac{1}{2}|h - \hat{h}|^2, \quad (3.8)$$

where h is the exact channel coefficient and \hat{h} is the estimate of h . Note that the average energy of channel coefficients and transmitted signals are both normalized to one. The Cramer-Rao lower bound (CRLB), for the minimum variance unbiased (MVU) estimator using N_t samples in estimation, is also provided to evaluate the performance. Consider the observations when the signals are propagated through

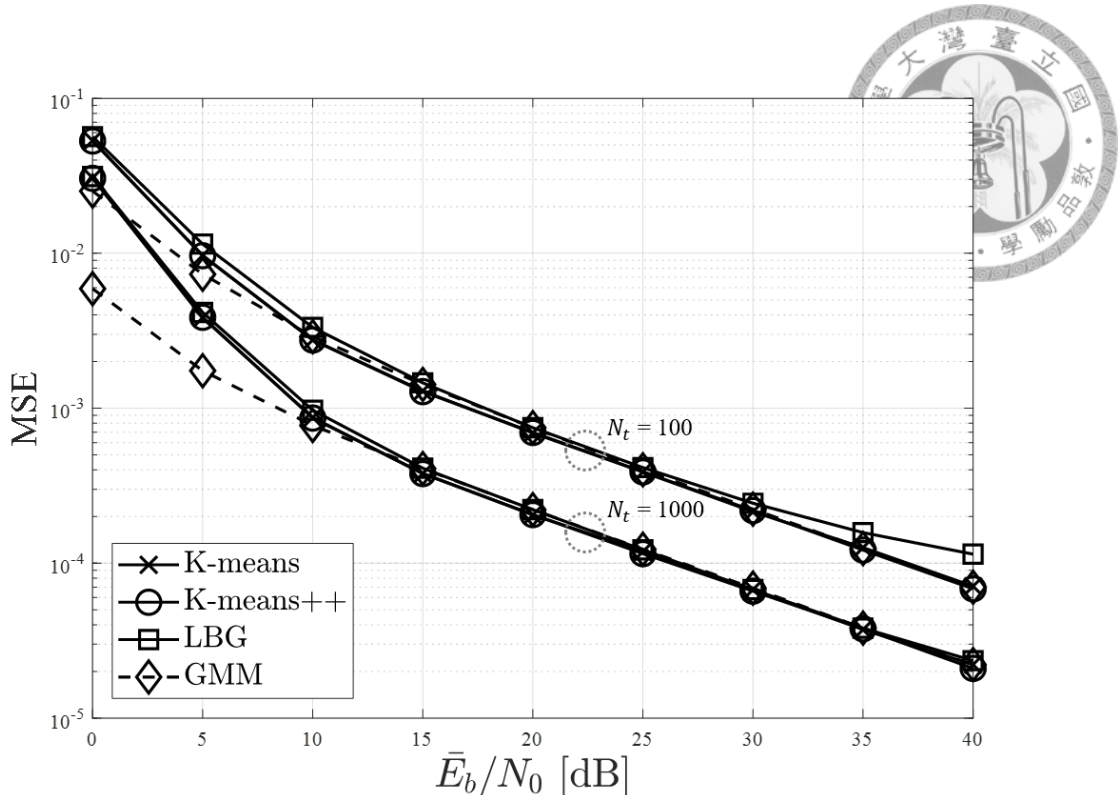


Figure 3.13: MSE performances of the cluster-based estimation applied to quasi-static Rayleigh flat-fading channels in the case of $P = 2$ and BPSK transmissions.

the channel with AWGN as

$$r(n) = h + w(n), \quad n = 0, 1, \dots, N_t - 1, \quad (3.9)$$

where h is the parameter to be estimated and $w(n)$ is AWGN with variance σ_w^2 . The MVU estimator of h can be derived as

$$\hat{h} = \frac{1}{N_t} \sum_{n=0}^{N_t-1} r(n), \quad (3.10)$$

and the variance of \hat{h} is the CRLB written as

$$\sigma_{\hat{h}}^2 = \frac{\sigma_w^2}{N_t}. \quad (3.11)$$

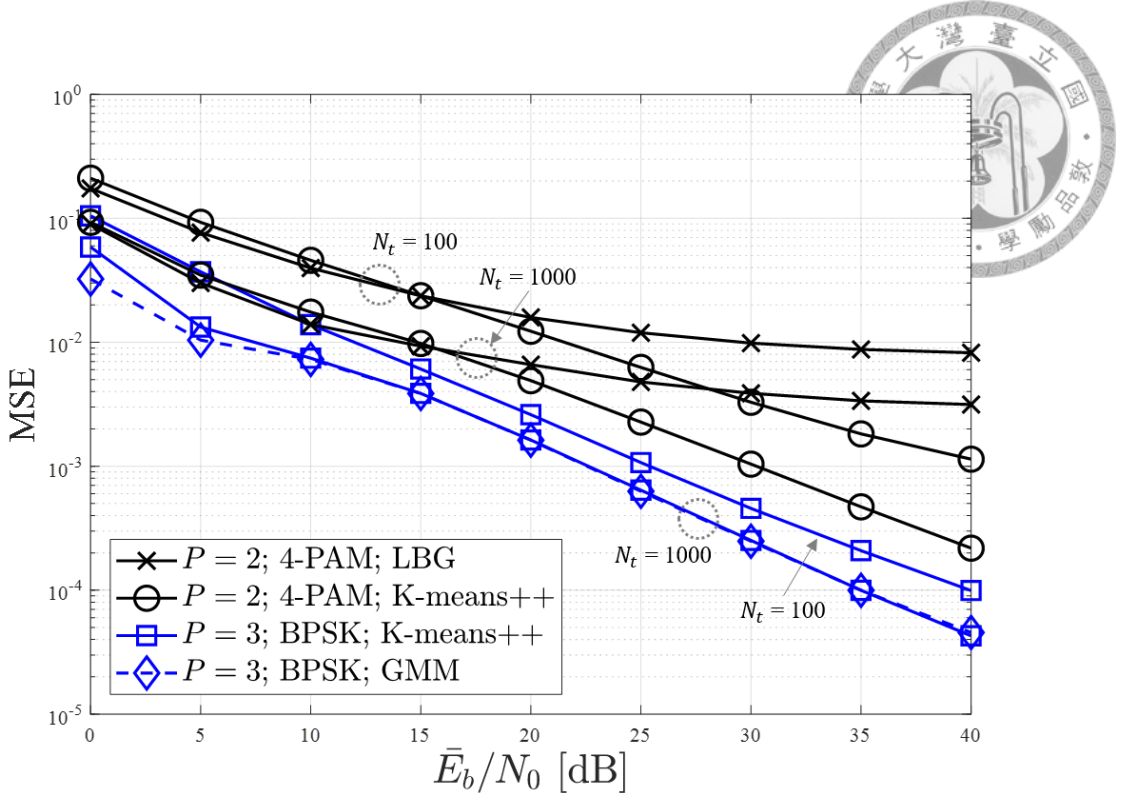


Figure 3.14: MSE performances of the cluster-based estimation applied to quasi-static Rayleigh flat-fading channels.

In addition to the effect of channel noise, clustering techniques cannot guarantee that the correct solution will be found and the probability that the samples are not properly classified also has a large impact on the estimation, especially for the cases with $P > 1$.

In the case of $P = 1$, the MSE performances shown in Fig. 3.12 are almost the same regardless of the choice of hard clustering algorithm. By using the EM clustering with GMM, the performances can be further improved such that the MSEs can approach to the CRLB in low-SNR region. Recall that the soft clustering can allow multiple groups to have highly overlapped areas, which is the case when the power of channel noise is relatively large. In the case of $P = 2$ and BPSK transmissions as shown in Fig. 3.13, the standard k-means algorithm results in the

same MSE performances as that of the k-means++, and the LBG algorithm with $N_t = 100$ has worst performance in high-SNR region. However, a larger time complexity is needed for standard k-means than the other algorithms as shown in Table 3.1 and 3.2. In the case of $P = 2$ and 4-PAM transmissions, there are evident estimation error floors when the LBG algorithm is applied and the performances of k-means++ can still be improved when the SNR is increasing. As mentioned before, the LBG algorithm is highly dependent on the accuracy of training samples and the solutions might be stuck in the local minima regardless of the initialization.

3.3 Resolving Phase Ambiguity

Although we can have the estimates of channel coefficients through the clustering, there is still an uncertain phase ambiguity due to the estimation using signals that carry messages. An easy way to remove the ambiguity is to differentially encode the message. However, the differential encoding results in a loss of error performance because of the effect of error propagation. Therefore, we introduce some of the methods to overcome the problem of phase ambiguity and also enhance the reliability in this section.

3.3.1 Differential Encoding

Differentially encoded (DE) modulation uses the difference between symbols to carry message. In the transmission of PSK, message is embedded in the difference of phases between two consecutive symbols and coherent detection can still be

applied, resulting in differentially encoded coherently detected PSK (DE-PSK).

Therefore, the phase offset resulted from uncertain ambiguity in blind estimation will not affect the detection of data in DE-PSK transmissions. The block diagram of DE-BPSK scheme is provided in Fig. 3.15.

When the differential encoding is applied, the performances of the uncoded GDMA systems employing cluster-based channel estimation over Rayleigh flat-fading channels are simulated in Fig. 3.17-3.19. The performances of systems with ideal channel estimation (CE) are also provided for comparison. The transmissions with differential encoding require additional 2~3 dB in SNR to achieve the same error rate as that without differential encoding. Moreover, there are error floors in high-SNR region of the BER performances when cluster-based estimation is applied with $P > 1$.

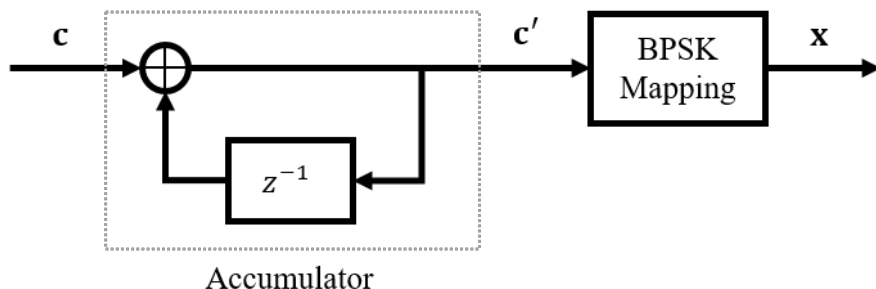


Figure 3.15: Modulation scheme for DE-BPSK transmission.

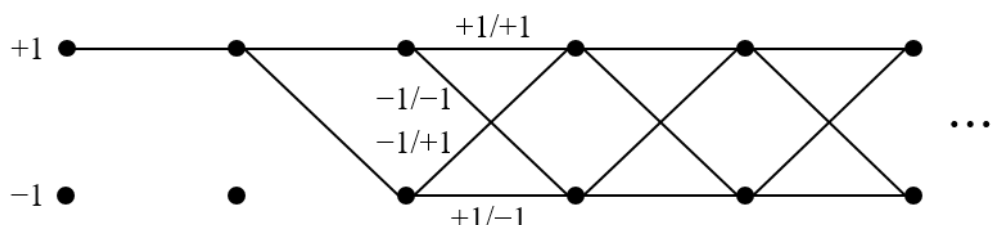


Figure 3.16: Representation of DE-BPSK in Trellis diagram.

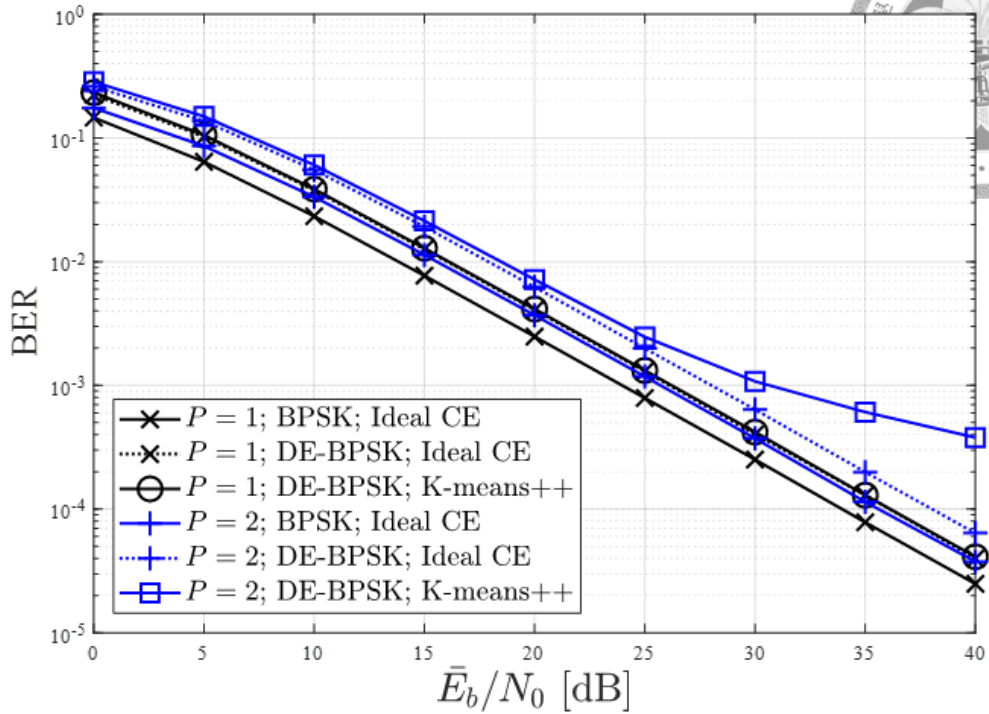
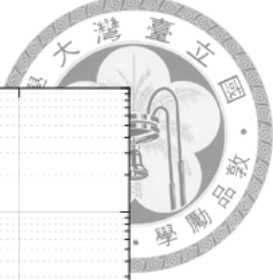


Figure 3.17: BER performances of GDMA-BPSK system employing cluster-based estimation with $N_t = 100$ over quasi-static Rayleigh flat-fading channels.

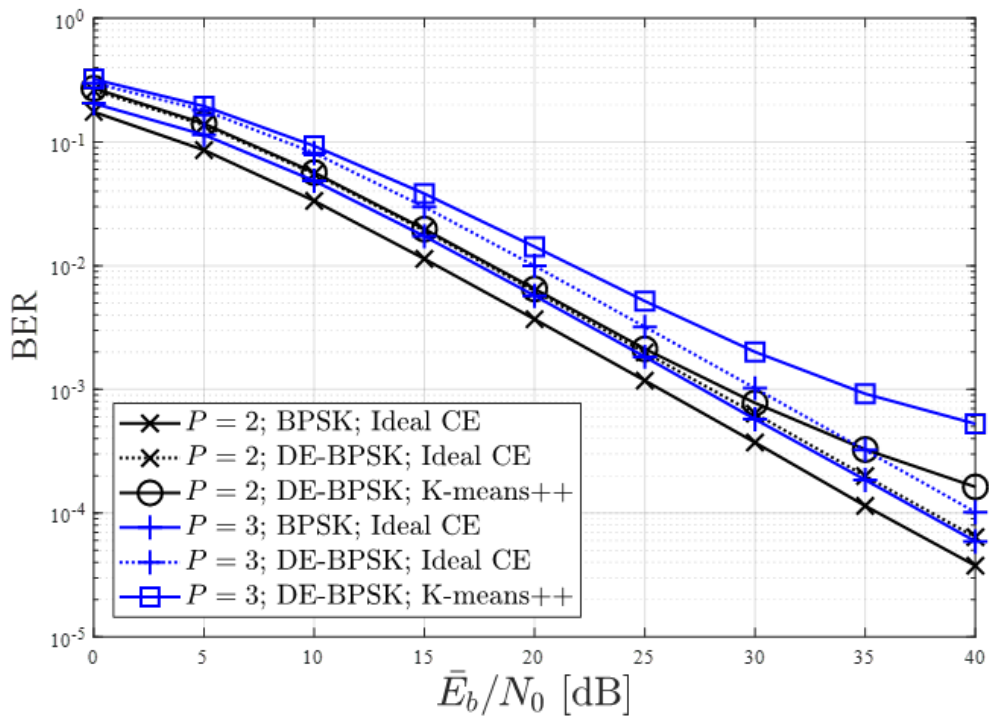


Figure 3.18: BER performances of GDMA-BPSK system employing cluster-based estimation with $N_t = 1000$ over quasi-static Rayleigh flat-fading channels.

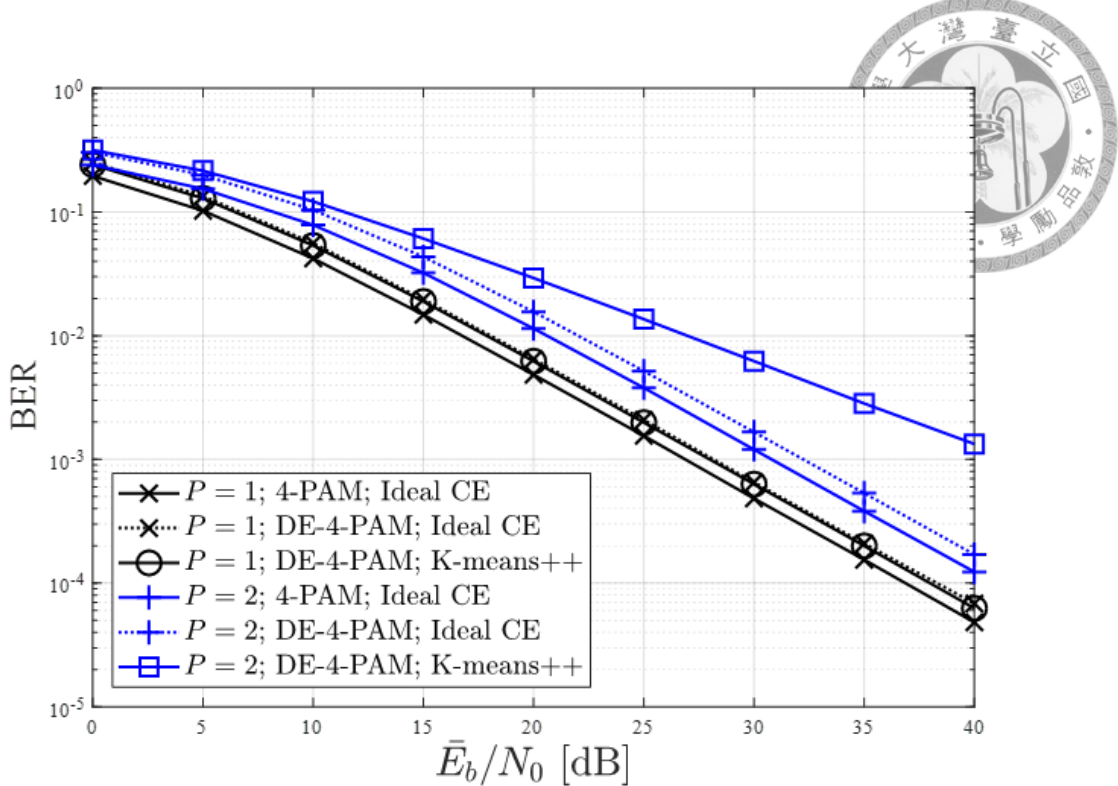


Figure 3.19: BER performances of GDMA-4-PAM system employing cluster-based estimation with $N_t = 1000$ over quasi-static Rayleigh flat-fading channels.

3.3.2 Turbo Principle

Differential encoding can be represented as a trellis diagram, shown in Fig. 3.16 for DE-BPSK and the notation on each edge represents input/output signal of the modulator, and hence the Viterbi algorithm or the Bahl – Cocke – Jelinek – Raviv (BCJR) algorithm [20] can be applied to the demodulator. The soft-in-soft-out (SISO) demodulation implemented by the BCJR algorithm, which detects the messages in the MAP criterion, can accept not only soft channel values but also *a priori* information, then outputs *a posteriori* probabilities. In [21], the extrinsic information delivered from the outer SISO decoder is fed back as *a priori* information to the inner SISO demodulator to form the iterative processing, also called the turbo principle.

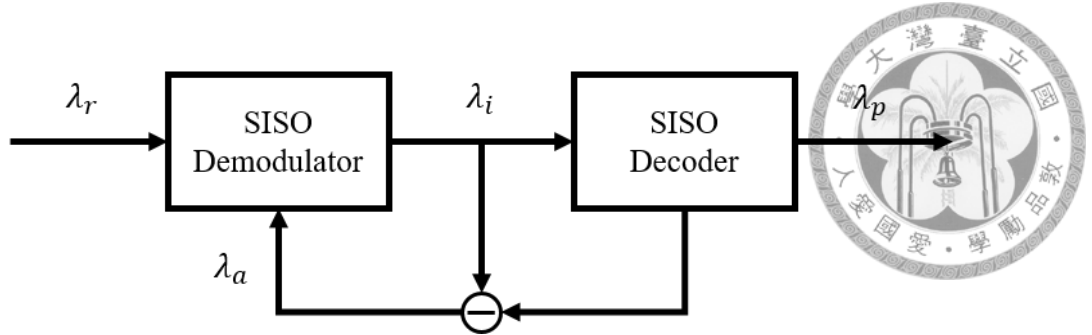


Figure 3.20: Turbo processor: iterative demodulation and decoding.

The turbo processing was originally designed for differentially encoded differentially detected PSK (DPSK) in [21]. Here we apply the turbo principle to mitigate the performance loss resulted from the differential encoding with the help of FEC coding. The block diagram of turbo processor is shown in Fig. 3.20 where λ_r and λ_a are the channel values and *a priori* information respectively, and the operation is in the log-domain without loosing optimality.

3.3.3 Joint Decoding

An LDPC code can be represented as a Tanner graph, defined by the parity-check matrix \mathbf{H} with two kinds of nodes: check nodes associated to rows of \mathbf{H} , and variable nodes associated to columns of \mathbf{H} . The differential encoding for DE-BPSK is implemented by an accumulator which sums the input bit $c(n)$ in \mathbf{c} with the previous output bit $c'(n - 1)$ to get the output bit $c'(n)$ in \mathbf{c}' recursively for each n as shown in Fig. 3.15. A graphical representation of an LDPC code concatenated with differential encoding for DE-BPSK is shown in Fig. 3.21. The intermediate check nodes represent the parity-check equations defined by the outer LDPC code and the input nodes represent the LDPC-coded bit sequence \mathbf{c} . The output check

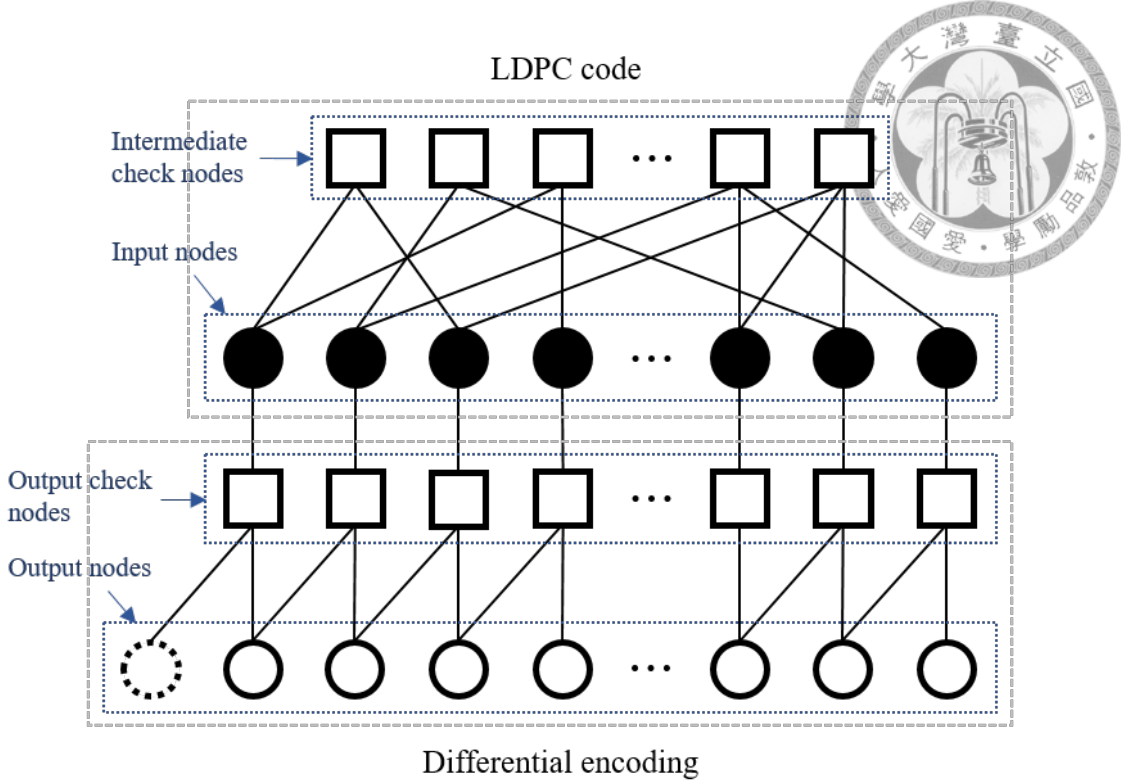


Figure 3.21: Serial concatenation of differential encoding and an LDPC code represented in Tanner graph for DE-BPSK transmission.

nodes are defined by the differential encoding, i.e., $c(n) \oplus c'(n - 1) \oplus c'(n) = 0$ for each n , and the output nodes are the bits in \mathbf{c}' after differential encoding. The variable node represented as dotted circle in Fig. 3.21 is the additional reference bit for differential encoding.

In the Tanner graph that combines the LDPC code and differential encoding, we can perform the sum-product algorithm (SPA) along the edges in the corresponding Tanner graph [9] to recover the messages by treating the two component codes as a single graph-based code. Therefore, two component codes will exchange the informations to each other in the decoding. An advantage of applying joint decoding is that the joint channel decoding using generalized SPA (G-SPA) can also be used to recover the messages of P users simultaneously.



3.3.4 Noncoherent Block-Coded Modulation

In [22], a novel block-coded modulation (BCM) scheme with noncoherent detection called noncoherent block-coded MPSK (NBC-MPSK) was proposed. The ambiguity can be easily removed without applying differential encoding by partitioning the code space as long as the generator matrix of a linear block code containing an all-one row.

The original code space C' is divided into $C' = \{C, C \oplus \mathbf{1}\}$, where $\mathbf{1}$ is an all-one vector, and the generator matrix \mathbf{G} of C is found by removing the all-one row in the generator matrix of C' . We only select the codewords from C to be transmitted, i.e., encode the message with \mathbf{G} , which results in a rate loss of one bit. At the receiver side, if the signal is BPSK-modulated, the codeword \mathbf{c}' corresponding to the received signal would be \mathbf{c} or $\mathbf{c} \oplus \mathbf{1}$ due to an uncertain phase ambiguity of 180° where \mathbf{c} is the transmitted codeword in C . To remove the uncertain ambiguity, we just need to detect whether the decoded codeword $\tilde{\mathbf{c}}$ is in C or not and the resultant codeword is

$$\hat{\mathbf{c}} = \begin{cases} \tilde{\mathbf{c}}, & \text{if } \tilde{\mathbf{c}} \in C \\ \tilde{\mathbf{c}} \oplus \mathbf{1}, & \text{if } \tilde{\mathbf{c}} \notin C \end{cases} \quad (3.12)$$

For higher order modulation scheme, the multi-level coding in BCM can be decoded by multi-stage decoding as shown in [22]. The code space identification in (3.12) can be implemented by checking the number of satisfied parity-check equations. However, the bit errors after decoding might result in erroneous identification and redundant bit-flipping.



Simulation Results

To compare the schemes that remove the ambiguity, simulated performances of systems with ideal CE and $P = 1$ are provided. In the transmission over quasi-static Rayleigh flat-fading channel, a (3,6)-regular rate-1/2 (1008,504) LDPC code is considered in Fig. 3.22 and 3.23, and the maximum number of decoding iterations is set to 50. Moreover, the (1008,504) LDPC-coded MC-DS-CDMA system over quasi-static frequency-selective Rayleigh fading channel with the same parameters as stated in Sec. 2.4.1 is considered in Fig. 3.24. In the system employing noncoherent block coding (NBC), the ambiguity is removed only by selecting the codeword suitably from the code space to be transmitted and the block error rate (BLER) is not affected since the decoding capability remains the same. However,

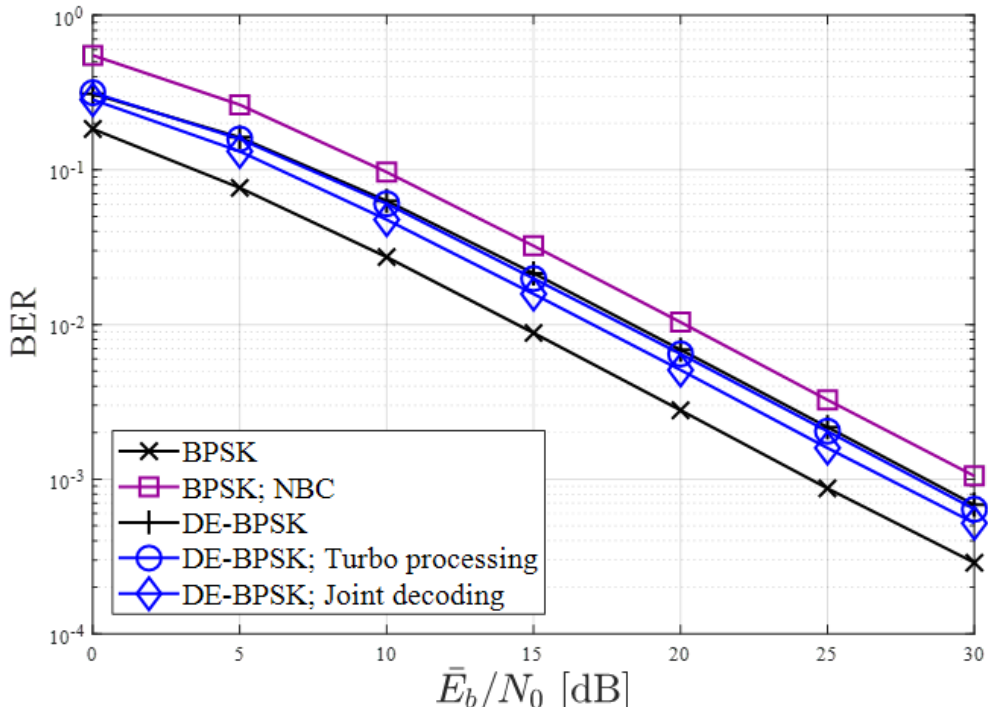


Figure 3.22: BER performances of schemes that remove the phase ambiguity in LDPC-coded system over quasi-static Rayleigh flat-fading channel.

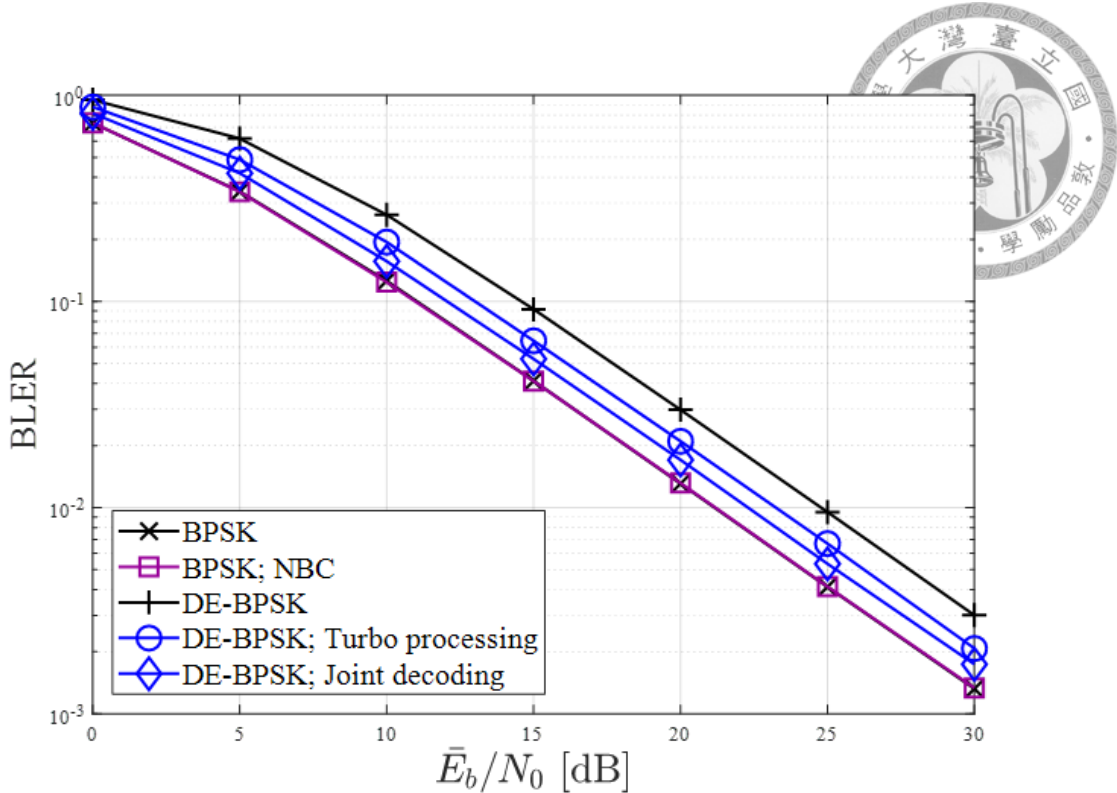


Figure 3.23: BLER performances of schemes that remove the phase ambiguity in LDPC-coded system over quasi-static Rayleigh flat-fading channel.

the NBC scheme yields the worst BER performance since the erroneous identification of code space in (3.12) with redundant bit-flipping results in much more bit errors than it originally has. The turbo principle and the joint decoding both achieve better performances than that of the system with only differential decoding by exchanging the extrinsic informations between two component codes. In addition, the joint decoding results in the best BER performance. Note that the NBC scheme cannot be applied to multi-carrier systems since the estimation is performed on each of the sub-channels separately and the codeword bits carried by different sub-carriers might have different phase offset independently.

The simulated performances of the systems employing cluster-based channel estimation are provided in Fig. 3.25-3.27. Besides the (3,6)-regular (1008,504)

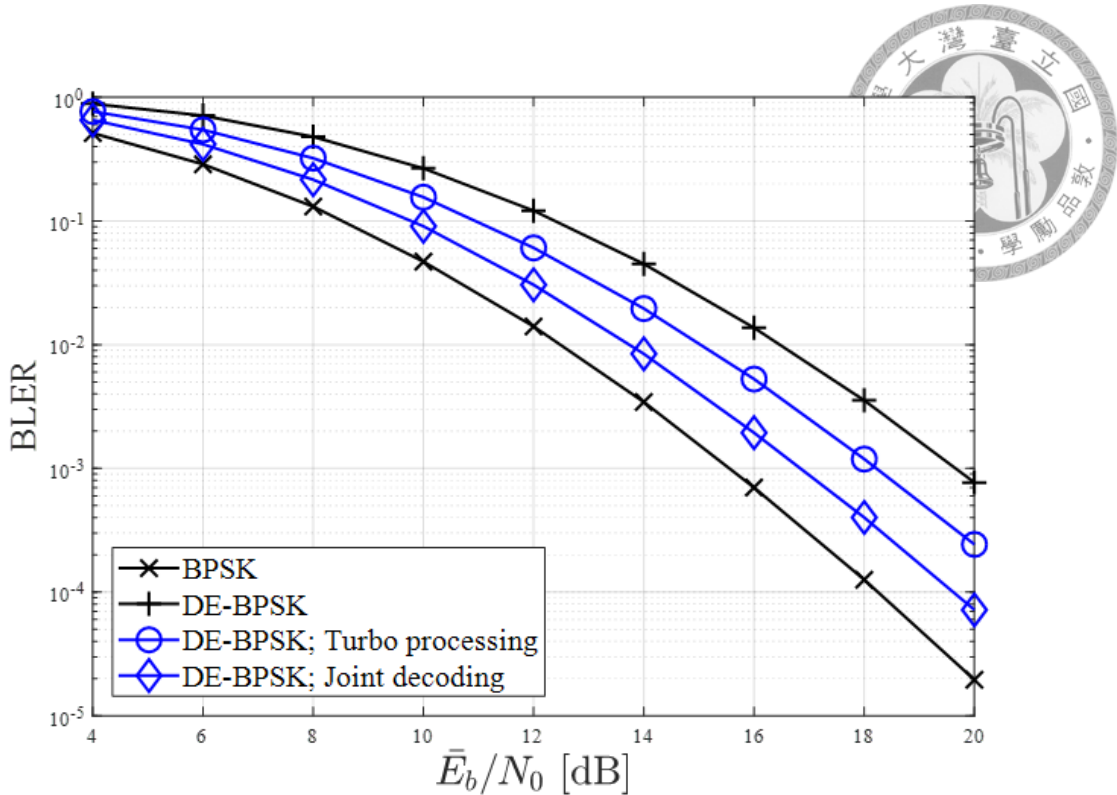


Figure 3.24: BLER performances of schemes that remove the phase ambiguity in LDPC-coded MC-DS-CDMA system over quasi-static frequency-selective Rayleigh fading channels.

LDPC code, a rate-1/2 (256,128) Polar code is also considered in the GDMA-SCD system over quasi-static Rayleigh flat-fading channels and the decoding algorithm is the SCL decoding. The list size in Polar decoding is set to 32. The NBC scheme and the joint decoding are employed to the systems with single-carrier transmission and multi-carrier transmission respectively to attain minimum performance degradation resulted from the removing of phase ambiguity. Moreover, the number of training samples for the cluster-based estimation in single-carrier transmission is equal to the length of codeword on the assumption that the signals are BPSK-modulated, i.e. $N_t = N_c$, and $N_t = N_c/Q$ in the multi-carrier system with Q sub-channels. Note that the bit streams transmitted through different sub-channels are differentially encoded separately in multi-carrier system. By using the cluster-

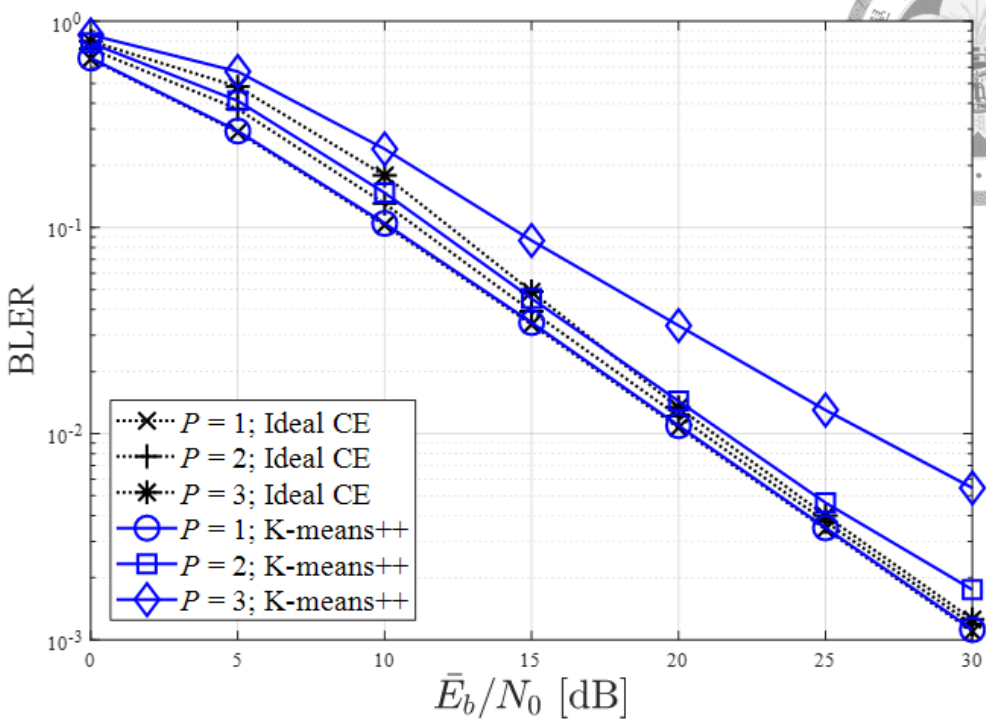
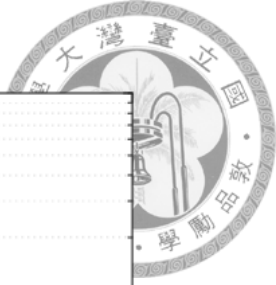


Figure 3.25: BLER performances of (256,128) Polar-coded GDMA-SCD system employing cluster-based estimation over quasi-static Rayleigh flat-fading channels.

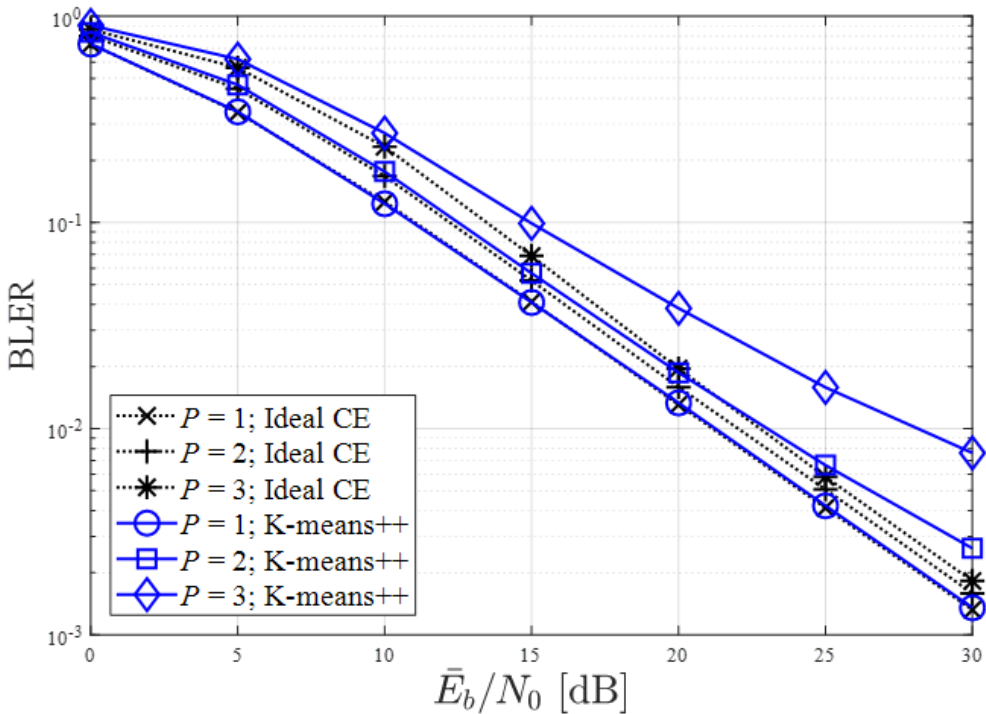


Figure 3.26: BLER performances of (1008,504) LDPC-coded GDMA-SCD system employing cluster-based estimation over quasi-static Rayleigh flat-fading channels.

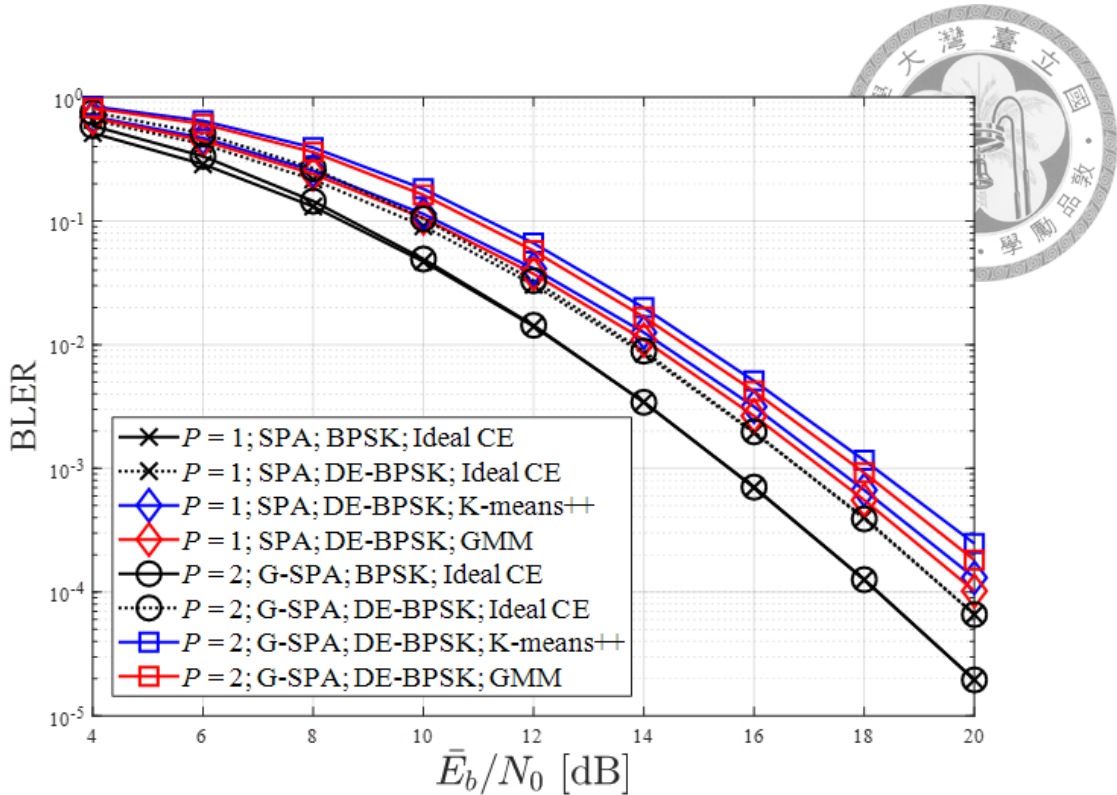


Figure 3.27: BLER performances of (1008,504) LDPC-coded MC-DS-CDMA-GDMA system employing cluster-based estimation over quasi-static frequency-selective Rayleigh fading channels.

based estimation scheme, the performances of GDMA-SCD systems over quasi-static Rayleigh flat-fading channels shown in Fig. 3.25 and 3.26 can approach to that of the differentially coded systems with perfect CSI in the cases of $P = 1$ and $P = 2$. Moreover, the performances of MC-DS-CDMA-GDMA system employing cluster-based estimation scheme over quasi-static frequency-selective Rayleigh fading channels shown in Fig. 3.27 have 0.4 dB and 1 dB performance losses in the cases of $P = 1$ and $P = 2$ respectively compared to the differentially coded systems with perfect CSI. The proposed estimation scheme is a kind of blind estimation, which can attain high spectral efficiency since the additional pilot signal is avoid. Note that a loss of 3 dB in SNR is introduced by the differential encoding in multi-carrier transmissions.

3.4 System Impairments



So far we have introduced the cluster-based channel estimation. In this section, the estimation scheme is employed to the systems with some impairments to see the robustness of the proposed scheme.

3.4.1 Unknown Timing Drifts

The assumption that the symbol timings are perfectly aligned for all users may not be practical in the scenario for uplink transmissions. To consider the situation that the synchronization of users has some inaccuracies in GDMA system, we assume that all users are transmitting signals with independent timing drifts which are uniformly distributed and unknown to the receiver. The block diagram of asynchronous transmission is shown in Fig. 3.28. The received continuous-time signal can be written as

$$r(t) = \sum_{p=1}^P h_p z_p(t - \tau_p) + w(t), \quad (3.13)$$

where τ_p is the timing offset of user- p and $w(t)$ is the complex AWGN.

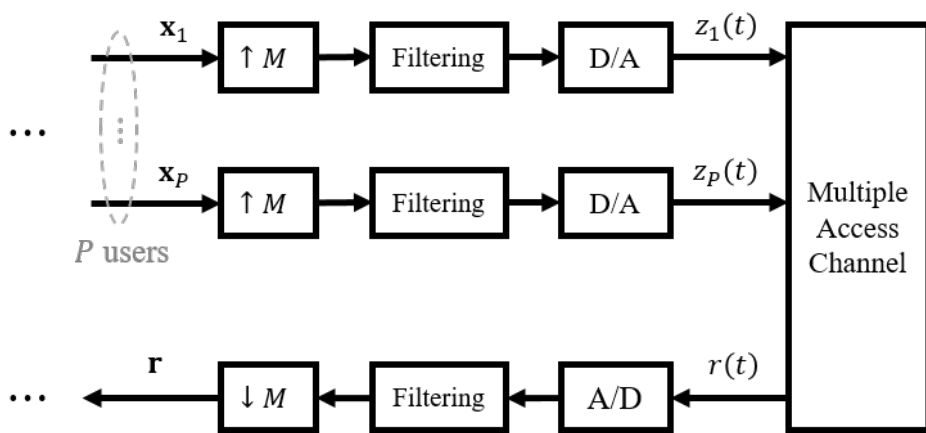


Figure 3.28: System model for asynchronous transmissions.

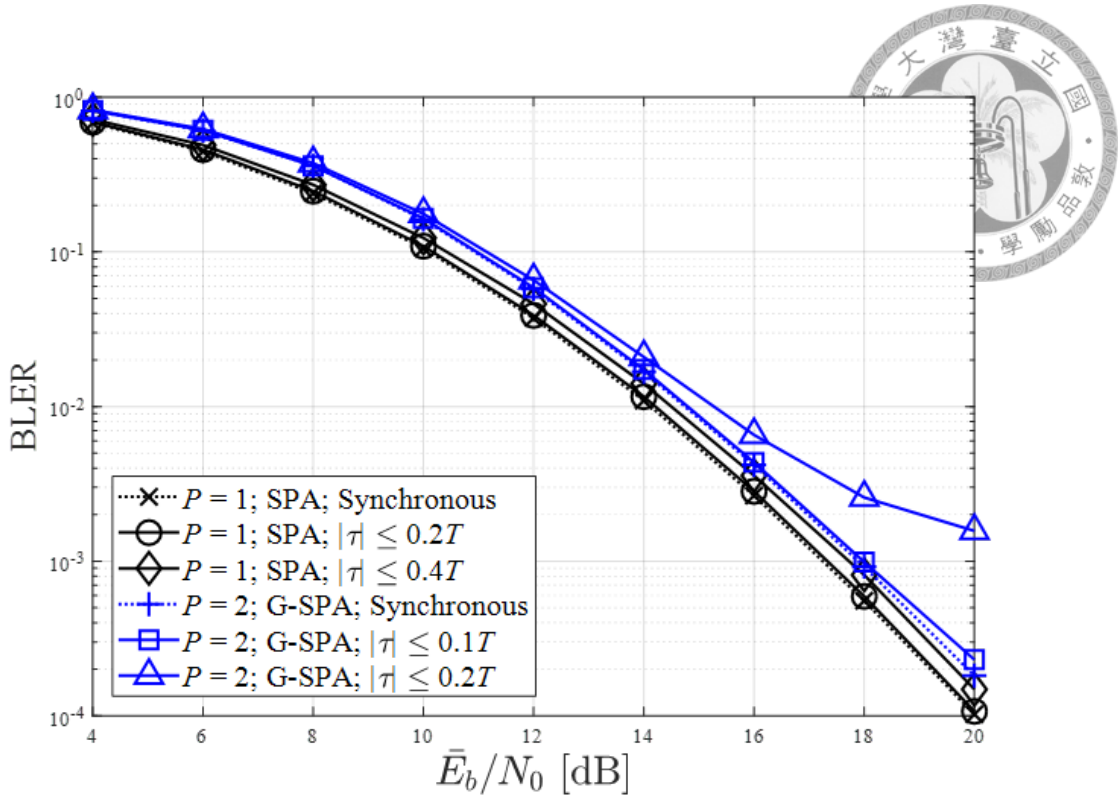


Figure 3.29: BLER performances of (1008,504) LDPC-coded MC-DS-CDMA-GDMA system employing cluster-based estimation over quasi-static frequency-selective Rayleigh fading channels with independent timing drifts.

In the simulations, the transmitting filter and receiving filter are both square root raised cosine function with roll-off factor $\beta = 0.22$, and the up-sampling and down-sampling rate are both set to $M = 4$. The timing drifts of transmissions are independent and uniformly distributed random variables within the interval $[-\alpha T, \alpha T]$, where T is the symbol period. The performances of asynchronous transmissions in the (1008,504) LDPC-coded MC-DS-CDMA system with the same parameters as stated in Sec. 2.4.1 are provided in Fig. 3.29. The cluster-based estimation scheme is implemented by the EM clustering with GMM. Since the number of users in system is doubled in the case of $P = 2$, the ISI effect is more evident when the symbol timings are not perfectly aligned and there is an error floor in the BLER performance when $KP = 32$ and timing drifts are within $0.2T$.



3.4.2 Doppler Effect

When either the transmitter, receiver or scatterers are in motion, the received signal will be dispersed in frequency as a result of the Doppler effect. The maximum Doppler frequency can be calculated by

$$f_d = \frac{f_c \cdot v}{c}, \quad (3.14)$$

where f_c is the carrier frequency, v is the speed of user equipment (UE) and $c = 3 \times 10^8$ m/sec is the speed of light. The spreading in signal spectrum caused by the Doppler effect implies the variation of channel.

An important assumption in the cluster-based estimation is that the channels of P users remain unchanged within N_t consecutive symbols. Therefore, we further simulate the performances of cluster-based estimation in time-varying channels [23]. In simulations, carrier frequency $f_c = 2$ GHz and chip rate 30.72 MHz are considered. Moreover, $\bar{f}_d = f_d T_s$ is the normalized maximum Doppler frequency

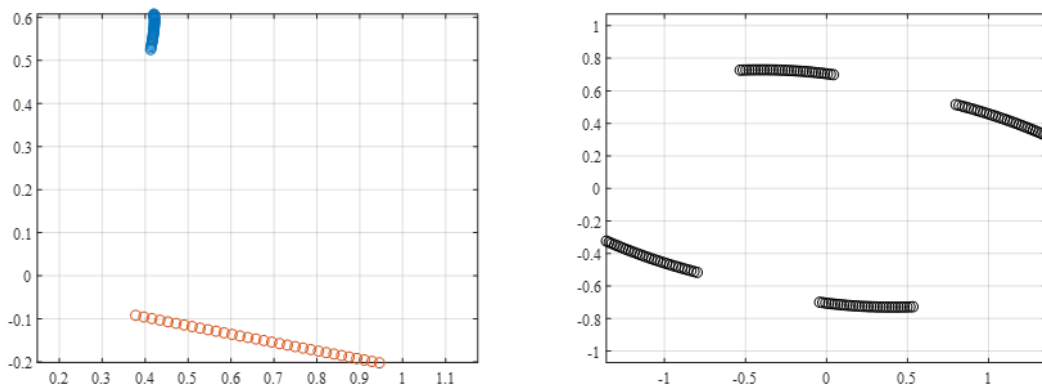


Figure 3.30: Traversal of channel coefficients and the corresponding superimposed levels in the case of $m = 1$ and $P = 2$.

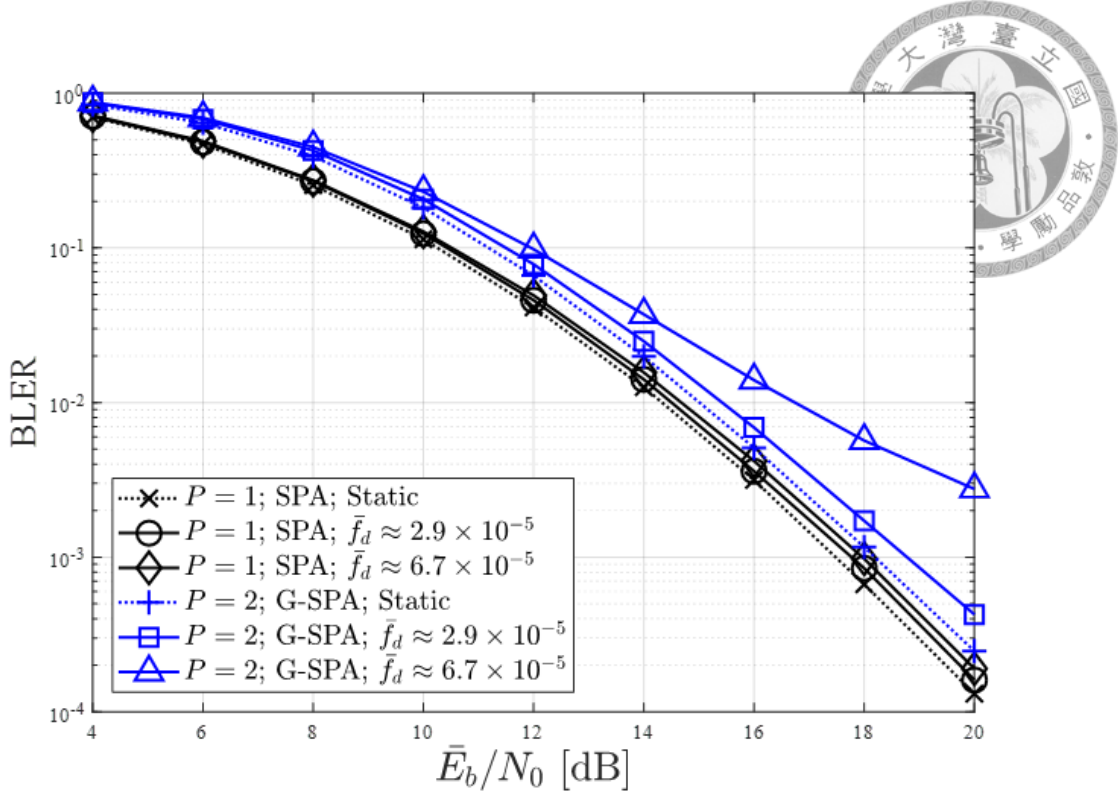


Figure 3.31: BLER performances of transmissions over time-varying frequency-selective Rayleigh fading channels in (1008,504) LDPC-coded MC-DS-CDMA-GDMA system employing cluster-based estimation.

and T_s is the period of an OFDM symbol. An example of channel coefficients varying with time is shown in Fig. 3.30, where the left one is the traversal of coefficients and the right one is the corresponding superimposed levels in the case of $m = 1$ and $P = 2$ when $\bar{f}_d \approx 6.7 \times 10^{-5}$. The (1008,504) LDPC-coded MC-DS-CDMA-GDMA system is considered and the results are provided in Fig. 3.31. The cluster-based estimation scheme is implemented by the EM clustering with GMM.

In the estimation scheme for $P = 2$ case, the geometrical configuration of the received signal is more critical than that for $P = 1$ case since the estimates are derived from the midpoints on the edges of parallelogram formed by connecting the centroids. Therefore, the variation of channels has larger impact on the $P = 2$ case than $P = 1$ as shown in Fig. 3.31.



Chapter 4

Concatenation of LDPC Codes and Differential Encoding in Multi-Edge Framework

In Chapter 3, the scheme for cluster-based channel estimation was introduced.

The proposed scheme is a kind of blind estimation, and there is still an uncertain phase ambiguity in the estimate since the clustering takes the signals that carry messages as training samples. In Sec. 3.3, some of the schemes to remove the ambiguity were discussed and a loss of 3 dB in performance is introduced by applying differential encoding in multi-carrier transmissions. In this chapter, we focus on the scheme that the differential encoding is employed, and the optimization of outer LDPC codes in multi-edge framework is then investigated to further relieve the performance degradation. Multi-edge type LDPC (MET-LDPC) codes [7] are a generalization of irregular LDPC codes. Before we exploit the advantages provided in MET framework, definitions and properties of both standard LDPC codes and MET-LDPC codes are reviewed.

4.1 Multi-Edge Type LDPC Codes



Unlike standard LDPC codes which consist of only one statistically equivalent type of edges, several edge-types can be simultaneously defined in MET-LDPC codes and every nodes are characterised by the number of connected edges of each edge-type in MET setting. Moreover, each of the edge-types has its own degree distributions and thus a great flexibility is introduced in the corresponding code structure. The MET framework gives rise to ensembles not possible in the irregular LDPC codes and provides an unifying representation for graph-based codes, which allow one to explore codes under specific constraints.

Standard irregular LDPC codes are specified by a pair of degree distributions, usually taken from edge-perspective, denoted as $\lambda(X)$ and $\rho(x)$ for variable nodes and check nodes respectively. In the polynomial

$$\lambda(X) = \sum_{d=1}^{d_v} \lambda_d X^{d-1}, \quad (4.1)$$

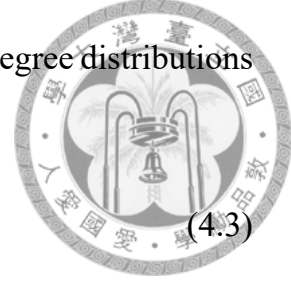
λ_d represents the fraction of all edges connected to variable nodes of degree- d and d_v is the maximum degree of variable nodes. Similarly, in the polynomial

$$\rho(X) = \sum_{d=1}^{d_c} \rho_d X^{d-1}, \quad (4.2)$$

ρ_d represents the fraction of all edges connected to check nodes of degree- d and d_c is the maximum degree of check nodes. The degree distributions may also be represented from node-perspective using the notation $\tilde{\lambda}(X)$ and $\tilde{\rho}(x)$ where $\tilde{\lambda}_d$ is the fraction of all variable nodes that have degree- d and $\tilde{\rho}_d$ is the fraction of all check

nodes that have degree- d . The coefficients of node-perspective degree distributions can be derived as

$$\tilde{\lambda}_d = \frac{\lambda_d/d}{\int_0^1 \lambda(X) dX}, \quad (4.3)$$



and

$$\tilde{\rho}_d = \frac{\rho_d/d}{\int_0^1 \rho(X) dX}. \quad (4.4)$$

In the representation of MET-LDPC codes, it is preferred to specify the code ensemble by a pair of node-perspective degree distributions related to variable nodes and check nodes, respectively,

$$L(\mathbf{r}, \mathbf{x}) = \sum_{\mathbf{b}, \mathbf{d}} L_{\mathbf{b}, \mathbf{d}} \mathbf{r}^{\mathbf{b}} \mathbf{x}^{\mathbf{d}}, \quad (4.5)$$

and

$$R(\mathbf{x}) = \sum_{\mathbf{d}} R_{\mathbf{d}} \mathbf{x}^{\mathbf{d}}. \quad (4.6)$$

Let n_e be the number of edge-types. The vector $\mathbf{d} = [d_1, \dots, d_{n_e}]$ is called multi-edge degree or node-type, and $\mathbf{x} = [x_1, \dots, x_{n_e}]$ denotes variables. We use $\mathbf{x}^{\mathbf{d}}$ to denote $\prod_{i=1}^{n_e} x_i^{d_i}$ where d_i is the number of connected edges of edge-type i for the nodes of node-type \mathbf{d} . For example, a node specified by $x_1^3 x_2^5$ is connected to three edges of edge-type 1 and five edges of edge-type 2. Let n_r be the number of different bit-channels that a codeword bit may be transmitted to. Let $\mathbf{b} = [b_0, \dots, b_{n_r}]$ be a vector that has one entry set to 1 and the rest set to 0, and $\mathbf{r} = [r_0, \dots, r_{n_r}]$ denotes variables corresponding to received bit-channels. We use $\mathbf{r}^{\mathbf{b}}$ to denote $\prod_{i=0}^{n_r} r_i^{b_i}$. The specification of bit-channels is utilized in the design of MET-LDPC codes for

high-order modulation schemes. Typically, the vector \mathbf{b} has only two entries to describe that a codeword bit is either punctured, $\mathbf{b} = [1 \ 0]$ and $\mathbf{r}^{\mathbf{b}} = r_0$, or transmitted through a single channel, $\mathbf{b} = [0 \ 1]$ and $\mathbf{r}^{\mathbf{b}} = r_1$, for binary-input channels.

Finally, the coefficients $L_{\mathbf{b}, \mathbf{d}}$ and $R_{\mathbf{d}}$ are non-negative real numbers corresponding to the fractions of variable nodes of node-type (\mathbf{b}, \mathbf{d}) and the fraction of check nodes of node-type \mathbf{d} respectively, where the fractions are relative to the number of transmitted variable nodes, i.e., unpunctured variable nodes.

Node-perspective degree distributions can be converted to edge-perspective via the following multinomials, where $\lambda_i(\mathbf{r}, \mathbf{x})$ and $\rho_i(\mathbf{x})$ are the edge-perspective degree distributions of edge-type i associated with variable nodes and check nodes respectively:

$$(\lambda_1(\mathbf{r}, \mathbf{x}), \lambda_2(\mathbf{r}, \mathbf{x}), \dots, \lambda_{n_e}(\mathbf{r}, \mathbf{x})) = \left(\frac{L_{x_1}(\mathbf{r}, \mathbf{x})}{L_{x_1}(\mathbf{1}, \mathbf{1})}, \frac{L_{x_2}(\mathbf{r}, \mathbf{x})}{L_{x_2}(\mathbf{1}, \mathbf{1})}, \dots, \frac{L_{x_{n_e}}(\mathbf{r}, \mathbf{x})}{L_{x_{n_e}}(\mathbf{1}, \mathbf{1})} \right), \quad (4.7)$$

and

$$(\rho_1(\mathbf{x}), \rho_2(\mathbf{x}), \dots, \rho_{n_e}(\mathbf{x})) = \left(\frac{R_{x_1}(\mathbf{x})}{R_{x_1}(\mathbf{1})}, \frac{R_{x_2}(\mathbf{x})}{R_{x_2}(\mathbf{1})}, \dots, \frac{R_{x_{n_e}}(\mathbf{x})}{R_{x_{n_e}}(\mathbf{1})} \right), \quad (4.8)$$

where $L_{x_i}(\mathbf{r}, \mathbf{x}) = \frac{\partial}{\partial x_i} L(\mathbf{r}, \mathbf{x})$, $R_{x_i}(\mathbf{x}) = \frac{\partial}{\partial x_i} R(\mathbf{x})$, and $\mathbf{1}$ is an all-one vector. There are n_e pairs of degree distributions defining the code ensemble in MET-LDPC codes. By setting $n_e = 1$, the representation of standard irregular LDPC codes can be obtained. If a node is connected to d_i edges of edge-type i , we will state that this node has d_i sockets for edge-type i and an edge in the graph is a pairing of sockets for the same edge-type. In MET framework, the total number of sockets on the variable node side is the same as that on the check node side for each edge-

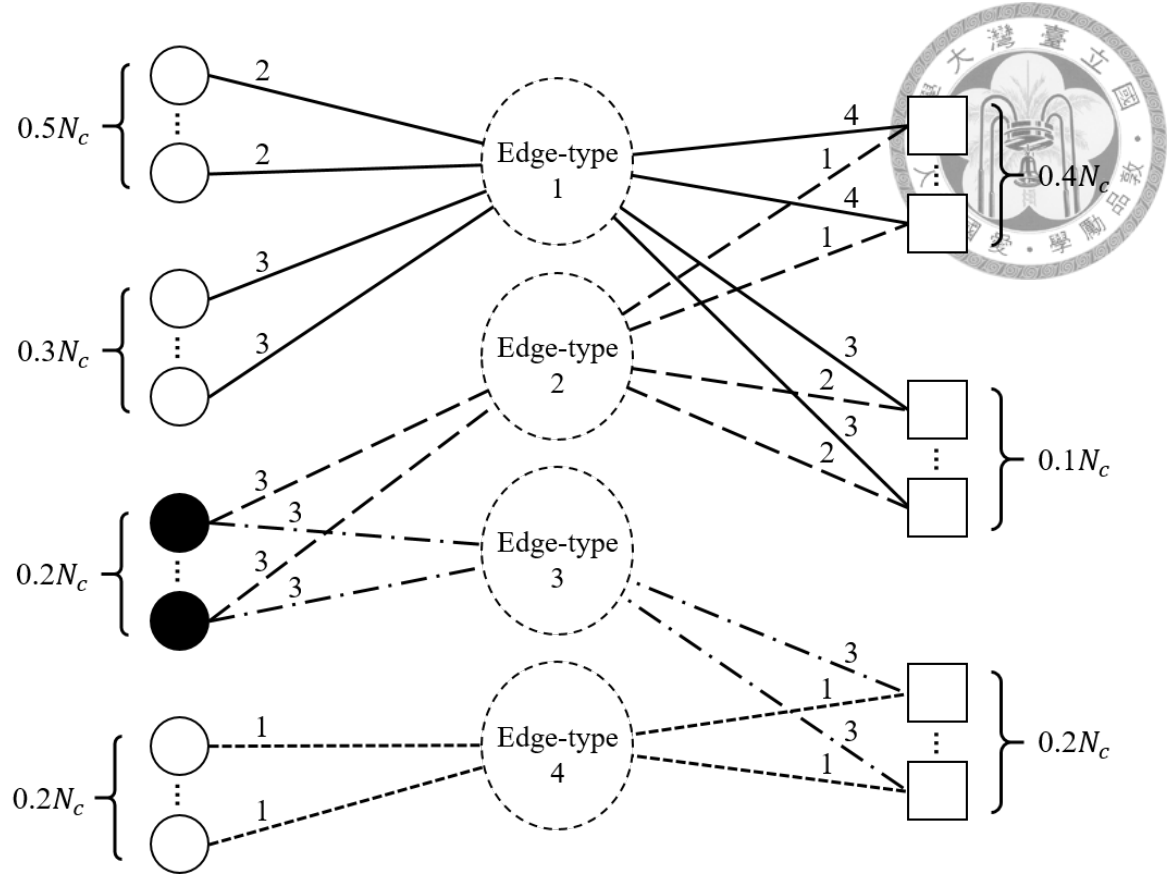


Figure 4.1: Graphical representation of a four-edge-type MET-LDPC code.

type. To ensure the validity of code structure, the following socket count equality constraints should be satisfied:

$$L_{x_i}(\mathbf{1}, \mathbf{1}) = R_{x_i}(\mathbf{1}), \quad i = 1, 2, \dots, n_e. \quad (4.9)$$

Assuming that all parity-check constraints are linearly independent, the nominal code rate of MET-LDPC codes is given by

$$R_c = L(\mathbf{1}, \mathbf{1}) - R(\mathbf{1}). \quad (4.10)$$

A graphical representation of a rate-1/2 four-edge type MET-LDPC code ensemble given in Table VI of [7] is shown in Fig. 4.1 as an example. The correspond-

ing node-perspective degree distributions of the example are given by $L(\mathbf{r}, \mathbf{x}) = 0.5r_1x_1^2 + 0.3r_1x_1^3 + 0.2r_0x_2^3x_3^3 + 0.2r_1x_4$ and $R(\mathbf{x}) = 0.4x_1^4x_2 + 0.1x_1^3x_2^2 + 0.2x_3^3x_4$ where r_0 denotes the punctured variable nodes and r_1 denotes the unpunctured variable nodes. The black solid circles in Fig. 4.1 represent the punctured variable nodes and N_c is the number of transmitted codeword bits in a block. The edge-perspective degree distributions of the example are also provided as

$$(\lambda_1(\mathbf{r}, \mathbf{x}), \lambda_2(\mathbf{r}, \mathbf{x}), \lambda_3(\mathbf{r}, \mathbf{x}), \lambda_4(\mathbf{r}, \mathbf{x})) = \left(\frac{10}{19}r_1x_1 + \frac{9}{19}r_1x_1^2, r_0x_2^2x_3^3, r_0x_2^3x_3^2, r_1 \right), \quad (4.11)$$

and

$$(\rho_1(\mathbf{x}), \rho_2(\mathbf{x}), \rho_3(\mathbf{x}), \rho_4(\mathbf{x})) = \left(\frac{16}{19}x_1^3 + \frac{3}{19}x_1^2x_2^2, \frac{2}{3}x_1^4 + \frac{1}{3}x_1^3x_2^2, x_3^2x_4, x_3^3 \right). \quad (4.12)$$

4.2 Ensemble Behavior

Belief propagation (BP) decoding, or sum-product algorithm as mentioned previously, is applied to the decoding of LDPC codes and MET-LDPC codes. In the BP decoding, there are three types of messages passed along the edges in the corresponding Tanner graph: channel message, variable-to-check message and check-to-variable message. Let m_0 denote the channel message, $m_{v \rightarrow c}^{(l)}$ denote the message from variable node v to check node c and $m_{c \rightarrow v}^{(l)}$ denote the message from check node c to variable node v at the l -th decoding iteration. The variable-to-check mes-



sage and check-to-variable message can be computed as follows:

$$m_{v \rightarrow c}^{(l)} = \begin{cases} m_0 & \text{if } l = 1, \\ m_0 + \sum_{c' \in C_v \setminus c} m_{c' \rightarrow v}^{(l-1)} & \text{if } l > 1, \end{cases} \quad (4.13)$$

$$m_{c \rightarrow v}^{(l)} = 2 \tanh^{-1} \left(\prod_{v' \in V_c \setminus v} \tanh \left(\frac{m_{v' \rightarrow c}^{(l)}}{2} \right) \right). \quad (4.14)$$

where $C_v \setminus c$ is the set of check nodes connected to variable node v excluding check node c , and $V_c \setminus v$ is the set of variable nodes connected to check node c excluding variable node v . Note that the variable-to-check message in (4.13) is passed from the unpunctured variable node that is transmitted to the channel, and the channel message will not be included if the variable node is punctured. The decoded LLR of variable node v after a predefined number of decoding iterations is obtained as

$$\mathcal{L}_v = \sum_{c \in C_v} m_{c \rightarrow v}^{(l)}, \quad (4.15)$$

which is the summation of all check-to-variable messages on the edges connected to variable node v .

A code ensemble is defined as the set of all codes with a specific degree distributions. To analyse and design the MET-LDPC code, multi-edge type density evolution (MET-DE) is usually used as an analytical tool. The MET-DE determines the asymptotic behavior of the BP decoding for a given code ensemble by iteratively tracking the probability density functions (PDFs) of messages passed along the edges in the corresponding Tanner graph. By using MET-DE, we can estimate how codes from this ensemble behave on average in the asymptotic sense.

The MET-DE can be applied to binary-input (BI) and symmetric-output channels, and we restrict the discussions to the transmission over BI-AWGN channel. In addition, the MET-DE is valid on the assumptions that an all-zero codeword is transmitted, thus an all-one sequence is transmitted under the mapping of $(-1)^c$, with cycle-free and infinite-length codes. In the density evolution for standard irregular LDPC codes, the PDFs of messages emitted from nodes of different degrees are averaged and a single PDF represents the messages since all edges are statistically equivalent. In MET-DE, the PDFs of messages emerging from nodes of different node-types are averaged according to edge-perspective degree distributions and the messages are represented by n_e PDFs for different edge-types.

Let f_{m_0} be the PDF of channel message, $f_v^{(l)}[i]$ be the PDF of messages on the edges of edge-type i of variable nodes and $f_c^{(l)}[i]$ be the PDF of messages on the edges of edge-type i of check nodes at the l -th decoding iteration. The PDF of variable-to-check message from variable nodes of node-type (\mathbf{b}, \mathbf{d}) along edges of edge-type i at l -th decoding iteration can be computed as

$$f_{v_{\mathbf{b}, \mathbf{d}}}^{(l)}[i] = (f_{m_0})^{b_1} \otimes \left(f_c^{(l-1)}[i]\right)^{\otimes(d_i-1)} \otimes_{k \neq i} \left(f_c^{(l-1)}[k]\right)^{\otimes d_k}, \quad (4.16)$$

where \otimes is the operation of variable node convolution and the channel message m_0 is Gaussian distributed with $2/\sigma^2$ mean and $4/\sigma^2$ variance when σ^2 is the variance of AWGN. Note that the channel message is only fed to the variable nodes that are transmitted to channel, i.e., unpunctured variable nodes with $\mathbf{b} = [0 \ 1]$. Similarly, the PDF of check-to-variable message from check nodes of node-type \mathbf{d}

along edges of edge-type i at l -th decoding iteration can be computed as

$$f_{c_d}^{(l)}[i] = \left(f_v^{(l)}[i]\right)^{\boxtimes(d_i-1)} \bigotimes_{k \neq i} \left(f_v^{(l)}[k]\right)^{\boxtimes d_k}, \quad (4.17)$$



where \boxtimes is the operation of check node convolution. From (4.16) and (4.17), one can see that the MET-DE simulates the procedure of BP decoding in (4.13) and (4.14) and computes the PDFs of messages passed along the edges iteratively. The PDFs of messages emitting from nodes of different node-types are averaged by the edge-perspective degree distributions in (4.7) and (4.8) to attain $f_v^{(l)}[i]$ and $f_c^{(l)}[i]$ in each iteration. The PDF of the decoded message for the variable node of node-type (\mathbf{b}, \mathbf{d}) is

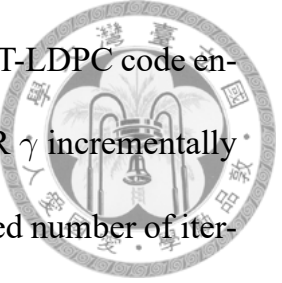
$$f_{v_{\mathbf{b}, \mathbf{d}}}^{(l)}[i] = (f_{m_0})^{b_1} \bigotimes_{i \in \{1, \dots, n_e\}} \left(f_c^{(l-1)}[i]\right)^{\boxtimes d_i}. \quad (4.18)$$

The procedure is terminated if the maximum number of iterations is reached or the error rate is less than a given threshold. Since an all-one word is transmitted on the assumption, the probability that the decoded LLR is less than zero is derived as the error rate, which is given by

$$\Pr[\epsilon] = \int_{-\infty}^0 f_{\mathcal{L}_v}^{(l)}(\tau) d\tau, \quad (4.19)$$

where $f_{\mathcal{L}_v}^{(l)}$ is the PDF of decoded message derived from averaging the PDFs in (4.18) across different node-types by the edge-perspective degree distribution.

A decoding threshold of a given code ensemble is defined as the worst channel parameter, e.g., channel SNR for the BI-AWGN channel, such that the reliable transmission is possible with infinite code length and infinite decoding iterations.



An analytical tool for determining the decoding thresholds of MET-LDPC code ensembles is the MET-DE. By decreasing the value of channel SNR γ incrementally until the error probability calculated by the MET-DE with a limited number of iterations in (4.19) is not smaller than a prescribed threshold (e.g., $\Pr[\epsilon] \leq 10^{-6}$), then the previous γ before termination is the decoding threshold γ^* . The MET-DE only determines the decoding threshold when a set of degree distributions is given. Usually, an outer global optimization algorithm is employed to search the parametric space of degree distributions for minimizing the decoding threshold with the constraints (4.9) and (4.10). Once the degree distributions with the minimum decoding threshold are found, one can construct MET-LDPC codes accordingly.

4.3 Serial Concatenation of LDPC Codes and Differential Encoding

In many schemes for blind channel estimation, e.g., cluster-based channel estimation proposed in Chapter 3, there is an inevitable phase ambiguity in the estimate and the differential encoding can be applied to resolve this problem. However, the differential encoding brings in a loss of 3 dB in the performance of multi-carrier transmission as shown in Chapter 3. By exploiting the great flexibility provided in multi-edge framework, we represent the concatenation of LDPC codes and differential encoding, referred to as DE-LDPC codes for brevity, as MET-LDPC codes and hence jointly analyse the two component codes to design the outer LDPC codes that can properly match the following differential encoding.

4.3.1 Multi-Edge Representation

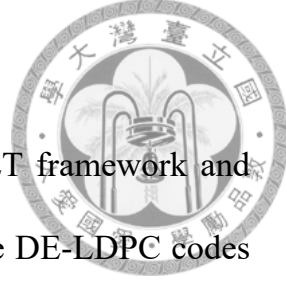
Recall that there are several edge-types defined in the MET framework and each of them has its own degree distributions. To represent the DE-LDPC codes as MET-LDPC codes, the edge-types in the corresponding Tanner graph should be defined. In Fig. 3.21, we showed the Tanner graph of DE-LDPC codes and here we also consider the transmission of DE-BPSK as example. The edge-type setting of DE-LDPC codes in the MET framework is configured as: the edges connecting intermediate check nodes and input nodes are defined as edge-type 1, the edges connecting input nodes and output check nodes are defined as edge-type 2, and the edges connecting output check nodes and output nodes are defined as edge-type 3. Note that the input nodes and output nodes represent the sequences \mathbf{v} and \mathbf{c} in Fig. 4.2 respectively. It is obvious that the connection of edges of edge-type 2 and edge-type 3 is deterministic, and the edges of edge-type 1 are connected with the degree distributions defined in the outer LDPC code.

DE-LDPC codes can be considered as MET-LDPC codes and the corresponding code ensemble can be represented by two node-perspective degree distributions associated with variable nodes and check nodes as follows:

$$L(\mathbf{r}, \mathbf{x}) = r_0 \sum_{i_v=1}^{d_v} L_{[i_v \ 1 \ 0]} x_1^{i_v} x_2 + r_1 L_{[0 \ 0 \ 2]} x_3^2, \quad (4.20)$$

$$R(\mathbf{x}) = \sum_{i_c=1}^{d_c} R_{[i_c \ 0 \ 0]} x_1^{i_c} + R_{[0 \ 1 \ 2]} x_2^1 x_3^2, \quad (4.21)$$

and the graphical representation in MET framework is shown in Fig. 4.4. The input



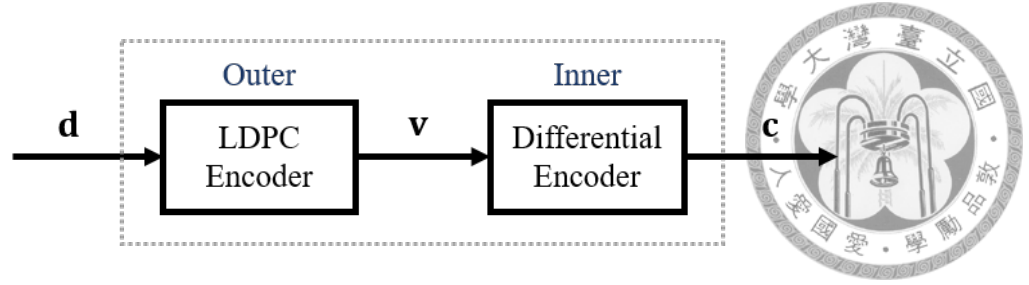


Figure 4.2: An encoder of DE-LDPC code for DE-BPSK transmission.

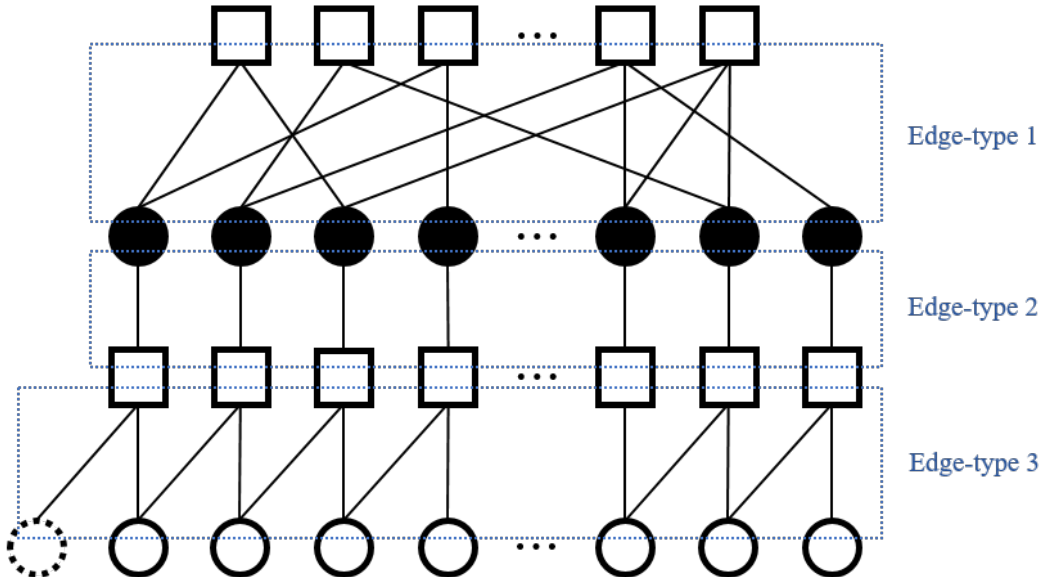


Figure 4.3: Configuration of edge-types for DE-LDPC codes represented in MET framework for DE-BPSK transmission.

nodes representing the codeword bits after outer LDPC encoding are punctured and hence are specified by r_0 . Moreover, since the codeword bits after differential encoding will be transmitted to the channel and then receive channel messages in the decoding, the output bits are specified by r_1 . The edge-perspective degree distributions associated with variable nodes and check nodes of the outer LDPC code can be derived from (4.20) and (4.21) as

$$\lambda(\mathbf{r}, \mathbf{x}) = \frac{L_{x_1}(\mathbf{r}, \mathbf{x})}{L_{x_1}(\mathbf{1}, \mathbf{1})} = r_0 \lambda(\mathbf{x}), \quad (4.22)$$

$$\rho(\mathbf{x}) = \frac{R_{x_1}(\mathbf{x})}{R_{x_1}(\mathbf{1})}. \quad (4.23)$$

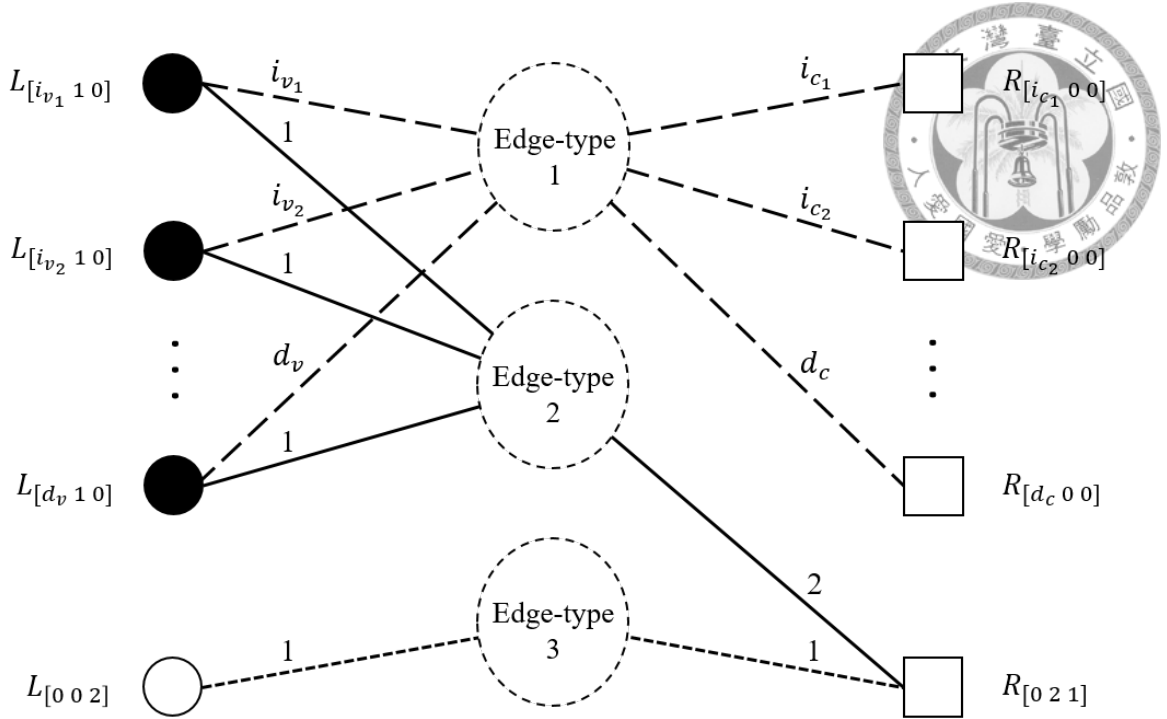


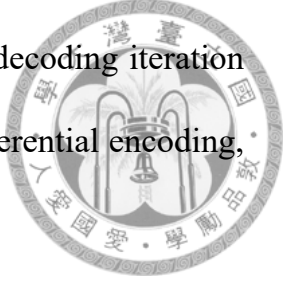
Figure 4.4: Graphical representation of DE-LDPC code ensemble in MET framework for DE-BPSK transmission.

4.3.2 Decoding Schemes

In Sec. 3.3.3, we discussed the joint decoding for DE-LDPC codes. A general definition of joint decoding is that one decoding iteration consists of L_o decoding iterations on the outer LDPC code, and L_i decoding iterations on the inner differential encoding. In the joint decoding, two component codes exchange the extrinsic informations simultaneously to each other. In addition to the joint decoding, the DE-LDPC codes can also be decoded by tandem decoding. The procedure of tandem decoding is that differential component is decoded first and the soft information is then sent to the LDPC component.

In [16], the decoding schemes were analysed and the authors concluded that the tandem decoding is sub-optimal compared to the joint decoding since the joint decoding always gives better performance than the tandem decoding. Hence, we

only consider the joint decoding for DE-LDPC codes and one decoding iteration consists of L iterations on both outer LDPC code and inner differential encoding, respectively.



4.3.3 Optimization in Multi-Edge Framework

Besides the density evolution, there are other approximate algorithms to analyse LDPC codes for less computational complexity, e.g., extrinsic information transfer (EXIT) chart analysis or Gaussian approximation. However, it was indicated in [24] that the assumption of symmetric Gaussian distribution for message passing in the EXIT chart analysis may not be accurate particularly at low rates and with punctured variable nodes. Since nearly half the variable nodes are punctured in the structure of DE-LDPC codes, the prediction of code ensemble using approximate algorithms might lose the optimality. If we consider DE-LDPC codes as MET-LDPC codes, we can search the space of degree distributions based on the MET-DE to construct DE-LDPC codes, which in turn helps to increase the accuracy since there is no approximation used in MET-DE. Recall that MET-DE tracks the messages iteratively with exact PDFs. Therefore, the MET framework provides a better chance to design the outer LDPC code component in consideration of the impact introduced by differential encoding on the error-correction capability. Moreover, the DE-LDPC codes employing the joint decoding scheme can be analysed by using the MET-DE. Since the MET-DE simulates the iterative procedure of BP decoding and computes the PDFs of messages in each iteration, we can easily adjust the scheme of MET-DE to estimate the asymptotic performances of

DE-LDPC codes under different decoding schemes.

To find the degree distributions of outer LDPC code component with minimum decoding threshold, besides the MET-DE, differential evolution [25] is also employed, which is a combination of hill-climbing algorithm and genetic algorithm.

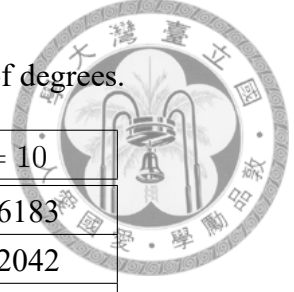
The fitness of each candidate in the differential evolution is the decoding threshold found by MET-DE and the goal is to find a set of degree distributions that minimizes the decoding threshold of DE-LDPC code. Once we find the degree distributions, the outer LDPC code is constructed by the improved progressive edge-growth (PEG) algorithm [26] [27] that maximize the local girth of variable nodes and approximate cycle extrinsic message degree (ACE) in Tanner graph. In the results of degree distributions found in MET framework, the maximum number of decoding iterations is less than 500 for the fairness in complexity. In the setting of MET-DE, the number of sample points in the quantization is 3000 and the quantization interval is 0.01.

4.3.4 Numerical Results

In [28], the design of LDPC codes concatenated with differential modulations was investigated and the optimized degree distributions, based on the EXIT chart analysis, of outer LDPC code were provided. The mutual information (MI) at the output of coded modulator (CM-SISO) was approximately computed based on Monte Carlo simulations in [28] and the authors stated that the predicted convergence thresholds are not accurate but it turns out to be in monotonic relationship. The decoding scheme considered in [28] was modified from the turbo principle



Table 4.1: Optimized degree distributions with a fixed set of degrees.



	$L = 1$	$L = 5$	$L = 10$
$\tilde{\lambda}_2$	0.903056	0.876163	0.846183
$\tilde{\lambda}_3$	0.002200	0.023773	0.002042
$\tilde{\lambda}_4$	0.094744	0.100064	0.151775
$\tilde{\rho}_3$	0.563524	0.576578	0.507446
$\tilde{\rho}_4$	0.349765	0.329838	0.390253
$\tilde{\rho}_8$	0.000988	0.000720	0.000955
$\tilde{\rho}_{15}$	0.085723	0.092864	0.101346
$\gamma_{(\text{dB})}^*$	0.99	0.99	1.01

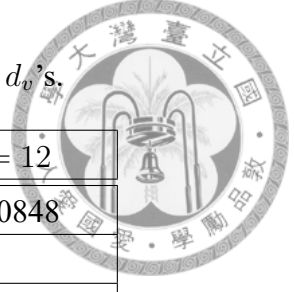
and the resultant complexity is high. To see the advantages, we compare the DE-LDPC codes designed in MET framework to the one given in [28] with the node-perspective degree distributions:

$$\tilde{\lambda}_2 = 0.5473 \quad \tilde{\lambda}_3 = 0.0116 \quad \tilde{\lambda}_4 = 0.4411$$

$$\tilde{\rho}_3 = 0.3157 \quad \tilde{\rho}_4 = 0.2259 \quad \tilde{\rho}_8 = 0.0273 \quad \tilde{\rho}_{15} = 0.4311, \quad (4.24)$$

and the joint decoding is employed. If the joint decoding is applied, the decoding threshold of (4.24) computed by MET-DE is 1.1 dB. Moreover, the decoding threshold of (3,6)-regular LDPC code computed by MET-DE when the differential encoding is concatenated is 2.18 dB, and 1.11 dB [29] without the differential encoding. With the same set of degrees for both variable nodes and check nodes as that of (4.24), the degree distributions optimized in the MET framework for different numbers of inner iterations based on MET-DE are tabulated in Table 4.1. In the sense of asymptotic performance, it is possible to find a better DE-LDPC code

Table 4.2: Optimized degree distributions for different d_v 's.



	$d_v = 10$	$d_v = 11$	$d_v = 12$
$\tilde{\lambda}_2$	0.831548	0.828379	0.830848
$\tilde{\lambda}_9$	0.006645		
$\tilde{\lambda}_{10}$	0.161807	0.068575	
$\tilde{\lambda}_{11}$		0.103045	0.018740
$\tilde{\lambda}_{12}$			0.150413
$\tilde{\rho}_3$	0.011435	0.000957	0.001150
$\tilde{\rho}_4$	0.733954	0.710731	0.647364
$\tilde{\rho}_8$	0.015334	0.031206	0.074233
$\tilde{\rho}_{15}$	0.239276	0.257105	0.277254
$\gamma_{(\text{dB})}^*$	0.74	0.73	0.71

ensemble with smaller decoding threshold than that found in [28]. In addition, let d_v denotes the maximum degree of variable nodes and the set of degrees for check nodes is the same as that of (4.24), the degree distributions optimized in the MET framework with different d_v 's are tabulated in Table 4.2.

In addition to the asymptotic performances, simulation results are also provided. In Fig. 4.5, the error rate performances of (12000,6000) DE-LDPC codes over BI-AWGN channel are simulated and the DE-LDPC code optimized in MET framework provided in Table 4.1 outperforms the DE-LDPC code in (4.24) when $L = 5$, especially in BLER performances. Since the density evolution is performed under the assumptions of infinite-length and cycle-free, the optimized codes are generally susceptible to high error floors due to short cycles and trapping sets. In particular, the presence of cycles involving degree-2 variable nodes makes the performance of iterative decoders unsatisfying [29]. In Fig. 4.5, a significant error floor can be observed since a large ratio of degree-2 variable nodes exist in the DE-LDPC codes

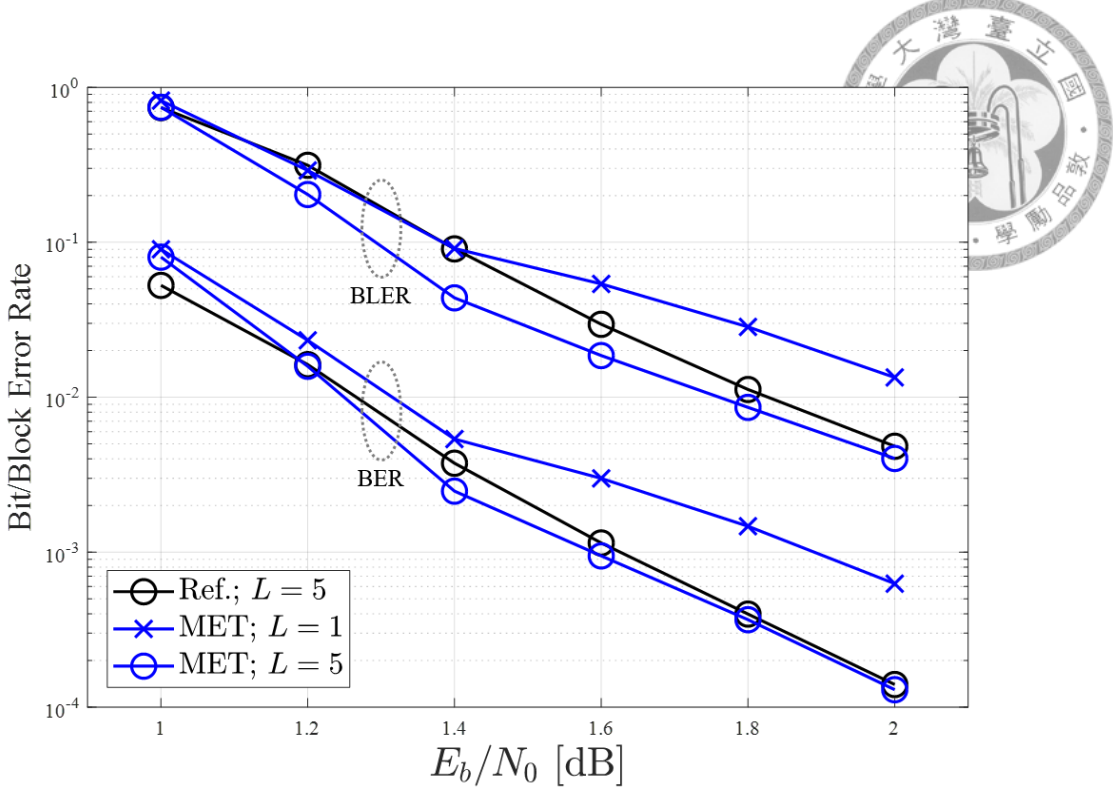


Figure 4.5: BER and BLER performances of (12000,6000) LDPC codes over AWGN channel.

optimized in MET framework.

In Fig. 4.6 and 4.7, the error rate performances of (6000,3000) LDPC codes over AWGN channel are provided. A (3,6)-regular LDPC code is simulated with or without differential encoding, and about 1 dB performance degradation is introduced by applying the differential encoding since the LDPC code is originally designed for memoryless channels. In addition, the performances of the DE-LDPC code optimized in MET framework provided in Table 4.2 with $d_v = 12$ is also simulated. The optimized outer LDPC code concatenated with inner differential encoding performs as good as (3,6)-regular LDPC code without differential encoding in low-SNR region. Therefore, if we can design the outer LDPC code in consideration of inner differential encoding, the resultant DE-LDPC code can evidently

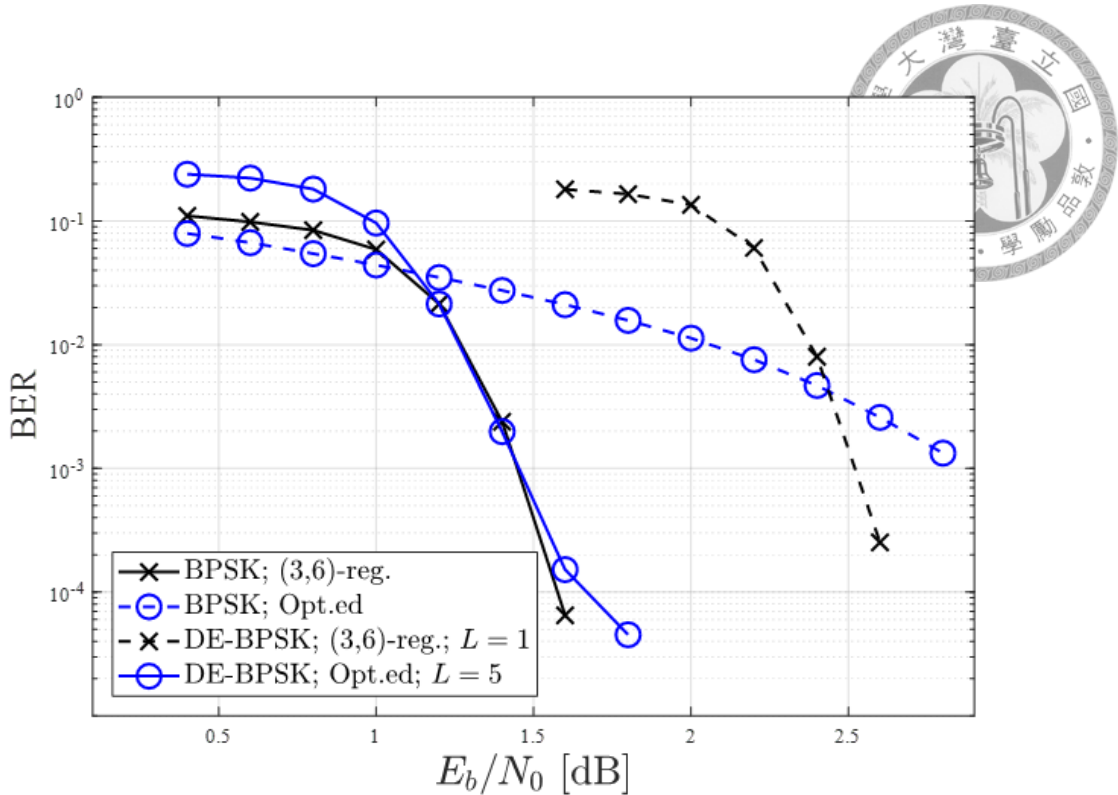


Figure 4.6: BER performances of (6000,3000) LDPC codes with or without differential encoding over AWGN channel.

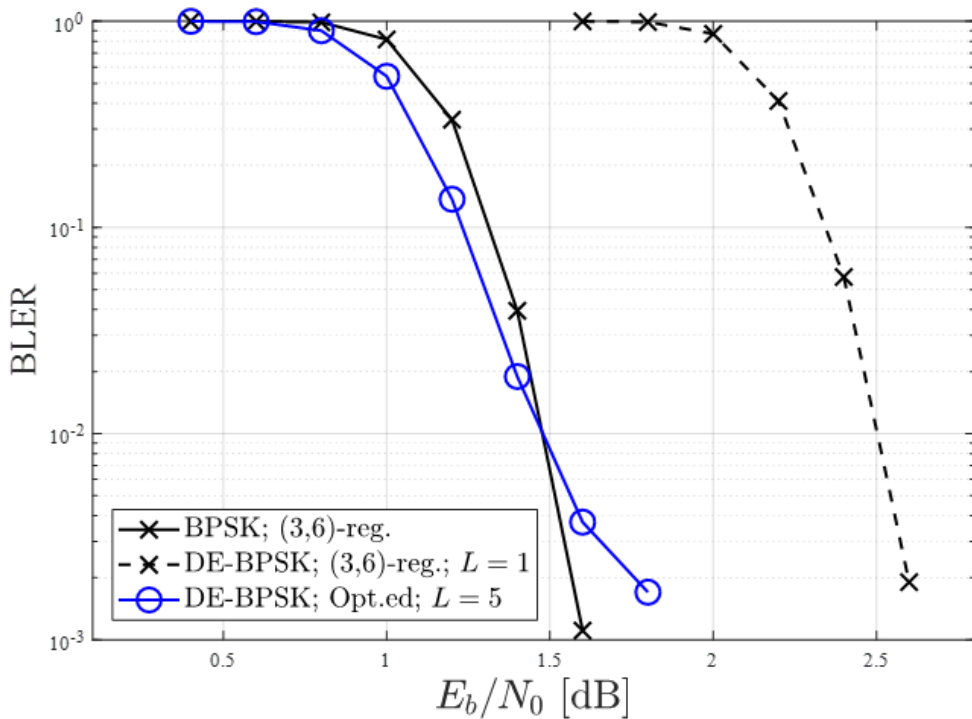


Figure 4.7: BLER performances of (6000,3000) LDPC codes with or without differential encoding over AWGN channel.

relieve the performance degradation and still remove the phase ambiguity in the estimates. However, there is an error floor in high-SNR region of the performance for DE-LDPC code optimized in MET framework.



In our study, the differential encoding is employed to overcome the problem of phase ambiguity caused by blind channel estimation. The outer LDPC code optimized specifically for inner differential encoding provided in Table 4.2 with $d_v = 12$ is also used in the MC-DS-CDMA-GDMA system employing cluster-based channel estimation in simulations. In Fig. 4.8 and 4.9, the BLER performances are provided and one can see that the performance can be further improved by 1 dB when the optimized DE-LDPC code is used.

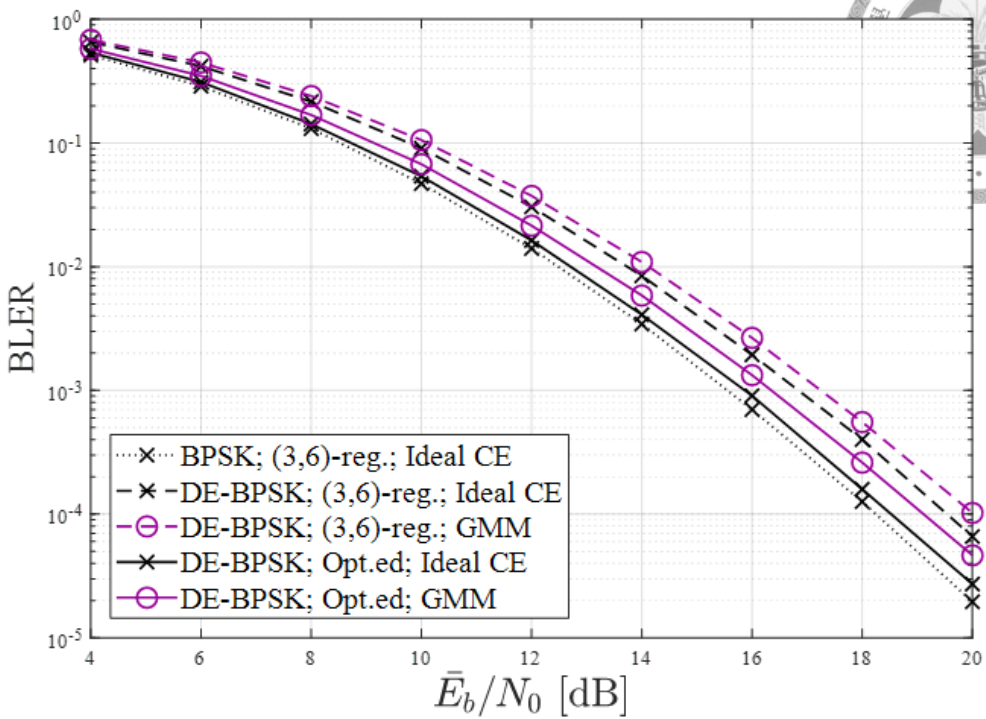
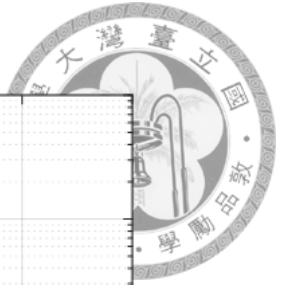


Figure 4.8: BLER performances of (1008,504) LDPC-coded MC-DS-CDMA system employing cluster-based estimation with $P = 1$ user over quasi-static frequency-selective Rayleigh fading channels.

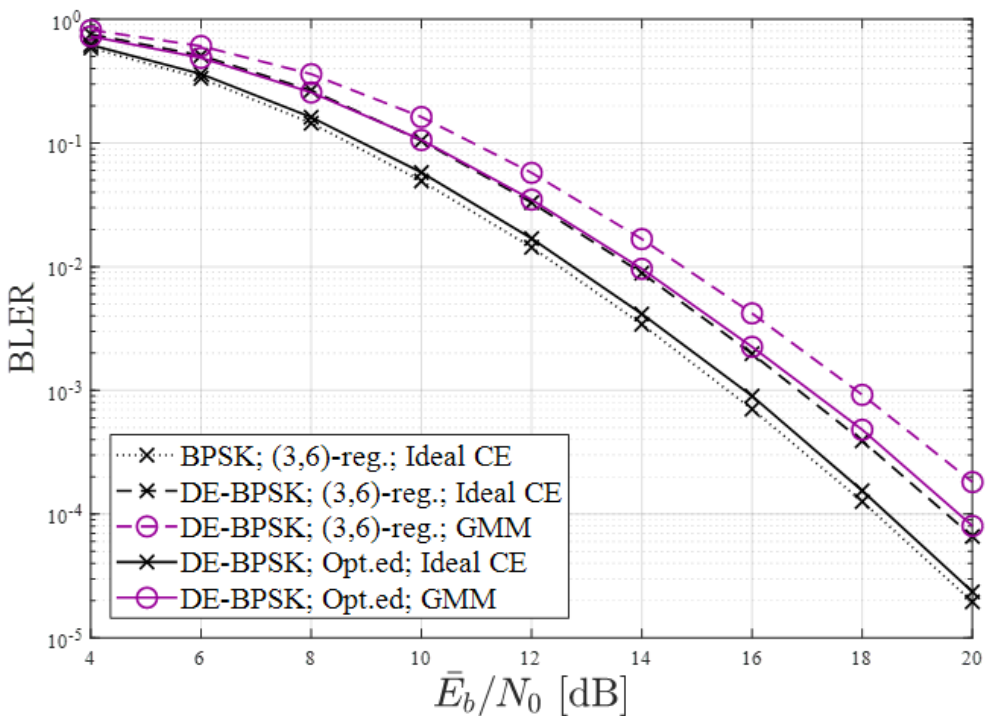


Figure 4.9: BLER performances of (1008,504) LDPC-coded MC-DS-CDMA-GDMA system employing cluster-based estimation with $P = 2$ users over quasi-static frequency-selective Rayleigh fading channels.



Chapter 5

Conclusion and Future Works

In this thesis, we presented the concept of GDMA, which exploits the distinct channels to separate the signals transmitted from multiple users over independent fading channels. Since the multi-level detection technique does not require additional user-specific resources, the GDMA concept can be easily combined with other multiple access systems to permit multiple users to share the same user-specific resource and make the resource allocation more flexible. Moreover, we proposed to utilize the clustering algorithms to classify the superimposed signals in GDMA system and further derive the channel coefficients of multiple users. The proposed cluster-based scheme for blind channel estimation can be applied to the transmissions over scalar channels and high spectral efficiency can be obtained since no additional pilot signal is needed for channel estimation. However, the proposed scheme is sensitive to the variation of channels.

Differential encoding is an easy way to remove the phase ambiguity in the estimates but it also introduce a loss in performance. Multi-edge representation for the serial concatenation of outer LDPC codes and inner differential encoding provides

an useful framework to design the outer LDPC codes and thus alleviate the performance degradation introduced by differential encoding. There are some other advantages can be further exploited in multi-edge framework, e.g., bit-channel specification in the design of MET-LDPC codes for high-order modulations, and better accuracy in the prediction of low-rate code ensembles compared to other approximate algorithms. Note that the multi-edge representation for DE-LDPC codes is restricted to DE-PAM schemes.

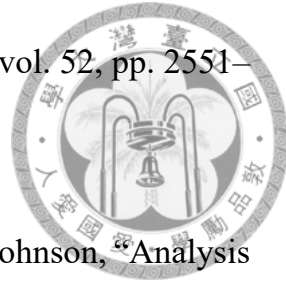




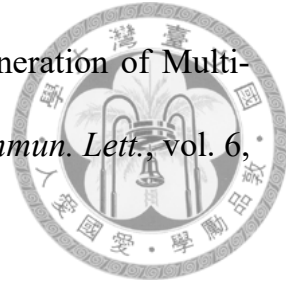
Bibliography

- [1] B.-H. Chang, “Multiple Access for Transmissions Over Independent Fading Channels,” Master’s thesis, National Taiwan University, 2018.
- [2] S. Zhang, S. Liew, and P. Lam, “Hot Topic: Physical Layer Network Coding,” in *Proc. International Conference on Mobile Computing and Networking (MobiCom)*, p. 358–365, 2006.
- [3] S. P. Lloyd, “Least Squares Quantization in PCM,” *IEEE Trans. Inf. Theory*, vol. IT-28, pp. 129–136, Mar. 1982.
- [4] Y. Linde, A. Buzo, and R. M. Gray, “An Algorithm for Vector Quantizer Design,” *IEEE Trans. Commun.*, vol. COM-28, pp. 84–95, Jan. 1980.
- [5] D. Arthur and S. Vassilvitskii, “K-Means++: The Advantages of Careful Seeding,” in *Proc. Symp. Discrete Algorithms*, p. 1027–1035, 2007.
- [6] A. P. Dempster, N. M. Laird, and D. B. Rubin, “Maximum Likelihood from Incomplete Data via the EM Algorithm,” *Journal of the Royal Statistical Society. Series B (Methodological)*, vol. 39, no. 1, pp. 84–95, 1977.
- [7] T. J. Richardson and R. L. Urbanke, “Multi-Edge Type LDPC Codes,” in *Proc. 60th Birthday Workshop Honoring Prof. Bob McEliece*, p. 1–36, 2002.

- [8] D. Wübben and Y. Lang, “Generalized Sum-Product Algorithm for Joint Channel Decoding and Physical-Layer Network Coding in Two-Way Relay Systems,” in *IEEE Proc. Global Communications Conference (GLOBECOM)*, Feb. 2010.
- [9] F. R. Kschischang, B. J. Frey, and H.-A. Loeliger, “Factor Graphs and the Sum-Product Algorithm,” *IEEE Trans. Inf. Theory*, vol. 47, pp. 498–519, Feb. 2001.
- [10] D. Wübben, “Joint Channel Decoding and Physical-Layer Network Coding in Two-Way QPSK Relay Systems by a Generalized Sum-Product Algorithm,” in *Proc. 7th International Symposium on Wireless Communication Systems (ISWCS)*, Sept. 2010.
- [11] E. Arikan, “Channel Polarization: A Method for Constructing Capacity-Achieving Codes for Symmetric Binary-Input Memoryless Channels,” *IEEE Trans. Inf. Theory*, vol. 55, pp. 3051–3073, July 2009.
- [12] I. Tal and A. Vardy, “List Decoding of Polar Codes,” *IEEE Trans. Inf. Theory*, vol. 61, pp. 2213–2226, May 2015.
- [13] D. J. C. MacKay, “Fountain Codes,” *IEE Proc. Commun.*, vol. 152, pp. 1062–1068, Dec. 2005.
- [14] M. Luby, “LT Codes,” in *Proc. 43rd Annu. IEEE Symp. Found. Comput. Sci.*, pp. 271–280, Nov. 2002.



- [15] A. Shokrollahi, “Raptor Codes,” *IEEE Trans. Inf. Theory*, vol. 52, pp. 2551–2567, June 2006.
- [16] S. Jayasooriya, M. Shirvanimoghaddam, L. Ong, and S. J. Johnson, “Analysis and Design of Raptor Codes Using a Multi-Edge Framework,” *IEEE Trans. Commun.*, vol. 65, pp. 5123–5136, Dec. 2017.
- [17] H.-M. Wang, “A Design of Systematic Physical-Layer Raptor Codes for High Throughput and Low Complexity,” Master’s thesis, National Taiwan University, 2018.
- [18] S. M. Alamouti, “A Simple Transmit Diversity Technique for Wireless Communications,” *IEEE Journal Select. Areas Commun.*, vol. 16, p. 1451–1458, Oct. 1998.
- [19] S.-H. Chang, “A Design of 16 ADQAM BICM,” Master’s thesis, National Taiwan University, 2013.
- [20] L. R. Bahl, J. Cocke, F. Jelinek, and J. Raviv, “Optimal Decoding of Linear Codes for Minimizing Symbol Error Rate,” *IEEE Trans. Inf. Theory*, vol. IT-20, pp. 284–287, Mar. 1974.
- [21] P. Hoeher and J. Lodge, ““Turbo DPSK” : Iterative Differential PSK Demodulation and Channel Decoding,” *IEEE Trans. Commun.*, vol. 47, pp. 837–843, June 1999.
- [22] R.-Y. Wei, “Noncoherent Block-Coded MPSK,” *IEEE Trans. Commun.*, vol. 53, pp. 978–986, June 2005.



- [23] Y. R. Zheng and C. Xiao, “Improved Models for the Generation of Multiple Uncorrelated Rayleigh Fading Waveforms,” *IEEE Commun. Lett.*, vol. 6, pp. 256–258, June 2002.
- [24] S. Jayasooriya, M. Shirvanimoghaddam, L. Ong, G. Lechner, and S. J. Johnson, “A New Density Evolution Approximation for LDPC and Multi-Edge Type LDPC Codes,” *IEEE Trans. Commun.*, vol. 64, pp. 4044–4056, Oct. 2016.
- [25] R. Storn and K. Price, “Differential Evolution—A simple and efficient heuristic for global optimization over continuous spaces,” *J. Global Optim.*, vol. 11, no. 4, pp. 341–359, 1997.
- [26] H. Chen and Z. Cao, “A Modified PEG Algorithm for Construction of LDPC Codes with Strictly Concentrated Check-Node Degree Distributions,” in *Proc. IEEE Wireless Communications and Networking Conference (WCNC 2007)*, Mar. 2007.
- [27] H. Xiao and A. H. Banihashemi, “Improved Progressive-Edge-Growth (PEG) Construction of Irregular LDPC Codes,” *IEEE Commun. Lett.*, vol. 8, pp. 715–717, Dec. 2004.
- [28] M. Franceschini, G. Ferrari, R. Raheli, and A. Curtoni, “Serial Concatenation of LDPC Codes and Differential Modulations,” *IEEE J. Sel. Areas Commun.*, vol. 23, pp. 1758–1768, Sep. 2005.

- [29] W. Ryan and S. Lin, *Channel Codes: Classical and Modern*. New York, NY, USA: Cambridge Univ. Press, 2009.
- [30] S. Kay, *Fundamentals of Statistical Signal Processing, Volume I: Estimation Theory*. Prentice Hall, 1993.
- [31] T. J. Richardson and R. Urbanke, *Modern Coding Theory*. Cambridge, U.K.: Cambridge Univ. Press, 2008.
- [32] B. Vucetic and J. Yuan, *Space-Time Coding*. Chichester, U.K.: Wiley, 2003.

